

Milena Suemi Irie

Microtomografia computadorizada: comparação de parâmetros utilizados na aquisição, reconstrução e processamento de imagens no estudo do processo de reparo ósseo e aplicabilidade na análise do efeito de diferentes terapias

Microcomputed tomography: comparison of parameters in image acquisition, reconstruction and processing for the evaluation of the bone repair process and its application to assess the effect of different therapies

Tese apresentada à
Faculdade de Odontologia da
Universidade Federal de Uberlândia,
como requisito parcial para obtenção
do Título de Doutora em Odontologia
na Área de Concentração de Clínica
Odontológica Integrada.

Uberlândia, 2021

Milena Suemi Irie

Microtomografia computadorizada: comparação de parâmetros utilizados na aquisição, reconstrução e processamento de imagens no estudo do processo de reparo ósseo e aplicabilidade na análise do efeito de diferentes terapias

Microcomputed tomography: comparison of parameters in image acquisition, reconstruction and processing for the evaluation of the bone repair process and its application to assess the effect of different therapies

Tese apresentada à Faculdade de Odontologia da Universidade Federal de Uberlândia, como requisito parcial para obtenção do Título de Doutora em Odontologia na Área de Concentração de Clínica Odontológica Integrada.

Orientadora: Prof^a. Dr^a. Priscilla Barbosa Ferreira Soares

Banca Examinadora:

Prof^o. Dr^o. Gustavo Davi Rabelo

Prof^o. Dr^o. Mario Taba Jr

Prof^o. Dr^o. Rubens Spin-Neto

Prof^a. Dr^a. Paula Barbar Dechichi

Prof^a. Dr^a. Priscilla Barbosa Ferreira Soares

Uberlândia, 2021

Ficha Catalográfica Online do Sistema de Bibliotecas da UFU
com dados informados pelo(a) próprio(a) autor(a).

168 2021	<p>Irie, Milena Suemi, 1990- Microtomografia computadorizada: comparação de parâmetros utilizados na aquisição, reconstrução e processamento de imagens no estudo do processo de reparo ósseo e aplicabilidade na análise do efeito de diferentes terapias [recurso eletrônico] / Milena Suemi Irie. - 2021.</p> <p>Orientadora: Priscilla Barbosa Ferreira Soares. Tese (Doutorado) - Universidade Federal de Uberlândia, Pós-graduação em Odontologia. Modo de acesso: Internet. Disponível em: http://doi.org/10.14393/ufu.te.2021.362 Inclui bibliografia.</p> <p>1. Odontologia. I. Soares, Priscilla Barbosa Ferreira, 1975-, (Orient.). II. Universidade Federal de Uberlândia. Pós-graduação em Odontologia. III. Título.</p> <p style="text-align: right;">CDU: 616.314</p>
-------------	--

Bibliotecários responsáveis pela estrutura de acordo com o AACR2:

Gizele Cristine Nunes do Couto - CRB6/2091



UNIVERSIDADE FEDERAL DE UBERLÂNDIA
 Coordenação do Programa de Pós-Graduação em Odontologia
 Av. Pará, 1720, Bloco 4L, Anexo B, Sala 35 - Bairro Umarama, Uberlândia-MG, CEP 38400-902
 Telefone: (34) 3225-8115/8108 - www.ppgoufu.com - copod@umarama.ufu.br



ATA DE DEFESA - PÓS-GRADUAÇÃO

Programa de Pós-Graduação em:	Odontologia				
Defesa de:	Tese Doutorado, número 68, PPGODONTO				
Data:	Trinta de Julho de Dois Mil e Vinte e Um	Hora de início:	08:30	Hora de encerramento:	[12:56]
Matrícula do Discente:	11713ODO016				
Nome do Discente:	Milena Suemi Irie				
Título do Trabalho:	Microtomografia computadorizada: comparação de parâmetros utilizados na aquisição, reconstrução e processamento de imagens no estudo do processo de reparo ósseo e aplicabilidade na análise do efeito de diferentes terapias				
Área de concentração:	Clínica Odontológica Integrada				
Linha de pesquisa:	Processo de Reparo				
Projeto de Pesquisa de vinculação:	Processo de Reparo				

Reuniu-se em Web Conferência pela plataforma Zoom, em conformidade com a PORTARIA Nº 36, DE 19 DE MARÇO DE 2020 da COORDENAÇÃO DE APERFEIÇOAMENTO DE PESSOAL DE NÍVEL SUPERIOR - CAPES, pela Universidade Federal de Uberlândia, a Banca Examinadora, designada pelo Colegiado do Programa de Pós-graduação em Odontologia, assim composta: Professores Doutores: Paula Dechichi Barbar (UFU); Gustavo Davi Rabelo (UFSC); Mario Taba Júnior (USP); Rubens Spin-Neto (AU); Priscilla Barbosa Ferreira Soares (UFU) orientadora da candidata.

Iniciando os trabalhos a presidente da mesa, Dra. Priscilla Barbosa Ferreira Soares, apresentou a Comissão Examinadora e o candidata, agradeceu a presença do público, e concedeu ao Discente a palavra para a exposição do seu trabalho. A duração da apresentação do Discente e o tempo de arguição e resposta foram conforme as normas do Programa.

A seguir o senhor(a) presidente concedeu a palavra, pela ordem sucessivamente, aos(às) examinadores(as), que passaram a arguir o(a) candidato(a). Ultimada a arguição, que se desenvolveu dentro dos termos regimentais, a Banca, em sessão secreta, atribuiu o resultado final, considerando o(a) candidato(a):

[A]provado(a).

Esta defesa faz parte dos requisitos necessários à obtenção do título de Doutor.

O competente diploma será expedido após cumprimento dos demais requisitos, conforme as normas do Programa, a legislação pertinente e a regulamentação interna da UFU.

Nada mais havendo a tratar foram encerrados os trabalhos. Foi lavrada a presente ata que após lida e achada conforme foi assinada pela Banca Examinadora.



Documento assinado eletronicamente por **Priscilla Barbosa Ferreira Soares, Professor(a) do Magistério Superior**, em 30/07/2021, às 12:56, conforme horário oficial de Brasília, com fundamento no art. 6º, § 1º, do [Decreto nº 8.539, de 8 de outubro de 2015](#).



Documento assinado eletronicamente por **Mario Taba Junior, Usuário Externo**, em 30/07/2021, às 12:57, conforme horário oficial de Brasília, com fundamento no art. 6º, § 1º, do [Decreto nº 8.539, de 8 de outubro de 2015](#).



Documento assinado eletronicamente por **Paula Dechichi Barbar, Professor(a) do Magistério Superior**, em 30/07/2021, às 12:57, conforme horário oficial de Brasília, com fundamento no art. 6º, § 1º, do [Decreto nº 8.539, de 8 de outubro de 2015](#).



Documento assinado eletronicamente por **Gustavo Davi Rabelo, Usuário Externo**, em 30/07/2021, às 12:59, conforme horário oficial de Brasília, com fundamento no art. 6º, § 1º, do [Decreto nº 8.539, de 8 de outubro de 2015](#).



Documento assinado eletronicamente por **Rubens Spin Neto, Usuário Externo**, em 30/07/2021, às 13:00, conforme horário oficial de Brasília, com fundamento no art. 6º, § 1º, do [Decreto nº 8.539, de 8 de outubro de 2015](#).



A autenticidade deste documento pode ser conferida no site https://www.sei.ufu.br/sei/controlador_externo.php?acao=documento_conferir&id_orgao_acesso_externo=0, informando o código verificador **2921269** e o código CRC **80F50287**.

DEDICATÓRIA

Por todo amor e enorme suporte,
dedico este trabalho à vocês:
pai, mãe, Maísa e Tiago.

AGRADECIMENTOS

Este poderia ser o capítulo mais longo desta tese, pois tenho muito a agradecer. Foram tantas pessoas que contribuíram para que eu conseguisse ter a capacidade intelectual e emocional para chegar até aqui que milhares de páginas seriam necessárias. Mas tentarei ser sucinta para não cansá-los.

Aos meus pais, Milton e Mary, por serem exemplos de caráter, honestidade e perseverança. Por priorizarem minha educação e da Maísa em detrimento de tantas coisas. Por todo o amor e apoio incondicional, que continua sendo extremamente fundamental para que eu siga sonhando, buscando e realizando. Se hoje tenho coragem e disciplina para tentar alcançar meus objetivos, foi pelo exemplo que eles me deram.

À minha irmã, Maísa, pela amizade mais sincera e pura que tenho. Por saber que mesmo distantes, nossos laços e sintonia são para sempre. A sua paciência e impaciência comigo me ensinaram muito.

Ao meu marido, Tiago, por tantos motivos que é difícil expressar em palavras a minha gratidão à ele. Amor, companheirismo, apoio, zelo, amizade, atenção, paciência, são algumas das inúmeras razões para agradecê-lo. Por valorizar a minha dedicação ao trabalho mesmo que isso significasse na minha ausência. Por me deixar feliz todos os dias, somente pelo fato de estar junto a mim. Por dividir seus sonhos e conquistas comigo, e principalmente, por tornar os meus sonhos, em nossos. Por todo seu esforço e dedicação para que seja possível realizá-los. Por todos os momentos maravilhosos que já vivemos juntos, seja conversando na sacada aqui de casa, ou por aí, conhecendo algum canto do mundo. Difícil imaginar Tiago sem Milena, e impossível Milena sem Tiago. Por melhor que eu possa tentar me expressar, não será digno do tamanho do meu amor e admiração por ele.

Aos meus avós paternos (*in memoriam*) pelos momentos felizes vividos juntos, e à minha Batian, por ser exemplo soberano para mim de garra e esforço.

À minha orientadora e Prof^a Priscilla Soares, por ser responsável, não somente pela possibilidade de realização de diversos trabalhos durante meu doutorado, mas pelo enorme amadurecimento que tive nestes últimos anos. Por

confiar em mim e no meu trabalho, por me ajudar sempre quando foi preciso, por acatar minhas ideias e propostas, por batalhar pelos projetos que construímos juntas, e sobretudo, por batalhar por mim. Ela me ensinou muito mais que metodologias de pesquisa, ela me mostrou que tudo é possível quando queremos, planejamos e estamos ao lado de pessoas dispostas a contribuir e crescer juntas. Ela me ensinou que oportunidades são dadas, mas cabe a mim torná-las proveitosas e relevantes. Minha imensa gratidão à essa mulher de garra, que além de orientadora, se tornou amiga por celebrar comigo a cada passo dado e por me dar suporte em cada queda.

Ao Prof^o Carlos Soares, por engrandecer a ciência brasileira em tantos aspectos, seja pela sua atuação administrativa, pela produção intelectual ou por oportunizar ensino de qualidade para novos pesquisadores. Sua contribuição para minha formação é imensurável, cada aula, cada frase, cada pergunta e cada resposta auxiliou diretamente no desenvolvimento dos trabalhos que tive a oportunidade de desenvolver nesse período. Agradeço por ter aberto não somente as portas da UFU para mim, mas também por nos acolher em diversos momentos na sua casa.

Ao Prof^o Rubens Spin-Neto, pessoa e profissional que é inspiração, não somente para mim, mas para muitos. O curto período de tempo que pudemos conviver foi suficiente para bastante aprendizado, mas que representa muito pouco diante de todo seu conhecimento e do que espero continuar aprendendo. Por toda receptividade, acolhimento e atenção dada em Aarhus, pelos muitos ensinamentos que ainda continuam por áudio ou reunião online, e principalmente, por conseguir ser exemplo de grandeza e humildade.

À todos os professores que tive durante essa trajetória acadêmica na UEM, na FORP e na UFU, em especial, à Prof^a Miriam Hidalgo, ao Prof^o Mario Taba Jr, ao Prof^o Danilo Maeda Reino, Prof^o Guilherme Oliveira, Prof^a Camilla Moura, Prof^a Paula Dechichi e Prof^o Gustavo Rabelo, Prof^o Pedro Limirio, tenho enorme gratidão a todos.

À minha amiga Nayara Teixeira, por sua amizade rara e especial, um dos melhores presentes que a UFU me deu. Uma pessoa que posso chamar de irmã, pelos laços fortes e resistentes que criamos e mantemos independente de

tudo. Os meus dias se tornaram mais alegres depois que a conheci. Meu agradecimento enorme a ela, por tudo que já me ajudou, pelos momentos juntas no trabalho e na vida, por me ensinar que a vida pode ser muito mais leve do que imaginamos e que amizades de infância podem ser feitas mesmo perto dos 30. Tenho imenso respeito pela profissional que ela é, mas minha admiração pela sua pessoa é ainda maior.

Ao meu amigo João Lucas Carvalho, por tantos momentos de discussão que sempre foram de grande aprendizado pra mim. Por toda ajuda, seja nas cirurgias dos animais, nas conversas sobre os projetos ou periodontia, ou num desabafo acolhedor. Homem honesto, com caráter e inteligência, minha admiração pela sua pessoa é enorme. Sua amizade foi essencial para mim neste período de doutorado, e sei que será para a vida.

À minha amiga Juliana Borges, que sempre me ajudou, desde o início do doutorado, quando eu não conhecia nada do laboratório e ela era aluna de iniciação científica. Por tantos momentos bons, risadas e conversas. Pessoa que admiro muito pela determinação, e por ser tão batalhadora. Tenho orgulho do seu crescimento profissional e da amizade que construímos.

Ao meu amigo Luis Gustavo, que também foi pessoa fundamental nesse período. Por me ensinar a ter mais paciência e sabedoria e a valorizar as pequenas coisas da vida. Pelos conselhos que somente ele tem. Pelos momentos tão felizes que compartilhamos juntos, seja em Uberlândia ou em Maringá. Que a pandemia permita nosso reencontro em breve.

Às amigas que também foram fruto da pós-graduação, em especial Carla Oliveira, Felipe Torres, Gabriela Leite, Angela Baptista e Lilian Oliveira. Aos colegas que tive a oportunidade de co-orientar durante o doutorado, Cláudia, Lucas, Clara, Guilherme, Nuryê, Tássio e Rômulo, agradeço pela paciência e pela oportunidade de aprendermos juntos.

Aos funcionários da FOUFU, em especial, Brenda, Lais, Graça, Eliete, John e Bruno.

À CAPES, ao CNPq e à FAPEMIG pela bolsa de doutorado e pelo apoio financeiro concedido para que as pesquisas dessa tese de doutorado pudessem ser desenvolvidas.

EPÍGRAFE

*“Nothing in life is to be feared, it is only to be understood.
Now is the time to understand more, so that we may fear less.”*

Marie Curie

SUMÁRIO

Resumo		10
Palavras-chave		10
Abstract		11
Keywords		11
1. Introdução e Referencial Teórico		12
2. Proposição		21
3. Capítulos		22
3.1 Capítulo 1	Artigo 1: Use of Micro-Computed Tomography for Bone Evaluation in Dentistry.	22
3.2 Capítulo 2	Artigo 2: Effect of microCT acquisition parameters and operator experience on the outcome of bone repair evaluation	35
3.3 Capítulo 3	Artigo 3: Is there any effect of data binning and averaging for microCT image acquisition on morphometrics outcome of the bone repair?	51
3.4 Capítulo 4	Artigo 4: Effect of ionizing radiation and LLLT (low-level laser therapy) on grafted and non-grafted lesions – an experimental study	67
4. Conclusões		98
5. Referências		100
6. Anexos		109

RESUMO

A utilização da microtomografia computadorizada (microCT) tem crescido enormemente. No entanto, questões relacionadas a sua aplicação e a definições de parâmetros, ainda carecem de investigações. O primeiro objetivo foi realizar uma revisão da literatura sobre o uso da microCT na Odontologia para o estudo do tecido ósseo e as etapas envolvidas na metodologia. A revisão de literatura demonstrou que para cada tipo de análise devem ser consideradas as características da amostra e os parâmetros a serem avaliados para que as etapas de aquisição, reconstrução e processamento da imagem sejam realizadas de forma ideal. O segundo objetivo foi investigar a influência de determinadas variáveis na análise microtomográfica do reparo ósseo, como: o tamanho do voxel e a espessura do filtro utilizado na aquisição de imagem, e a experiência dos examinadores no processamento dos dados. O objetivo 3 foi determinar se o binning da imagem e o número médio das projeções (*frame averaging*) obtidas durante a aquisição na microCT afetam os resultados morfométricos do reparo do tecido ósseo. Os objetivos 2 e 3 demonstraram que o tamanho do voxel e o binning da imagem afetam a análise dos dados, demonstrado pelas diferenças observadas nos parâmetros Tb.Th e BV/TV. Por último, no objetivo 4, a aplicação da microCT, em associação a outras metodologias, foi utilizada para avaliar o efeito da radioterapia e da laserterapia de baixa intensidade (LLLT) no reparo ósseo de defeitos enxertados com osso bovino mineralizado deproteínizado (DBBM) e não enxertados (coágulo). Pode-se concluir no objetivo 4, por meio da análise microtomográfica e histomorfométrica, que a quantidade de tecido ósseo neoformado observada foi menor nos grupos submetidos à radioterapia, sendo que não foi observada diferença nos resultados pela aplicação da LLLT. A incorporação das partículas do enxerto com o osso neoformado foi preservada demonstrando que a osteocondutividade do biomaterial foi mantida mesmo após a radioterapia.

PALAVRAS-CHAVE: Microtomografia por Raio-X; Processamento de Imagem Assistida por Computador; Compressão de Dados; Osso; Enxerto de Osso Alveolar; Osso Esponjoso; Lesões por radiação

ABSTRACT

The use of microcomputed tomography (microCT) has largely increased. Issues related to its application and parameter definitions still need to be investigated. The objective 1 of this work was to conduct a literature review on the use of microCT in Dentistry for bone tissue investigations and the steps involved in the methodology. The literature review indicated that the characteristics of the sample and the parameters to be evaluated should be considered so that the process of image acquisition, reconstruction and processing are properly carried out. The second objective was to investigate the influence of variables in the microtomographic analysis of bone repair, such as: voxel size and filter thickness used in image acquisition, and the experience of examiners in data analysis. Objective 3 was to determine whether image binning and frame averaging during microCT acquisition affect the morphometric results of bone tissue repair. Objectives 2 and 3 demonstrated that voxel size and image binning affect data analysis, demonstrated by the differences observed in the Tb.Th and BV/TV parameters. Finally, in objective 4, the application of microCT, in association with other methodologies, was used to assess the effect of radiotherapy and low-intensity laser therapy (LLLT) on bone repair of defects grafted with deproteinized mineralized bovine bone (DBBM) and defects filled by clot. It could be concluded, that the amount of neoformed bone tissue observed was smaller in the groups submitted to radiotherapy, and no difference was observed in the results in LLLT groups. The incorporation of graft particles with the newly formed bone was preserved, demonstrating that the osteoconductivity of the biomaterial was maintained even after radiotherapy.

Keywords: X-Ray Microtomography; Computer Assisted Image Processing; Data compression; Bone; Alveolar Bone Graft; Cancellous bone; Radiation injuries

1. INTRODUÇÃO E REFERENCIAL TEÓRICO

A microtomografia computadorizada (microCT) é uma metodologia de análise que permite a visualização da morfologia interna e externa de amostras em escala micrométrica (até 1 μm), fornecendo informações sobre geometria 3D (Kuhl *et al.*, 2010) em tempo de resposta relativamente curto com um alto rendimento (Chavez *et al.*, 2021). As informações obtidas por meio das análises microtomográficas revolucionaram o campo de pesquisa que envolve o estudo do tecido ósseo por permitir a visualização da microarquitetura de forma não destrutiva (Bouxsein *et al.*, 2010).

A reconstrução de estruturas *in vivo* e *ex vivo* com elevada resolução espacial permite que alta correlação entre análises de microTC e histomorfometria bidimensional convencional (2D) seja obtida, como demonstrado por estudos prévios (Müller *et al.*, 1998; Anavi *et al.*, 2011). Esta resolução permite análise tridimensional altamente precisa do volume ósseo, da rede trabecular (número trabecular, espessura trabecular, separação trabecular, padrão trabecular) e das corticais ósseas (Kalpakcioglu *et al.*, 2008; Guda *et al.*, 2014). Embora mais estudos sejam necessários para o aprimoramento do método, a evolução dos aparelhos microtomográficos pode possibilitar o diagnóstico e/ou acompanhamento de patologias ósseas por meio da análise de biópsias de pacientes com suspeita ou diagnóstico de doenças ósseas metabólicas (Hutchinson *et al.*, 2017). A microCT não fornece informações sobre as atividades celulares, mas diversas vantagens podem ser citadas, como análise da estrutura interna sem destruição da amostra, reconstrução tridimensional da amostra e possibilidade de posterior processamento histológico utilizando a mesma amostra (de Lange *et al.*, 2014).

A utilização de imagens obtidas por meio da microCT para análise do processo de reparo ósseo em estudos utilizando modelo animal tem crescido enormemente. Existem diversos sistemas disponíveis comercialmente que diferem em determinadas especificações, mas apresentam de forma semelhante os principais constituintes de um microtomógrafo, que são: tubo de raio-x com foco de dimensão micrométrica e campo de emissão cônico, a mesa com movimento de precisão rotacional e translacional, onde é fixado o objeto a ser

analisado e detector de radiação. Dentro disso, determinadas variáveis associadas a obtenção das imagens, processamento e análise dos dados podem afetar os resultados morfológicos (Christiansen, 2016). Dessa forma, o entendimento destas etapas é necessário para correta aplicação e interpretação dos dados.

1.1. Microtomografia computadorizada: aquisição, reconstrução e processamento da imagem

O funcionamento da microCT é similar ao da tomografia computadorizada (TC), que envolve uma fonte de radiação X em forma de feixe cônico com energia polienergética e detectores de radiação acoplados ao sistema computacional de aquisição e processamento da imagem adquirida (Versiani *et al.*, 2018). O princípio básico para obtenção de imagem nesta ferramenta consiste na emissão do feixe de raios X e sua atenuação ao atravessar a amostra (Boerckel *et al.*, 2014). A atenuação da radiação X depende da radiodensidade e do número atômico da amostra, conseqüentemente diferentes atenuações resultam em distintos tons na imagem captada pelo detector. Desta forma, o cálculo da atenuação é realizado pela comparação da intensidade da radiação proveniente da fonte com a intensidade da radiação captada pelo detector após passar pela amostra (Clark & Badea, 2014). No entanto, devido à heterogeneidade na densidade da amostra e da energia do feixe emitido pela fonte (fonte polienergética), o coeficiente de atenuação depende da intensidade de energia e das diferentes composições estruturais da amostra avaliada (Schulze *et al.*, 2011) Neste contexto, a formação de ruídos e artefatos na imagem obtida pode ocorrer devido à diferença entre o coeficiente de atenuação do material e a atenuação real mostrada pelo receptor (Pauwels *et al.*, 2012; Versiani *et al.*, 2018). O detector nos sistemas microtomográficos são cintiladores do tipo *flat panel* que emitem luminescência quando há incidência de radiação ionizante. Por serem acoplados a um sensor de luz (carga acoplada), a intensidade da radiação que incide no detector é captada e emitida por elétrons para geração de um sinal elétrico. Este sinal é convertido em informação digital (pixels) (Boerckel *et al.*, 2014). Este sistema tubo-detector

geralmente é fixo, e a amostra rotaciona em incrementos em torno do próprio eixo. No escaneamento de amostras *in vivo*, o posicionador de amostras é fixo e o sistema tubo-detector se movimenta circulamente em torno da amostra. No entanto, maior estabilidade e maiores resoluções são obtidas em equipamentos de bancada (*ex vivo*) (Bouxsein *et al.*, 2010).

Com o intuito de diminuir o artefato causado pela diferença de atenuação do raio X, filtros (colimadores) são utilizados para reduzir a intensidade dos fótons de baixa energia e minimizar as diferenças no comprimento de onda do feixe emitido (Schulze *et al.*, 2011). A colimação da radiação emitida diminui o espalhamento do feixe, reduzindo o artefato denominado *beam-hardening*, ou endurecimento do feixe (Jovanović *et al.*, 2013). Quando a amostra escaneada apresenta elevado número atômico e o feixe de baixa energia não é filtrado, este é facilmente atenuado ao atingir a amostra fazendo com que a energia média dos fótons restantes aumente, com maior capacidade de atravessar o objeto. Isso irá levar à formação de imagens que não correspondem à estrutura real da amostra escaneada, pois as bordas da amostra aparecem mais claras e o centro da imagem, mais escuro (Bouxsein *et al.*, 2010). Seguindo o mesmo raciocínio, amostras que apresentam elevada densidade, como implantes e outras estruturas metálicas, podem levar a maior atenuação do feixe que são representadas na imagem por linhas finas que prejudicam a qualidade da imagem de forma considerável (Schulze *et al.*, 2010). O escaneamento de amostras muito densas pode ser realizado com a rotação total (360°). Além disso, aumentar a tensão do feixe também auxilia na diminuição deste artefato (Kamburoglu *et al.*, 2013).

O detector possui sensibilidade variável, o que também pode resultar na formação de ruídos. A calibração do detector (*flat field correction*) deve ser realizada para minimizar essa diferença na sensibilidade. A falha na detecção dos feixes atenuados devido à ausência de sensibilidade pelo detector, pode gerar “pixel morto” (*dead pixel*). Devido à rotação do sistema tubo-detector, ou da amostra, essa falha na detecção irá resultar em artefatos em forma de anel (*ring artifacts*) (Anas *et al.*, 2011). O grau de rotação (*rotation step*) pode ser determinado pelo operador e depende das especificações do equipamento

utilizado (Cengiz *et al.*, 2017). A cada movimentação, seja da amostra ou do sistema fonte-detector, a projeção é obtida. É possível estabelecer o número de projeções obtidas a cada movimento de rotação e o tempo para aquisição de cada projeção pelo sistema computacional do equipamento. Dessa forma, a média das projeções obtidas é calculada instantaneamente pelo algoritmo do sistema computacional. A princípio, quanto maior o número de projeções, menor a quantidade de ruído, porém, o tempo de escaneamento é aumentado (Friedrichsdorf *et al.*, 2019). Desta forma, deve-se levar em consideração se a diminuição de ruído irá efetivamente melhorar a qualidade da imagem para compensar o tempo de escaneamento maior. Outra ferramenta do sistema computacional dos microtomógrafos é o *Binning* da aquisição. Este parâmetro permite a combinação de pixels vizinhos para formar um pixel único maior. O pixel é o menor elemento que constitui uma imagem 2D. A imagem digital é processada por meio de dígitos binários (bits), então, uma imagem de 8 bits permite que o pixel apresente 256 (2^8) tons de cinza. Desta forma, ao unir pixels vizinhos pelo uso do Binning, possíveis ruídos da imagem podem ser reduzidos. Por outro lado, pode ocorrer diminuição da resolução da imagem por reduzir o nível de detalhamento (McDougald *et al.*, 2017).

Após a aquisição das imagens, a reconstrução 3D é geralmente realizada usando-se o algoritmo Feldkamp-David-Kress (FDK). Então, o modelo de matriz bidimensional é substituído pelo modelo de matriz volumétrica tendo o voxel como menor unidade de medida. Na etapa de pré-processamento da imagem, ferramentas de diminuição de ruído e artefatos podem ser aplicadas. No entanto, a diminuição da qualidade da imagem pode ocorrer neste processo (Cho *et al.*, 2007). O enfoque dado para os métodos que têm como objetivo melhorar a qualidade da imagem, é decorrente da necessidade de diminuir os possíveis vieses da análise e para aplicação de métodos automatizados de mensuração.

O processo de binarização da imagem obtida é necessário para que seja possível a realização de cálculos numéricos de informações advindas dessa imagem, ou seja, na determinação do que é considerado osso ou não, sendo este processo de segmentação realizado após a escolha do *threshold*. Esta

etapa da análise pode apresentar grande influência nos resultados da morfologia óssea (Bouxsein *et al.*, 2010). A maioria dos estudos em animais utiliza *threshold* global. Este pode ser obtido pela segmentação visual por meio da determinação do valor obtido pela comparação da binarização com a imagem original, ou pelo método Otsu que é calculado de forma automática pelos softwares do sistema pela análise do histograma (Queiroz *et al.*, 2017). Métodos de *threshold* locais utilizam algoritmos que determinam um valor de limiarização para cada voxel, baseado nos valores de limites locais dos voxels vizinhos em vez de um único valor de limite global (Waarsing *et al.*, 2004). No entanto, o método de escolha do *threshold* não é padronizado entre os grupos de pesquisa. De acordo com o *guideline* de Bouxsein e colaboradores (2010), independentemente do método de binarização utilizado, recomenda-se comparar visualmente as escalas de cinzas para confirmar se a segmentação determinada representa realmente a estrutura do osso. O processo de binarização da estrutura óssea, torna-se ainda mais difícil em regiões de processo de reparo, uma vez que as trabéculas ósseas neoformadas apresentam mais heterogeneidade em relação a sua densidade. Dessa forma, em estruturas de dimensões muito reduzidas, como trabéculas de ratos, o tamanho do voxel poderá influenciar significativamente no processo de binarização, e conseqüentemente, nos resultados morfológicos obtidos (Müller *et al.*, 1996).

1.2. Processo de reparo ósseo

A qualidade do tecido ósseo depende de suas propriedades estruturais, como geometria, macro e microarquitetura e das propriedades do tecido, como o módulo de elasticidade, densidade mineral, qualidade da matriz óssea e comportamento celular (Farlay & Boivin., 2012). Para avaliar o comportamento do tecido ósseo sob várias condições sistêmicas e locais, defeitos ósseos criados cirurgicamente em modelos animais são usados para fornecer melhor compreensão do processo de reparo e procedimentos regenerativos (Schindeler *et al.*, 2018).

O osso em condições fisiológicas passa por constante remodelação, onde uma estrutura hierárquica complexa é responsável pela homeostase

mineral, equilíbrio ácido-base, reserva de tecido hematopoiético, citocinas e fatores de crescimento (Mackiewicz *et al.*, 2011). O trauma neste tecido desencadeia eventos que objetivam sua regeneração. O processo de reparo ósseo pode ocorrer diretamente por meio de ossificação intramembranosa, indiretamente por ossificação endocondral ou pela combinação de ambas, como em situações de fraturas ou distrações osteogênicas (Borrelli *et al.*, 2011).

O reparo ósseo foi bem documentado em estudos histológicos em ossos longos de animais após lesão tecidual (Schindeler *et al.*, 2018). A formação do coágulo sanguíneo dá início ao processo de reparo ósseo em três fases: inflamatória, fibroblástica e remodeladora. O estágio inflamatório apresenta fenômenos vasculares como a vasodilatação e aumento da permeabilidade capilar, que permite maior migração leucocitária. Com isso, ocorre a cascata de eventos celulares que resultam na formação da rede de fibrina devido à coagulação sanguínea. Nesse ambiente, há intensa proliferação celular proveniente da cavidade medular e do periósteo. Ocorre a diferenciação das células osteoprogenitoras que dão origem à síntese de osteóide sobre o tecido conjuntivo. A mineralização ocorre progressivamente para formação do tecido ósseo primário (*woven bone*). Nesta etapa, numerosas trabéculas de osso imaturo se formam e substituem a maior parte do tecido de granulação precoce. Podem ser observadas no defeito trabéculas ósseas e espaços fibrovasculares. A borda cortical adjacente ao defeito sofre reabsorção e os vasos sanguíneos dos canais haversianos unem-se por anastomoses aos vasos do defeito. Um novo osso passa a ser depositado ao redor deste vaso formando o novo sistema haversiano composto parcialmente de osso cortical pre-existente e do novo osso do defeito. O osso imaturo incorpora-se ao osso cortical e sofre remodelação até ser completamente substituído por osso lamelar (Mueller *et al.*, 1991; Schilling *et al.* 1998).

1.3. Efeito da radiação ionizante no processo de reparo

O processo de reparo pode sofrer influências de fatores intrínsecos e extrínsecos (Borrelli *et al.*, 2011). A irradiação do tecido ósseo altera a atividade metabólica celular levando a diversas alterações teciduais. Estudos que utilizam

biópsias humanas fornecem informações importantes sobre os mecanismos biológicos da radioterapia no osso (Brown *et al.*, 2008). No entanto, estudos pré-clínicos permitem isolar diversos fatores a serem investigados, além de permitir análises que não são possíveis em ensaios clínicos (Higham & Faithfull., 2015). Dessa forma, a associação de metodologias como ensaios mecânicos (Donnelly.,2011; Soares *et al.*, 2020), microtomografia computadorizada e histomorfometria contribuem enormemente para o avanço do conhecimento dos efeitos da irradiação (Dalle Carbonare *et al.*, 2005; Koontz *et al.*; 2017; Soares *et al.*, 2019).

Alterações estruturais e biológicas no tecido ósseo decorrente da radioterapia, como apoptose celular, reabsorção trabecular, alterações corticais, maior fragilidade óssea, têm sido demonstradas em estudos com roedores (Szymczyk *et al.*, 2004; Wong *et al.*, 2008; Rabelo *et al.*, 2010; Limirio *et al.*, 2019; Green & Rubin, 2014; Mendes *et al.*, 2020; Borges *et al.*, 2021). Ocorre redução na proliferação e diferenciação de osteoblastos com modificação da morfologia óssea devido à hipocelularidade e à redução na vascularização (Fenner *et al.*, 2010). As alterações vasculares, que se iniciam com o aumento da permeabilidade do endotélio, resultam em fibrose, estreitamento luminal e hipóxia (Baselet *et al.*, 2018). As alterações a nível celular e vascular provocadas por altas doses de radiação no tecido ósseo resultam na formação de osso desorganizado e rico em tecido fibrótico. Essas alterações podem comprometer consideravelmente o reparo ósseo do tecido irradiado fibrótico (Barth *et al.*, 2011; Lucatto *et al.*, 2011; Bartlow *et al.*, 2018; Mendes *et al.*, 2020).

O uso de biomateriais como substitutos ósseos tem sido utilizado para o tratamento de defeitos ósseos devido as suas propriedades osteocondutoras (Iocca *et al.*, 2017). A osteocondutividade é uma propriedade do biomaterial de servir como arcabouço para que as células osteoprogenitoras do hospedeiro possam se proliferar. O uso de osso bovino (xenógeno) ou de materiais aloplásticos tem sido proposto, podendo ser usados isoladamente ou associados aos enxertos autógenos (Mendoza-Azpur *et al.*, 2019). A utilização de enxerto ósseo particulado xenógeno é considerada tratamento previsível. No tecido ósseo saudável, a utilização de biomateriais particulados é mais eficiente para

diminuir alterações dimensionais quando comparado ao alvéolo preenchido somente por coágulo após exodontia (Iocca *et al.*, 2017).

Neste contexto, o uso de biomateriais representa uma possível abordagem de tratamento a ser realizado antes de iniciar as sessões de radioterapia, seja para preservação alveolar em sítios pós-extração dentária, visando futura instalação de implantes, seja para preenchimento de *gaps* em implantes imediatos instalados no período pré radioterapia. Implantes instalados prévios ao tratamento radioterápico têm demonstrado melhores resultados quando comparado aqueles instalados no período pós radioterapia (Alberga *et al.*, 2021). Essa abordagem diminui o risco de desenvolvimento de osteorradionecrose (ORN) pela realização da intervenção cirúrgica antes da radioterapia, e por permitir que a osseointegração se inicie no tecido que ainda não sofreu os efeitos da radiação (Arnold *et al.*, 1998; Schoen *et al.*, 2004). Apesar das evidências favoráveis ao uso de substitutos ósseos particulados nas condições do tecido não irradiado, no melhor conhecimento dos autores desse trabalho, até o presente momento não existem estudos experimentais que avaliem o reparo ósseo de lesões que foram enxertadas previamente à radioterapia.

Abordagens terapêuticas e preventivas para minimizar os efeitos deletérios da radiação no tecido ósseo precisam ser investigadas. A busca por protocolos a serem aplicados não apenas para o tratamento de sequelas decorrentes da radiação, mas também para prevenir possíveis complicações, é extremamente necessária. A tentativa de acelerar o processo de reparo ósseo de lesões que podem existir no período muito próximo do início das sessões de radioterapia, como em alvéolos pós extração, é de grande relevância. Neste contexto, as aplicações clínicas da laserterapia têm sido amplamente estudadas. Os lasers de baixa potência emitem luz no espectro não ionizante, visível, próximo do infravermelho, que atuam em fotoceptores das células (parede celular ou organelas citoplasmáticas) (Gupta *et al.*, 2014). Ocorre uma interação fotoquímica capaz de induzir aumento do metabolismo celular e consequentemente diferentes efeitos biológicos gerais como o analgésico, anti-inflamatório e bioestimulativo (Garcia *et al.*, 2010).

A Terapia com Laser de Baixa Intensidade (LLLT) mostra-se bastante eficaz no reparo do tecido ósseo (de Oliveira *et al.*, 2018). O efeito biológico da LLLT é denominado fotobiomodulação, o qual induz alteração celular de forma não-destrutiva (Gupta *et al.*, 2014). Especificamente no tecido ósseo, ocorre aumento no número de osteócitos e pode influenciar positivamente no seu reparo (Dörtbudak *et al.*, 2002). Os efeitos positivos do LLLT (830nm) na cicatrização têm sido relatados em relação à maior quantidade de osso neoformado e aumento da vascularização na região de fratura (Fávaro-Pípi *et al.*, 2010). A LLLT também pode estimular o reparo ósseo em defeitos preenchidos com biomateriais, como osso inorgânico bovino e hidroxiapatita (Obradović *et al.*, 2009), tornando válida a investigação desta terapia no processo de reparo de lesões enxertadas que serão submetidas aos efeitos deletérios da radiação ionizante.

Em suma, com a tecnologia agregada à Odontologia, principalmente no campo de aquisição e processamento de imagens, o entendimento da biologia óssea e os fatores que afetam seu metabolismo ganhou novas proporções (Schneider *et al.*, 2012). Apesar da literatura abordar o uso da microCT (Buie *et al.*, 2007; Bouxsein *et al.*, 2010), algumas questões relacionadas a sua aplicação na Odontologia e, também, a definições de parâmetros, ainda carecem de investigações. É necessário o melhor entendimento dos efeitos destes parâmetros, relacionados à aquisição da imagem, processamento e análise, nos resultados morfométricos obtidos. Aplica-se neste contexto, o uso da microCT e outras metodologias para a avaliação de terapias que possam auxiliar no processo de reparo submetido à radioterapia (RTX) por meio da análise de seus efeitos nas características morfométricas do tecido ósseo.

2. PROPOSIÇÃO

O objetivo desta tese de doutorado é fornecer informações relevantes à literatura referentes ao uso da microCT para análise do reparo ósseo por meio da avaliação de diferentes parâmetros de aquisição e processamento da imagem. Além disso, a aplicação da microCT, em associação a outras metodologias, foi utilizada para avaliar o efeito da radioterapia e do LLLT no reparo ósseo de defeitos enxertados (DBBM) e não enxertados. Desta forma, este trabalho foi dividido em quatro objetivos:

- Objetivo 1: realizar uma revisão da literatura sobre o uso da (microCT) na Odontologia para análise do reparo ósseo;

- Objetivo 2: investigar a influência do tamanho do voxel e da espessura do filtro utilizado na aquisição de imagem, e a experiência dos examinadores no processamento dos dados na análise microtomográfica do reparo ósseo;

- O objetivo 3: determinar se o binning da imagem e o número médio das projeções (*frame averaging*) obtidas durante a aquisição na microCT afetam os resultados morfométricos do reparo do tecido ósseo;

- Objetivo 4: aplicação da microCT, em associação a outras metodologias para avaliar o efeito da radioterapia e da laserterapia de baixa intensidade (LLLT) no reparo ósseo de defeitos enxertados, com osso bovino mineralizado deproteinizado (DBBM), e não enxertados (coágulo).

3. CAPÍTULOS

3.1. Capítulo 1

Artigo publicado no periódico *Brazilian Dental Journal*

Irie MS, Rabelo GD, Spin-Neto R, Dechichi P, Borges JS, Soares PBF. Use of Micro-Computed Tomography for Bone Evaluation in Dentistry. *Braz Dent J.* 2018 May-Jun;29(3):227-238. doi: 10.1590/0103-6440201801979. PMID: 29972447.



Use of Micro-Computed Tomography for Bone Evaluation in Dentistry

Milena Suemi Irie¹, Gustavo Davi Rabelo¹, Rubens Spin-Neto², Paula Dechichi³, Juliana Simeão Borges¹, Priscilla Barbosa Ferreira Soares¹

¹Department of Periodontology and Implantology, UFU - Universidade Federal de Uberlândia, Uberlândia, MG, Brazil
²Department of Dentistry and Oral Health, Aarhus University, Aarhus, Denmark
³Institute of Biomedical Sciences, UFU - Universidade Federal de Uberlândia, Uberlândia, MG, Brazil

Correspondence: Priscilla Barbosa Ferreira Soares, Av. Pará, 1720, Bloco 4L, Anexo A, 38400-902, Campus Umuarama, Uberlândia, MG, Brasil. Tel: +55-34-3225-8119. e-mail: pbfsoares@yahoo.com.br

Micro computed tomography (μ CT) follows the same principle of computed-tomography used for patients, however providing higher-resolution. Using a non-destructive approach, samples can be scanned, and each section obtained is used to build a volume using tridimensional reconstruction. For bone analysis, it is possible to obtain information about the tissue's microarchitecture and composition. According to the characteristics of the bone sample (e.g. human or animal origin, long or irregular shape, epiphysis or diaphysis region) the pre-scanning parameters must be defined. The resolution (i.e. voxel size) should be chosen taking into account the features that will be evaluated, and the necessity to identify inner structures (e.g. bone channels and osteocyte lacunae). The region of interest should be delimited, and the threshold that defines the bone tissue set in order to proceed with binarization to separate the voxels representing bone from the other structures (channels, resorption areas, and medullary space). Cancellous bone is evaluated by means of the trabeculae characteristics and their connectivity. The cortex is evaluated in relation to the thickness and porosity. Bone mineral density can also be measured, by the amount of hydroxyapatite. Other parameters such as structure-model-index, anisotropy, and fractal dimension can be assessed. In conclusion, intrinsic and extrinsic determinants of bone quality can be assessed by μ CT. In dentistry, this method can be used for evaluating bone loss, alterations in bone metabolism, or the effects of using drugs that impair bone remodeling, and also to assess the success rate of bone repair or surgical procedures.

Key-Words: bone, micro-computed tomography, resolution, segmentation, texture analysis.

Introduction

Micro-computed tomography (μ CT) follows the basic principles of medical computed tomography in which the sample is placed in the path of an x-ray beam forming a projection image on the scintillator or other x-ray-sensitive detector array (1). The sample is rotated and imaged at a large number of angles, and the sequence of projection images is "back-projected" to reconstruct the x-ray absorption at each point within the scanned volume (1,2). The μ CT is currently used to evaluate bone morphometric characteristics as the complimentary alternative of conventional histological analysis (2), when considering a tridimensional volume of the sample over two-dimensional histological sections. Using μ CT allows a more representative analysis in the whole sample extension, being the most advantage compared to histology analysis, although, it should be emphasized that histology remains as the most indicated method to evaluate cells, proteins and composition.

The μ CT as non-destructive method provides 3D information without destroying the sample, allowing its inner reconstruction by radiographic image sections. The same sample can later be prepared for histologic analysis, generating complementary information of the same tissue areas. In addition, using μ CT it is possible to measure bone quality based on other parameters such as mineral properties. Also, microarchitecture analyzed in a

representative bone volume will assess distinct sites, and not just on the few sections provided in histology methods (3).

μ CT and HR-pQCT (high-resolution peripheral quantitative computed tomography system) are nowadays the most useful high-resolution imaging of trabecular and cortical bone ultrastructure (4). The μ CT equipment's are available for in vivo and in vitro imaging for bone analysis. μ CT has been widely used in medicine and dentistry fields to assess the bone quality defined by several structural parameters, making possible to evaluate the repair and regeneration of the bone tissue in animal and human samples (5). A large number of studies have used μ CT in order to identify alterations and changes due to systemic diseases and conditions (e.g. osteoporosis, osteoarthritis, hypercalcemia, diabetes, etc) and also metabolic diseases and their respective treatment (e.g. anti-resorptive treatment, corticoids, etc) (6). High correlations and excellent agreement between conventional histomorphometry and μ CT data have been demonstrated (7).

At the largest length scales, two types of bone structure are evidenced: trabecular and cortical bone. Trabecular or cancellous bone micro-architecture shows a porous network with small filaments inter-woven which results in higher porosity (80%-85%) comparing to cortical area (2-5%) (7,8). Trabecular bone can be 10 times thinner than the

cortical structure. High resolution images are necessary to analyze trabecular portions, particularly in rodent models, which can exhibit 0.2 mm of thickness in healthy mice (9). Cortical bone should be evaluated concerning structure by CT methods, and possible alterations on cortex structure are relevant to bone strength. If the cortex is thick, images of low resolution may be sufficient for analysis, however, if the cortices are thin, measurement of the morphological features could be a challenge (10).

Bone quality involves bone mass, structural properties: geometry, macro and micro-architecture, and tissue properties: modulus of elasticity, mineral density, collagen quality, cell and marrow behavior (11). Mechanical and biological behavior of bone tissue play important role in clinical practice, especially for evaluating distinct systemic and local conditions (diseases, therapies or lesions). This property can also contribute to better understanding of bone regenerative procedures, such as: alveolar ridge and maxillary sinus augmentation procedures, bone repair and fracture healing (12), surgical reconstruction and rehabilitation, and implant osseointegration (13). μ CT has shown to be the most indicated technique for assessment of the bone mass and morphology in animal models (3). In addition, particularly in dentistry, this method is extremely useful to the study of human jaw bone tissue associated with different conditions and diseases, also to assess the changes when the bone is evolved by lesions or submitted to surgical procedures (14–16).

Before starting a μ CT analysis, it is important to previously define all the crucial parameters to answer the study question. Variables in the analysis should be considered, including: type of the sample (i.e. bone site, size, thickness); sample preparation (not allowing dryness, excessive heating, mimicking the surrounding tissues as muscles); the next step of the assessment (histological processing, mechanical tests); the necessary resolution (different equipment, in vivo or in vitro condition, influence on binarization process), and at last the parameters to be evaluated (e.g. considering separated analysis of cortical and cancellous bone, bone repair, etc). Therefore, the aim of the present study was to review and discuss the equipment, sample preparation, scanning parameters, and analysis methods applied to bone tissue evaluation in dentistry using μ CT-based methodology.

Review of Literature

Before Image Acquisition

Sample Preparation

For bone tissue analyses, the sample preparation and the stabilization of the sample holder inside the μ CT unit should be standardized. Some systems have an open platform to fit the sample, so it is important to make sure

that the entire sample fit this space and remain inside the field of view during the whole scanning (in 180° or 360° rotation). Otherwise, the image has to be reconstructed locally reducing image quality (17). Sample preparation will vary according to the type of specimen, however mostly samples are excised, and then the soft tissue may be removed. Moreover, specimens can be aligned with the vertical or horizontal axis of the unit, in this case the vertical positioning is more adequate. Horizontal placement is compromised with a slightly reduced image quality due to beam-hardening along and perpendicular to the long bone. No relative displacement is desirable during the measurement; if the sample changes the initial positioning during the scan, motion artifacts may appear (3).

The μ CT scanning of bone tissue can be done by maintaining the sample in liquid or air environment. However, if quantitative measurements of tissue mineral density are required, is recommended to scan in a liquid medium. Changes in medullary density can happen if the bone is dehydrated. Scans can take 10 to 11 hours, to avoid sample dehydration and shrinkage during scanning is recommended to scan samples inside liquid-filled tubes. The operator needs to assure all specimens are scanned in the same type and volume of the medium. Saline, ethanol, and neutral buffered formalin medium have been used for bone storage medium during μ CT scanning (18). If the specimens are stored in ethanol, they should be rehydrated in saline solution (0.9%) by overnight immersion or over a weekend before scanning. Bone samples also can be harvested without chemical fixation and store frozen at -20°C immersed in saline inside a tube or wrapped in saline-soaked gauze (19). The bone samples can also be fixed and stored in the phosphate-buffered saline (PBS). However, attention should be given in cases of long term storage in PBS, because partial change to acetic acid may occur, leading to bone demineralization (20). To avoid air bubbles formation, all these liquids should be inserted using a syringe (3). To maintain normal hydration of bone during scanning, the specimens can be wrapped in paper tissue, inserted into a tube and then, moister the paper with water or saline solution to avoid dehydration during scanning (20). If the sample will follow for histology after μ CT scan, first it should be fixed (usually in paraformaldehyde), and during the scan it should be kept in a saline or buffered solution. In cases of biomechanical tests and μ CT performed in the same sample, for example, the sample should not be fixed and maintained frozen until scan.

Scanning and Quantitative Assessment

Image Acquisition and Image Resolution

Before scan, some parameters should be defined in order to have better quality in the images that will be

reconstructed. Besides resolution and pixel size, the operator should define the use of filters. Aluminum or copper filters are used in order to reduce beam-hardening artifacts (3). By experience, the most used filter for bone evaluation is the aluminum with 0.5 mm.

Concerning resolution, the pixel size chosen will define the voxel size in the following step, *i.e.* the tridimensional reconstruction. Voxel unit from μCT is denominated as isotropic voxels because it has all three equal dimensions. The resolution chosen for a μCT volume has strong influence on the results of cortical and trabecular bone analysis if the voxel size is not compatible with the structures size (21). This influence is not relevant when thick trabecula is analyzed, such as human sample (100 to 200 mm). However, results from small structures (20 to 60 mm), like rodent's trabeculae, can be affected by voxel size resolution (7,22). Three-dimensional reconstructions of serial sections led to a new understanding of the branching patterns and remodeling processes of the cortex (2). The relation between voxel size and scanning time should also be considered. Scanning small and highly details structures with low resolution (>100 μm) can underestimate bone mineral density and overestimate sample thickness (3). Ideally, the smallest voxel size available should be used in order to obtain the highest amount of detail possible. However, resolution is time dependent, and high-resolution scanning (small voxel size) results on longer acquisition and reconstruction time, and large data sets. If μCT scanning is performed on live animals (*i.e. in vivo*) for long time, the high dose of radiation might become relevant and threaten the animal's health state (23).

When the ratio between voxel size and sample size decreases, in general, the measurement error is minimized. Thus, the ratio should be lower for more accurate μCT performance (3). Using the μCT evaluation based on nominal voxel sizes of 6, 10, 15, 20, and 30 μm there was a strong effect on the results of several commonly reported trabecular bone parameters in mice vertebral body trabecular bone (23). Since mice trabecular dimension is approximately 30 μm, scanning with larger voxel sizes can result on results which are poorly accurate. The trabecular bone structure outcomes are significantly affected by μCT scanning voxel size and by the global segmentation method (*i.e.* thresholding) used to separate bone from non-bone (23). Therefore, it is recommended that high-resolution scans should be used whenever possible to provide the most accurate estimation of trabecular bone microstructure.

Regions of Interest: Cortical and Trabecular Bone

To determine the region of interest (ROI) of a sample it is important to define the interest landmarks, the contoured region of interest, and the size. The starting point should

be known anatomical sites (*i.e.* landmarks), such as the proximal tibial plateau, the metaphyseal growth plate or another appropriate anatomic site in animal samples. For human samples, distinct characteristics should be considered, meaning differences between maxilla and mandible. According with the study question, the region analyzed in animal models should rely on the criteria: a) will cortical and cancellous bone be analyzed?; b) in studies of bone repair, the created lesion will be performed within the epiphysis or the diaphysis?; and for human studies, the criteria should follow similar questions: a) is it important to analyze cortical and cancellous bone separately?; b) should larger samples be segmented in smaller pieces?; c) is there standardization among the samples?; and just after these definitions, together with the criteria about the scanning phase (resolution, scanning time, sample preparation), the region of interest should be defined. The ROI size should be defined as the distance from the start point until the end of the defined region, set by number of sections to be scanned, based on the defined voxel size (3). The area and volume of the bone to be analyzed will depend on the type of study. To analyze trabecular bone in rats or mice, the metaphyseal region of long bones is mostly located a few millimeters adjacent to the metaphyseal growth plate. If the volume of interest is out of this region, more medullar areas are included reducing the mean value for the ratio bone volume/total volume. Thus, relevant differences between study groups can be masked (24). For the cortices, usually is selected diaphysis region, for the measurements of the cortical area, mean cortical thickness and total bone. For bone repair and regenerative procedures, the area should contain the whole lesion, in order to assess the new bone formation (Fig. 1).

3D Reconstruction

A volume image obtained from μCT consists of a stack of cross sections reconstructed according to the axis of rotation of the unit's gantry. The reconstruction software usually generate voxels that are isotropic, and the voxel dimensions are automatically calculated with the same accuracy as the imaging system's calibration (1). The bone-tissue reconstruction allows the identification the specimen section by section. Then it is possible to analyze the whole volume by the delimitation of the region of interest (ROI), including cortical and cancellous bone (Fig. 2). In X-ray microtomography, image information from a voxel with a very small physical size should be detected and the right choice of parameters for noise reduction becomes very important in the reconstruction step.

During reconstruction, the software usually allows to work on histogram, and also, to perform corrections such as: smoothing, ring artifacts reduction and beam-hardening

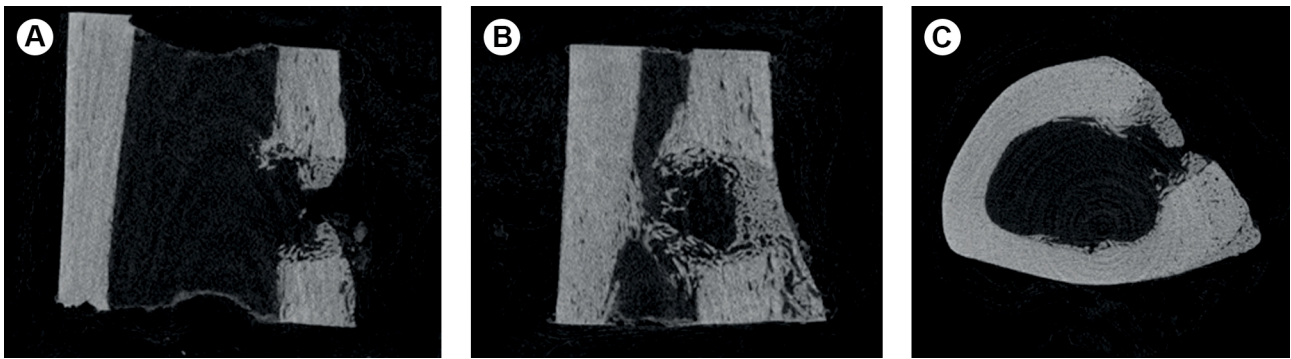
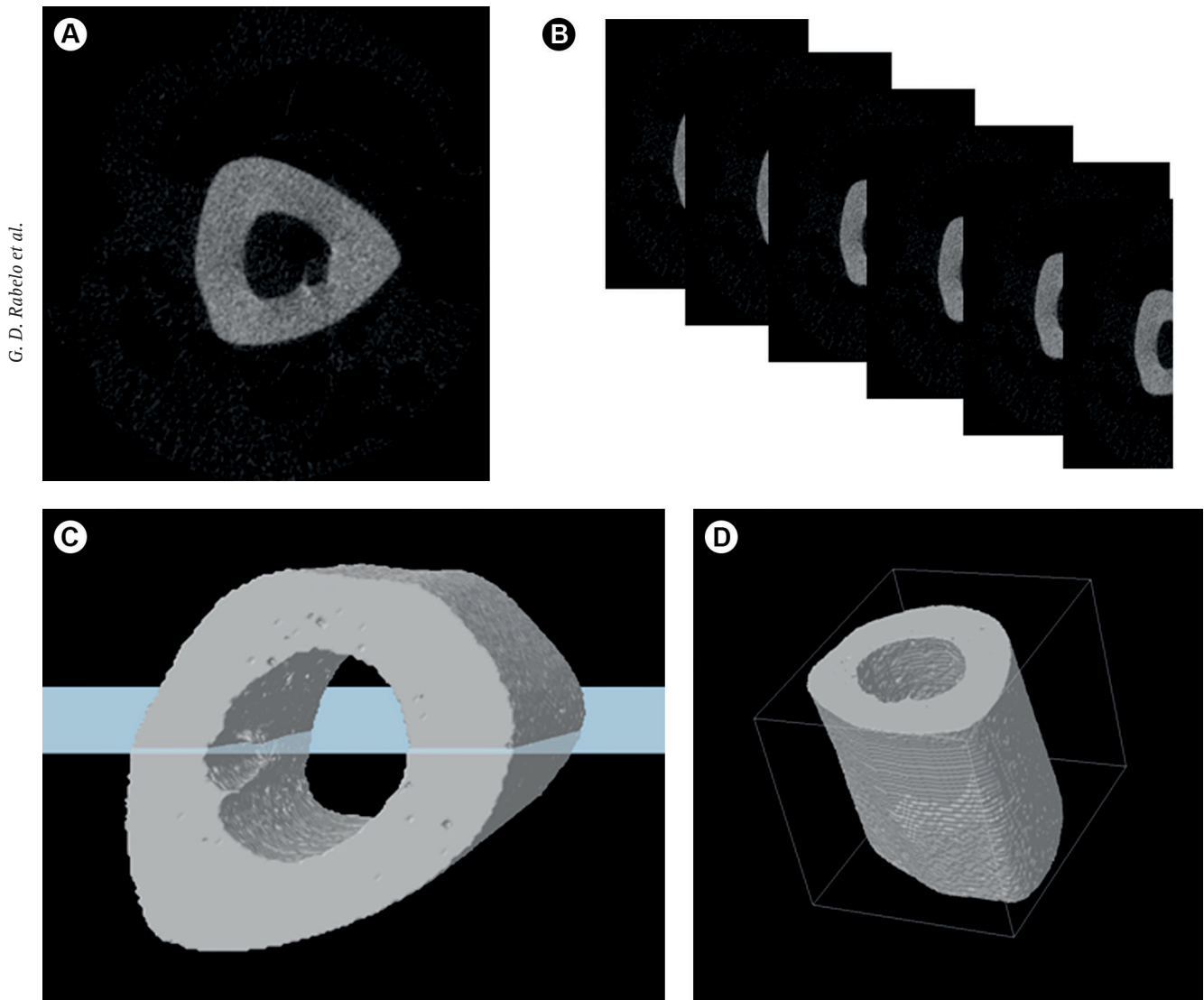


Figure 1. Rat femur with bone repair process evaluated 7 days after euthanization revealing new bone formation in the region of the created lesion using a drill (8 μm pixel size at 90 kV, 111 μA and 720 ms integration time; Rotation step 0.400 and Filter Al 0.5 + Cu 0.038). A: Coronal view. B: Sagittal view. C: Trans axial view.



G. D. Rabelo et al.

Figure 2. Rat tibiae scanned at the diaphysis in order to evaluate the cortices (15 μm pixel size at 90 kV, 111 μA and 1800 ms integration time; Rotation step 0.600 and Filter Al 0.5 + Cu 0.038). A: One single slice in gray-scale image revealing the cortex and the medullary channel in the center. B: Representation of the slices grouped in a seriated organization in order to allow the 3D reconstruction. C: 3D volume of the whole scanned segment of the tibiae (in gray) and the plate (in light blue) that can be used to segment the volume to visualization of the inner structures of the bone. D: Another view of the 3D volume obtained from the serial sections.

correction. The use of this tools enable to a more accurate 3D volume for analysis and noise reduction, however, they could increase the time of the reconstruction step.

Choosing the More Appropriated Parameters: What is the Study Question?

The parameters evaluated should answer the major study questions, so the acquired data will provide information for the major deliverables of the project. The use of μCT evaluation should be able to represent the structural organization (microarchitecture) and the bone composition (mineral density defined by X-ray absorption). Using three-dimensional imaging techniques like μCT, more complete information of bone microarchitecture became available, and it is already known that the complexity of the microarchitecture will have an important influence on the mechanical competence of bone (25). Bone strength analysis relies on the evaluation of intrinsic (mineral and collagen quality, presence of microcracks) and extrinsic determinants (geometry, bone mass and mineral density, macro, and microarchitecture) (11). The μCT method will provide crucial information on some of these determinants. The identification of changes in these determinants will aid to understand the influence of structure and composition on strength, toughness and stiffness of bone.

In human or animal bone, is possible to assess bone quality features by means of μCT with the use of X-rays. It is necessary to keep in mind what are the best parameters in cortical and cancellous bone that could differentiate two different conditions (i.e disease versus control). In addition, it should be possible to characterize different phases and the evolution of the specific situation in the study, such as in the cases of bone repair evaluation, fracture healing or osseointegration of the biomaterial or implant.

Binary Selection: Choosing the Threshold

An image is mathematically represented by a matrix of numbers, which contains a numerical value correspondent to the intensity value or pixel depth. Each image matrix element contains a numerical value that corresponds to the image intensity value or pixel depth (26). In μCT imaging, these intensities are often presented within a 8-bit grayscale, in 256 levels of gray, varying from 0 to 255. When proceeding binary selection, it means the process to convert the X-ray image acquired, and which is present in 256 levels of gray, to only two "colors": one including and the other excluding the evaluation tissue. To perform such step, the definition of a threshold which separates what is and what is not tissue, is rather important. Choosing two thresholds (upper and lower), defining a range of what to be considered as bone, will enable to differentiate the bone from the holes (non-bone material), in order to use the numeral values

obtained from each region to make the measurements. The question is whether the automatic segmentation from bone and non-bone parts within the image could compromise the final evaluation. The use of a global threshold refers to the use an automatic, easy and non-time consuming way to separate and differentiate the bone, however, careful should be taken in attention to this automated process. Problems such as noise, resolution limitations, and beam-hardening will be critical in the segmentation of the original reconstructed grayscale data sets to separate bone from non-bone. Inappropriate segmentation method will reduce the potential power of μCT and may introduce bias in the architectural measurements (27).

There is no consensus on a threshold that could be used for all studies, and extreme care must be taken in the definition of the best threshold (3). For instance, selecting a global threshold in studies where bone mineralization may not be constant (e.g. during bone repair) or when there are extreme ranges of bone volume fraction among groups, and one unique value is not adequate. In dentistry, using human or animal bone, the threshold should be defined taking into account the type, site, and inherent bone characteristics. It is necessary to distinguish the evaluation of cortical and trabecular bone separately. Also, when the region of interest includes bone repair or healing (i.e. the region of a created lesion for bone repair evaluation, the site of osseointegration of the implant or biomaterial, or the tooth extraction area - Fig. 3), should also be delimited and separated from the other parts included in the field of irradiation. The ability to measure cortical and trabecular bone density and architecture separately with high-resolution methods has enabled to better understand the changes that occur with age, diseases, differences between sexes and races, and the effects of drug treatment (28).

Cortical Bone Evaluation

Evaluation of the cortices should assess initially two important parameters: thickness (Ct.Th) and porosity (Ct.Po). The optimum resolution chosen is that one which allows the identification of the bone channels, including even the smaller ones. To assess cortical porosity in humans it should be known that the bone channels vary according to the site, age and systemic condition. In long bones they have a mean diameter of about 60 μm in aged women (29). In animals, for adult rats we found a mean diameter of 7 μm and for rabbits around 15 μm (unpublished data). The threshold should delimitate the bone matrix separated from the holes to make possible to reach the intracortical porosity by means of calculation of all pixels that do not correspond to bone tissue. By porosity, it is also possible to assess the differentiation between the open and closed porosity. When the open porosity is chosen, it will take

into account the open channels on the surfaces included in the ROI. On the other hand, the closed porosity will be related just to the intracortical porosity, by means of that only closed pores (channels) will be considered in the analysis. Besides thickness and porosity, the μ CT software also allows identifying other characteristics, such as: bone surface area (Ct.BS), which in this case is related to all pixels on the contour of all channels within the region of interest. Additionally, other features, like the percent of bone volume, meaning the inverse counting of pixels compared to the porosity are also possible to obtain. It should be emphasized that the majority of the studies had focused on the trabecular bone for the evaluation of bone fragility; however, the cortex is the major dictator on this characteristic (10). Non-vertebral fractures occur predominantly at cortical sites and most of bone loss occurs by intracortical remodeling, that cavitates the

cortex producing porosity, being more important in these cases the assessment of cortex than trabecular bone (10).

Cancellous Bone Evaluation

The trabeculae or "trabecular" bone is the primary anatomical and functional unit of cancellous bone, with high turnover rates compared with the cortical bone. In the prediction of bone strength, measurements of trabecular density and trabecular microstructure should be combined and performed in combination with cortical evaluation. Trabecular bone morphometry depends on the measurement of the bone volume (BV) and also on the characteristics of the trabeculae including: the trabecular number (Tb.N) calculated as the average number of trabeculae per unit length; the trabecular thickness (Tb.Th) as the mean thickness of trabeculae; and the trabecular separation (Tb.Sp) as the mean distance between trabeculae.

G. D. Rabelo et al.

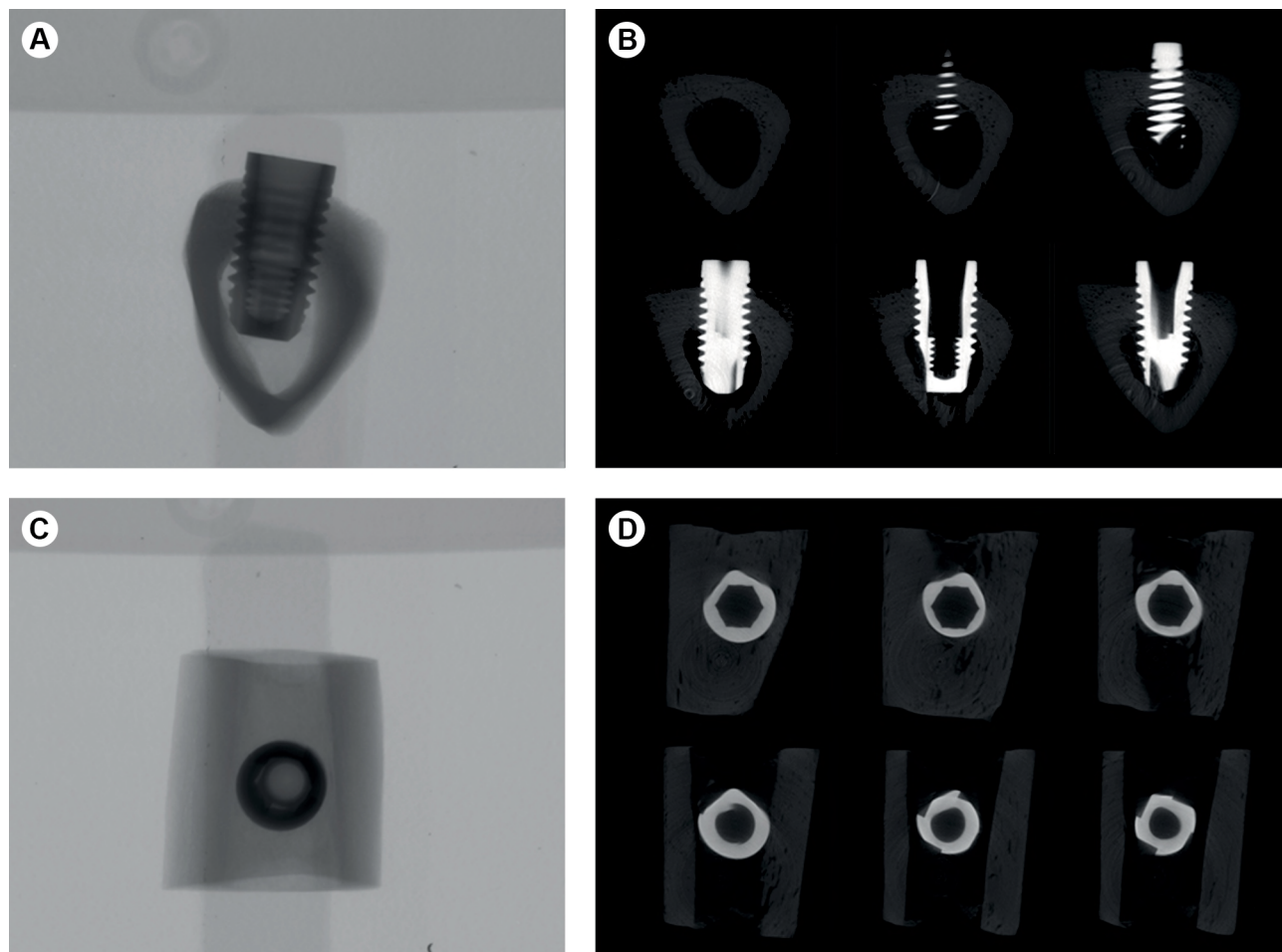


Figure 3. Implant installed in a rabbit tibia (8.5 μ m pixel size at 90 kV, 278 μ A and 1320 ms integration time; rotation step 0.400 and Filter Cu 0.1 mm; Reconstruction: Smoothing=2, Smoothing kernel=0 (Asymmetrical boxcar), Ring Artifact Correction=8 and Beam Hardening Correction (%)=80). A: μ CT original file in a coronal view of the implant inserted in the tibia. B: Random images representing a sequence of the slices going through the implant, starting from the tibia without the implant on the upper left corner and finishing at the end of the implant in the lower right corner. C: μ CT original file in a transaxial view of the implant inserted in the tibia. D: Random images representing a sequence of the slices going through the implant, starting from the superior part of the implant inserted within the cortex on the upper left corner and finishing at the end of the implant in the inferior part, inside the medullary portion in the lower right corner.

By means of algorithms included in the analysis software, it is also possible to measure the connectivity density (Conn.D), as one measurement that gives information on the trabeculae degree of connectivity and the structure model index (SMI). SMI is an indicator of the trabeculae format, being the ones with the value more close to 0 related to the parallel ones, and a value more close to 3 meaning more cylindrical rods shape of the trabeculae (3). In osteoporosis for example, there is a conversion of plates into rods (6). Besides these parameters, others also could be measured as the bone surface density, but the majority of the studies in the literature focused on the ones previous mentioned.

Additional Analysis and "Unthresholded" Methods

Additional measurements using μCT are available through developed algorithms in order to assess architecture parameters and features do not associated with the classical analysis. The spatial organization of the cortical and trabecular bone gives additional information how these tissues are structured and the influence on their mechanical properties. The texture analysis enables to reach improvements in bone microarchitectural evaluation from low resolution images (e.g. radiographs, Dual-energy X-ray absorptiometry - DXA) or add a new mathematical way to measure structure parameters, based on the size, shape and distribution of elements within the tissue. Some parameters of the texture analysis are included in the conventional μCT software's, and others can be acquired using plugins and download free software's, like Image J (NIH). This analysis evaluates local variations in gray levels, the degree of complexity, given by numerical values as how a structure fills up the space; and quantifies the emptiness, by an indicator of the degree of gap distribution over a certain surface (30,31). The most used additional analysis on μCT are the degree of anisotropy, fractal dimension, and lacunarity, disposable in the evaluation software, except for the lacunarity.

Emphasizing anisotropy measurement, the degree of anisotropy gives information on the orientation of trabeculae in space. A preferential orientation of the trabecular plates observed along the direction of the strains exerted on bone is related to high anisotropy (6). Concerning the cortex, cortical structure follows a preferential orientation and hierarchical arrangement, inducing strong anisotropy (32).

The Fractal Dimension (FD) is another parameter that may be extracted by μCT analysis. This parameter indicates how much an object occupies its underlying metric space, meaning that is a measure that characterizes how much an object occupies the space that contains it (31). The fractal geometry analysis has been used for describing

irregular patterns with self-similarity at different scales, for example, it has been used to characterize the microstructure of porous media within the cortical bone (33). Fractal geometry analysis of cancellous bone identifies architectural features not easily recognized by conventional bone histomorphometric (34). A decrease in fractal dimension was already evidenced when there are alterations of trabecular bone, meaning loss of trabecular connectivity and increase in porosity (35). The complexity of trabecular bone microarchitecture, expressed by the mean value of the fractal dimension, was higher in cases of fracture compared with control cases (36).

Another important parameter is the lacunarity, which measures the gap or lacuna distribution, meaning higher the lacunarity, bigger will be the variation of pixels distribution within an image. High lacunarity means that pixels are grouped in a wide variety of sizes of islands, surrounded by a widely variant emptiness, indicating heterogeneity of spatial pattern or texture (31). Lacunarity plots characterize the spatial organization of an image, including the average size of any structural sub-unit(s) within the image, making them potentially useful in representing the trabecular thinning and perforation of vertebral trabecular bone associated with osteoporosis (37). In dentistry, the lacunarity measurements should be employed attempting to understand the heterogeneity of bone channels network in cortical bone and to evaluate the homogeneity in the trabeculae distribution in cancellous bone. Lacunarity decreases with the increase of regularity of gaps distribution (38). This parameter can be measured in both threshold and non-threshold methods, using free download software's. The use of non-threshold images (original acquisition images), without binarization, could overcome some problems like low resolution, once the measurement works with the distribution of gray-level pixels in the image.

Results of μCT Evaluation: Interpretation and Significance

Morphometry and Mineral Density Measurements: Clinical Significance

Morphometry, an important parameter extracted by μCT analysis, is related to the measurement of bone architecture. Data obtained for analysis of the different conditions of bone integrity, reflects on the biomechanics behavior of this connective tissue. Using μCT, the assessment of the spatial organization of bone structure and their mineral composition is possible to identify alterations caused by diseases or physiological adaptation, with important clinical significance.

Data extracted from μCT datasets make possible to explore the bone architecture in its macro and microscale.

When the bone quality is compromised, alterations in trabecular bone are evidenced. Trabecular bone volume, trabecular thickness and trabecular number are significantly decreased in osteoporosis (39) and in osteoarthritis (40). Bone trabeculae decreases in aging due to constant osteoblastic depression, and this usually leads to a progressive conversion of the trabeculae format from plates into rods (6). In relation to cortical bone, cortical thickness and porosity are the parameters that are directly related to bone strength, so being crucial concerning the clinical significance when analyzing the bone in diseases or distinct conditions. Cortical porosity is increased in several diseases, with increased osteoclast resorption activity. Cortical bone porosity is responsive to disease, therapy, and metabolic alterations, with the pore structure intimately related to biomechanical properties, for example, with the pores becoming increasingly interconnected and convoluted as age progresses (2). This cortical bone loss is one of the major responsible for the reduction in strength. The porosity is increased in diseases like diabetes (41), chronic kidney disease (42), osteoporosis (39), rheumatologic diseases and others, which present high risk of fractures. All these conditions have clinical relevance, and studies conducted in human or animal studies should apply techniques that are able to evaluate the bone quality, such as the μ CT.

G. D. Rabelo et al.

Animal Studies: Bone Repair, Modeling, and Remodeling

The majority of studies concerning bone repair are concentrated in the application of synthetic bone substitutes, biomimetic molecular agents, physical stimulation, systemic or local conditions known to have deleterious effects on bone, or a combination of them (43,44). The evaluation of the bone repair process in conditions that affects bone turnover and metabolism, may be compromised by external causes and systemic conditions, can be investigated by using μ CT. Experimental studies in rats revealed alterations in bone healing, for example due to radiotherapy, which affects the bone repair (12). For evaluation of dental implants osseointegration process, the μ CT associated with animal model also is commonly used, and allows the assessment of the new bone formation process around the implant. Nevertheless, some of these studies were focused on histomorphometric findings and have some limitations, one of them related to the 2D evaluation of a few slides. By using μ CT, the advantage could be the 3D evaluation by assessing the whole bone repair process, including the whole microstructure of the new bone formation.

The bone healing cascade follows a process of: an early phase that enables temporarily fracture stabilization and further endochondral bone formation, characterized

by the recruitment of mesenchymal cells and successive chondrogenesis resulting in a soft callus formation. The second stage is distinguished by deposition of the collagen and subsequent mineralization resulting in a woven bone formation and the last stage is characterized by the bone remodeling which restores the original bone structure and strength (44). Irrespective of the study question, using μ CT by means of the whole 3D volume representative of the bone repair region, it is possible to achieve answers which provide insights into how the bone neoformation and healing took place (Fig. 4).

In the evaluation of new bone formation, when using μ CT analysis, the bone volume (BV) is the most important assessed parameter. It means the new bone amount within the region of interest, represented by the lesion filled with bone, or the callus on fracture healing, or even the new bone surrounding implants. The same parameters for the trabecular bone can be evaluated. The characterization of the new bone trabeculae formation, and in the late phase, new formed cortices also can be evaluated by the parameters described previously (Fig. 4). Additionally, the parameters related to bone composition can be measured and differentiate the new bone, like bone mineral density (BMD) measure as the volumetric density of calcium hydroxyapatite (CaHA) in terms of $\text{g}\cdot\text{cm}^{-3}$. By μ CT of fracture healing, using different ranges of voxel brightness (thresholds) to identify mineralized tissue of different densities, with values in a range for less dense new bone and calcified cartilage, another range for very dense cortical bone and other range for non-mineralized tissue (45).

Final Recommendations

The use of μ CT for bone tissue evaluation should be extensive and thorough, taking into consideration the maximum possible tissue extension through the whole tridimensional reconstruction of the sample.

The bone samples should be prepared and maintained in an adequate medium before and during the scanning. If histological processing will follow the scan, the correct fixation of the material should be made (with alcohol or paraformaldehyde, according to the next steps of the sample processing). Although, if is the case to perform mechanical tests, the storage should take place in adequate frozen conditions.

Small and standardized bone samples will provide better scanning conditions, with influence on the final results regarding the possibility to scan with better resolution in this condition.

With regards to image acquisition, the resolution should be able to give accurate results concerning the structures to be evaluated. In cortical bone, the better resolution should allow the identification and measurement of the bone

channels, even the smaller ones. In cases that is necessary to assess the osteocytes lacunae, high-resolution around 1 μm can be defined, but the longer scan time and a small analyzed area should be considered.

Trabecular bone should be evaluated in order to allow the correct identification of the trabeculae, with the resolution choice considering the average of the trabeculae thickness. The same patterns for the trabeculae bone should be considered for bone repair, with the new bone formation at the initial stages presenting a trabecular-like arrangement.

Other parameters during image acquisition should also be carefully defined, as the use of filters (aluminum, copper), the equipment potential and the correct location of the region that should be scanned.

Regarding to the reconstruction process, care should be taken with the correct delimitation of the region of interest, also, with the parameters such as the beam hardening correction, the smoothing and the ring artifact correction.

By the analysis of the bone parameters, the structural analysis should be able to compare different groups or conditions, following the same conditions in order to avoid bias (use of different thresholds for cortices and trabecular bone, but the same thresholds for the comparisons among the different groups). At the cortex, it should be possible to identify if one bone is more porous than the other, or if the bone channels morphology or spatial distribution are altered in a specific condition. Within the trabecular bone, the number, thickness, size and shape of the trabeculae,

together with their connectivity, should be possible to be analyzed and differentiate conditions with better or worst features related to an ideal bone quality and strength (Fig. 5).

Concerning the bone material composition, the mineral density could be evaluated and aid to differentiate health and disease condition, by means of higher or lower X-ray absorbance of the scanned bone. In this analysis, careful should be taken related to the use of a calibrated μCT , by the use of phantoms of known amounts of hydroxyapatite.

Attention on the use of right nomenclatures should be taken by using guidelines and following the correct information on operator manuals of the different μCT systems.

Studies should describe all the parameters related to scanning, reconstruction, and analysis, in order to allow comparison and discussion with other studies.

Micro CT bone evaluation within dentistry has unlimited applications, including: evaluation of diseases and conditions affecting bone metabolism and structure; analysis of repair and regenerating procedures; evaluation of new therapies and surgical interventions; evaluation of the effectiveness and use of biomaterials; and more. When it is possible to analyze human jaw samples, the evaluation by this high-resolution method enables to acquire several information, both on cortices and cancellous structure and composition (Fig. 6). Both type of studies, in experimental animal conditions or human samples are able to be investigated by the use of the μCT . Utilizing high-resolution

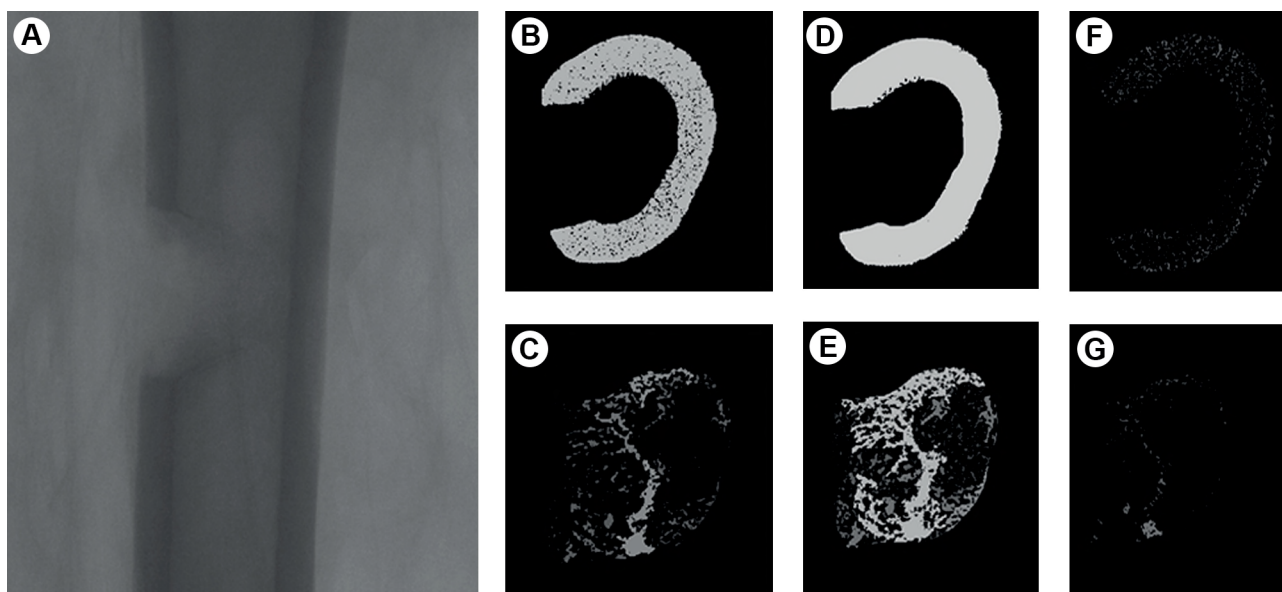


Figure 4. Rat femur with bone repair process evaluated 7 days after euthanization. A: μCT scout view of the femur with the lesion in the middle (8 μm pixel size at 90 kV, 111 μA and 720 ms integration time; Rotation step 0.400 and Filter Al 0.5 + Cu 0.038). B: Defined cortex after binarization with an ideal threshold. C: Defined lesion area (bone repair and medullar channel: after binarization, also with an ideal threshold. D and E: Both cortex and lesion area with over thresholding, revealing overestimation of the bone. F and G: Both cortex and lesion with under thresholding, revealing sub estimation of the bone definition.

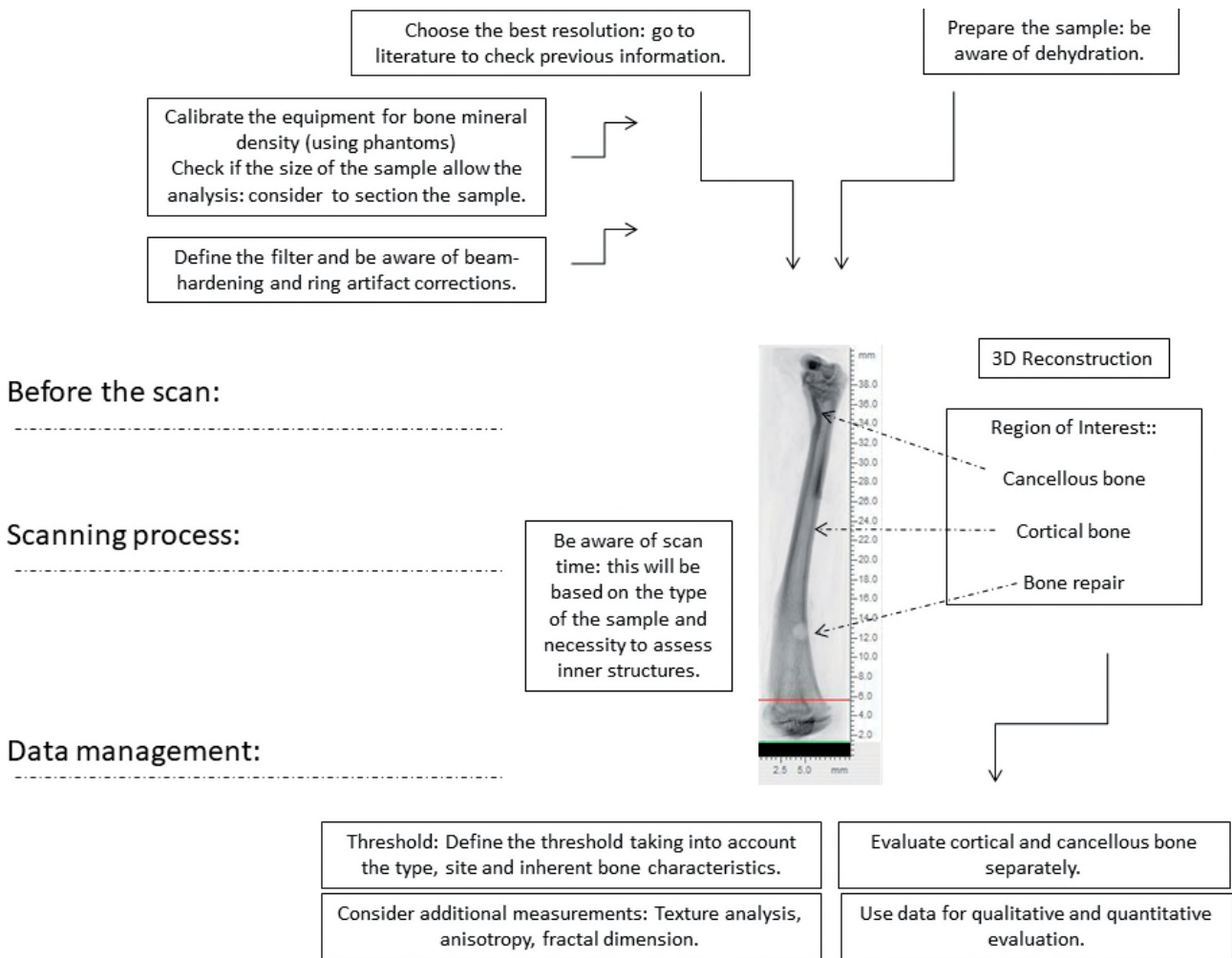


Figure 5. Flow chart with orientations for bone evaluation using microcomputed tomography. The inside figure reveals a scout view of a rat femur with a bone defect (lesion) at the diaphysis part, and both epiphysis where are possible to assess the cancellous bone.

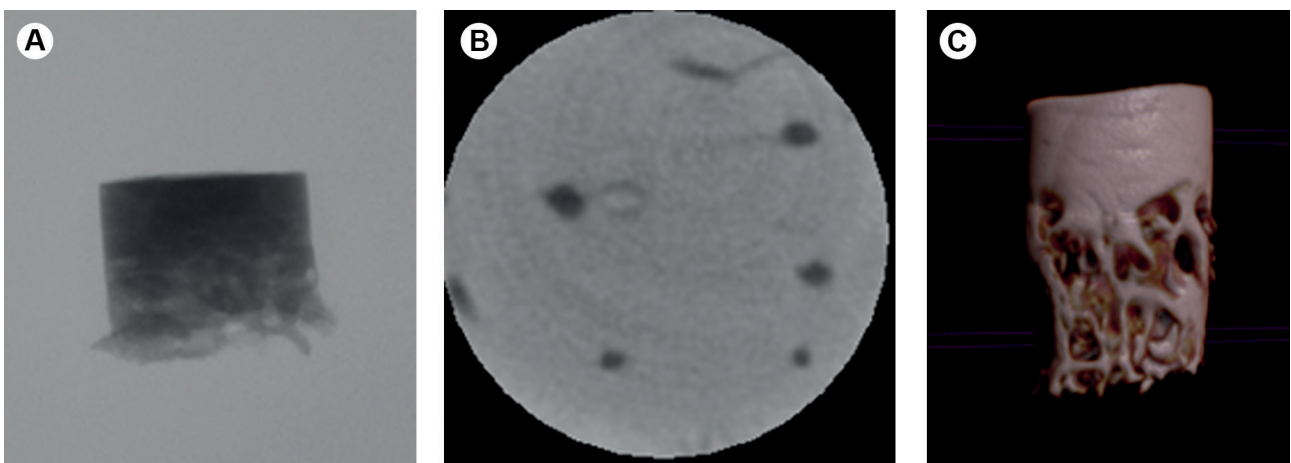


Figure 6. Human sample removed from the mandible of a patient (scan: 19 μ m pixel size at 50 kV, 800 μ A and 4000 ms exposure; Rotation step 0.600 and Filter Al 0.5 mm). A: Scout view revealing the bone sample, with the superior part composed by the cortex and the inferior part with cancellous bone. B: One of the slices within the cortex revealing the bone channels in dark and the bone matrix in gray. C: 3D reconstruction of the bone sample removed.

imaging technique will allow characterization and changes in the bone tissue at the microarchitectural level.

Acknowledgements

This study was supported by the research funding agencies FAPEMIG and CAPES.

Resumo

A microtomografia computadorizada segue o mesmo princípio da tomografia computadorizada utilizada para avaliação dos pacientes, mas neste caso, é empregada para pequenas amostras com alta resolução. De forma não destrutiva, as amostras podem ser escaneadas, e cada fatia obtida é organizada de forma seriada para formar um volume tridimensional (3D). Para análise óssea, é possível obter informações de microarquitetura e composição mineral, permitindo avaliação distinta entre diferentes sítios. De acordo com as características de cada amostra óssea, como amostras de humanos, animais, ossos longos ou achatados, epífise ou diáfise, etc, devem ser definidos os parâmetros pré-escaneamento com a resolução desejada, levando em consideração quais informações serão extraídas da avaliação. Depois do escaneamento e da reconstrução, deve-se proceder com a seleção da região de interesse (ROI), e depois seguir com o processo de binarização, que se caracteriza pela escolha de um limiar que define os voxels que compõem a região de osso e àqueles que compõem a região dos buracos (canais, áreas de reabsorção e espaço medular). No osso trabecular e no reparo os parâmetros avaliados se baseiam nas características das trabéculas e sua conectividade. No osso cortical os parâmetros estão relacionados com a espessura e porosidade. Além dos parâmetros de microarquitetura, também é possível avaliar a densidade mineral óssea, calculada por volume de hidroxiapatita. Outros parâmetros também podem ser mensurados, utilizando técnicas computacionais como a análise de textura. Parâmetros intrínsecos e extrínsecos da qualidade óssea podem ser avaliados pela microtomografia computadorizada. Na odontologia, este método pode ser empregado em estudos que objetivem avaliar doenças, alterações metabólicas e medicamentos com repercussão no metabolismo ósseo, e na avaliação do processo de reparo e de técnicas cirúrgicas.

References

- Metscher BD. MicroCT for comparative morphology: simple staining methods allow high-contrast 3D imaging of diverse non-mineralized animal tissues. *BMC Physiol* 2009;9:11.
- Tjong W, Nirody J, Burghardt AJ, Carballido-Gamio J, Kazakia GJ. Structural analysis of cortical porosity applied to HR-pQCT data. *Med Phys* 2014;41:13701.
- Bouxsein ML, Boyd SK, Christiansen BA, Guldberg RE, Jepsen KJ, Müller R. Guidelines for assessment of bone microstructure in rodents using micro-computed tomography. *J Bone Miner Res* 2010;25:1468-1486.
- Burghardt AJ, Link TM, Majumdar S. High-resolution computed tomography for clinical imaging of bone microarchitecture. *Clin Orthop Relat Res* 2011;469:2179-2193.
- Sinibaldi R, Conti A, Sinjari B, Spadone S, Pecci R, Palombo M, et al. Multimodal-3D imaging based on μ MRI and μ CT techniques bridges the gap with histology in visualization of the bone regeneration process. *J Tissue Eng Regen Med* 2018;12:750-761.
- Chappard D, Baslé MF, Legrand E, Audran M. Trabecular bone microarchitecture: A review. *Morphologie* 2008;92:162-170.
- Muller R, Van Campenhout H, Van Damme B, Van der Perre G, Dequeker J, Hildebrand T, et al. morphometric analysis of human bone biopsies: a quantitative structural comparison of histological sections and micro-computed tomography. *Bone* 1998;23:59-66.
- Roschger P, Paschalis EP, Fratzl P, Klaushofer K. Bone mineralization density distribution in health and disease. *Bone* 2008;42:456-466.
- Kohler T, Beyeler M, Webster D, Müller R. Compartmental bone morphometry in the mouse femur: Reproducibility and resolution dependence of microtomographic measurements. *Calcif Tissue Int* 2005;77:281-290.
- Zebaze R, Seeman E. Cortical bone: a challenging geography. *J Bone Miner Res* 2015;30:24-29.
- Farlay D, Boivin G. Bone mineral quality. *Osteoporosis* 2012;953-978.
- Rocha FS, Dias PC, Limirio PHJO, Lara VC, Batista JD, Dechichi P. High doses of ionizing radiation on bone repair: is there effect outside the irradiated site? *Injury* 2017;48:671-673.
- Fanusc MI, Chang TL. Three-dimensional morphometric analysis of human cadaver bone: Microstructural data from maxilla and mandible. *Clin Oral Implants Res* 2004;15:213-218.
- Rabelo GD, Coutinho-Camillo C, Kowalski LP, Portero-Muzy N, Roux J-P, Chavassieux P, et al. Evaluation of cortical mandibular bone in patients with oral squamous cell carcinoma. *Clin Oral Investig* 2018;22:783-790.
- Blok Y, Gravesteyn FA, Van Ruijven LJ, Koolstra JH. Micro-architecture and mineralization of the human alveolar bone obtained with microCT. *Arch Oral Biol* 2013;58:621-627.
- Romão MMA, Marques MM, Cortes ARG, Horliana ACRT, Moreira MS, Lascala CA. Micro-computed tomography and histomorphometric analysis of human alveolar bone repair induced by laser phototherapy: A pilot study. *Int J Oral Maxillofac Surg* 2015;44:1521-1528.
- Stauber M, Müller R. Micro-computed tomography: a method for the non-destructive evaluation of the three-dimensional structure of biological specimens. *Methods Mol Biol* 2008;455:273-292.
- van't Hof RJ. Analysis of bone architecture in rodents using microcomputed tomography. *Methods Mol Biol. Methods Mol Biol* 2012;816:461-476.
- Carriero A, Doube M, Vogt M, Busse B, Zustin J, Levchuk A, et al. Altered lacunar and vascular porosity in osteogenesis imperfecta mouse bone as revealed by synchrotron tomography contributes to bone fragility. *Bone* 2014;61:116-124.
- Bruker-MicroCT. Bruker Micro - CT Academy Bruker Micro-CT Academy. *Bruker Micro-CT Acad* 2015;2:1-2.
- Kim DG, Christopherson GT, Dong XN, Fyhrie DP, Yeni YN. The effect of microcomputed tomography scanning and reconstruction voxel size on the accuracy of stereological measurements in human cancellous bone. *Bone* 2004;35:1375-1382.
- Barak MM, Lieberman DE, Hublin JJ. Of mice, rats and men: Trabecular bone architecture in mammals scales to body mass with negative allometry. *J Struct Biol* 2013;183:123-131.
- Christiansen BA. Effect of micro-computed tomography voxel size and segmentation method on trabecular bone microstructure measures in mice. *Bone Rep* 2016;5:136-140.
- Christiansen BA. Assessment of Bone Mass and Microarchitecture in Rodents. In: *Primer on the Metabolic Bone Diseases and Disorders of Mineral Metabolism: 8th Edition* 2013. p. 59-68.
- Laib a, Barou O, Vico L, Lafage-Proust MH, Alexandre C, Rügsegger P. 3D micro-computed tomography of trabecular and cortical bone architecture with application to a rat model of immobilisation osteoporosis. *Med Biol Eng Comput* 2000;38:326-332.
- Shiffman D. Images and Pixels 2008. Available from: <https://processing.org/tutorials/pixels/>. Latest access: May 10, 2018.
- Waarsing JH, Day JS, Weinans H. An improved segmentation method for in vivo μ CT imaging. *J Bone Miner Res* 2004;19:1640-1650.
- Geusens P, Chapurlat R, Schett G, Ghasem-Zadeh A, Seeman E, de Jong J, et al. High-resolution in vivo imaging of bone and joints: a window to microarchitecture. *Nat Rev Rheumatol* 2014;10:304-313.
- Bernhard A, Milovanovic P, Zimmermann EA, Hahn M, Djonic D, Krause M, et al. Micro-morphological properties of osteons reveal changes in cortical bone stability during aging, osteoporosis, and bisphosphonate treatment in women. *Osteoporosis Int* 2013;24:2671-2680.
- Gudea A, Stefan A. Histomorphometric, fractal and lacunarity comparative analysis of sheep (*Ovis aries*), goat (*Capra hircus*) and roe deer (*Capreollus capreollus*) compact bone samples. *Folia Morphol* 2013;72:13.
- De Melo RHC, Conci A. How Succolarity could be used as another fractal measure in image analysis. *Telecommun Syst* 2013;52:1643-1655.
- Russell NA, Pelletier MH, Bruce WJ, Walsh WR. The effect of gamma irradiation on the anisotropy of bovine cortical bone. *Med Eng Phys*

- 2012;34:1117-1122.
33. Sanchez-Molina D, Velazquez-Ameijide J, Quintana V, Arregui-Dalmases C, Crandall JR, Subit D, et al. Fractal dimension and mechanical properties of human cortical bone. *Med Eng Phys* 2013;35:576-582.
 34. Fazzalari NL, Parkinson IH. Fractal dimension and architecture of trabecular bone. *J Pathol.* 1996;178:100-105.
 35. Pothuaud L, Benhamou CL, Porion P, Lespessailles E, Harba R, Levitz P. Fractal dimension of trabecular bone projection texture is related to three-dimensional microarchitecture. *J Bone Miner Res* 2000;15:691-699.
 36. Prouteau S, Ducher G, Nanyan P, Lemineur G, Benhamou L, Courteix D. Fractal analysis of bone texture: A screening tool for stress fracture risk? *Eur J Clin Invest* 2004;34:137-142.
 37. Dougherty G, Henebry GM. Lacunarity analysis of spatial pattern in CT images of vertebral trabecular bone for assessing osteoporosis. *Med Eng Phys* 2002;24:129-138.
 38. Melo RHC, Vieira ED, Conci A. Characterizing the lacunarity of objects and image sets and its use as a technique for the analysis of textural patterns. *Adv Concepts Intell Vis Syst Proc* 2006;4179:208-219.
 39. Boutroy S, Vilayphiou N, Roux JP, Delmas PD, Blain H, Chapurlat RD, et al. Comparison of 2D and 3D bone microarchitecture evaluation at the femoral neck, among postmenopausal women with hip fracture or hip osteoarthritis. *Bone* 2011;49:1055-1061.
 40. Goldring SR, Goldring MB. Changes in the osteochondral unit during osteoarthritis: structure, function and cartilage-bone crosstalk. *Nat Rev Rheumatol* 2016;12:632-644.
 41. Heilmeyer U, Patsch JM. Diabetes and bone. *Semin Musculoskelet Radiol* 2016;20:300-304.
 42. Marques IDB, Araújo MJCLN, Gracioli FG, Reis LM do., Pereira RM, Custódio MR, et al. Biopsy vs. peripheral computed tomography to assess bone disease in CKD patients on dialysis: differences and similarities. *Osteoporos Int* 2017;28:1675-1683.
 43. Von Rechenberg B. Animal models in bone repair. *Drug Discov Today Dis Model.* Elsevier Ltd; 2014;13:23-7. Available from: <http://dx.doi.org/10.1016/j.ddmod.2015.02.001>.
 44. Peric M, Dumic-Cule I, Grevic D, Matijasic M, Verbanac D, Paul R, et al. The rational use of animal models in the evaluation of novel bone regenerative therapies. *Bone* 2015;70:73-86.
 45. Freeman TA, Patel P, Parvizi J, Antoci V, Shapiro IM. Micro-CT analysis with multiple thresholds allows detection of bone formation and resorption during ultrasound-treated fracture healing. *J Orthop Res* 2009;27:673-679.

Received October 30, 2017
Accepted March 27, 2018

3.2 Capítulo 2

Artigo submetido ao periódico *Physics in Medicine and Biology*

Effect of micro-CT acquisition parameters and operator experience on the outcome of bone repair evaluation

Name of the authors:

Milena Suemi, Irie^a; Rubens, Spin-Neto^b; Lucas Henrique, de Souza Teixeira^a; Gustavo, Davi Rabelo^c; Nayara, Teixeira de Araújo Reis^a; Priscilla, Barbosa Ferreira Soares^a

Primary Institution: School of Dentistry, Federal University of Uberlândia, Uberlândia, Minas Gerais, Brazil

Authors affiliation

^a Department of Periodontology and Implantology, School of Dentistry, Federal University of Uberlândia, Avenida Pará s/n°, Campus Umuarama, Bloco 4L, Bairro Umuarama, 38400-902, Uberlândia, Minas Gerais, Brazil.

^b Department of Dentistry and Oral Health, Section of Oral Radiology, Health, Aarhus University, Arhuus C, 8000, Aarhus, Denmark

^c Dentistry Department, Federal University of Santa Catarina, Rua Delfino Conti SN, Trindade, Florianópolis, SC, 88040-370, Brazil.

Corresponding author: Priscilla Barbosa Ferreira Soares. Department of Periodontology and Implantology, School of Dentistry, Federal University of Uberlândia, Avenida Pará s/n°, Campus Umuarama, Bloco 4L, Bairro Umuarama, 38400-902, Uberlândia, Minas Gerais, Brazil. +55 3432258119; e-mail: pbfsoares@yahoo.com.br

Declarations

Conflicts of interest/Competing interests: On behalf of all authors, the corresponding author states that there is no conflict of interest of any kind.

Ethical approval: This study was approved by the Research Ethics Committee (approval number 093/17) and was carried out in strict compliance with the ethical principles for the care and use of laboratory animals, following the ARRIVE guidelines. All applicable international, national, and/or institutional guidelines for

the care and use of animals were followed. All procedures performed during studies involving animals were in accordance with the ethical standards of practice at the Universidade Federal de Uberlândia. This study only reports data from animal experiments.

Abstract

To *investigate whether* two acquisition parameters such as voxel size and filter thickness used in a microcomputed tomography (microCT) scan, together with the examiner experience, influence the outcome of a bone repair analysis in an experimental model. Bone defects were created in rat tibias, and then scanned using two voxel sizes of 6- or 12- μm , and two aluminum filter thickness of 0.5- or 1-mm. After the scan, bone volume fraction (BV/TV) and trabecular thickness (Tb.Th) were analyzed twice by two groups of operators: experienced and non-experienced examiners. For BV/TV, no significant differences were found between scanning voxel sizes of 6 and 12 μm for the experienced examiners; however, for the non-experienced, the analysis performed using 12 μm voxel size resulted in higher BV/TV values (32.4 and 32.9) than the ones acquired on 6 μm voxel size (25.4 and 24.8) ($p < 0.05$). For Tb.Th, no significant differences between the analyses performed by experienced and non-experienced groups were observed when used the 6 μm voxel size. However, non-experienced examiners analysis revealed higher Tb.Th values when using 12 μm voxel size compared with 6 μm (0.05 vs 0.03, $p < 0.05$). Filter thickness had no influence on the results of all groups. In conclusion, voxel size and operator experience affected the measured Tb.Th and BV/TV of a region containing new bone formation. Operators experience in micro-CT analysis is more critical for BV/TV than for Tb.Th, whereas voxel size has a major effect on Tb.Th evaluation. Operators at initial phases on research training should be calibrated for bone assessment.

Keywords: microcomputed tomography; bone architecture; trabecular bone; stereology; rodent; bone repair; animal models; imaging.

Introduction

Microcomputed tomography (microCT) analysis is a nondestructive method that provides three-dimensional reconstructions of interior structures and other bone properties (Bouxsein et al., 2010; Kühl et al., 2013). A strong correlation between microCT and histomorphometric analysis has been reported in several studies (Müller et al., 1998; Anavi et al., 2011). MicroCT has been widely used in research fields of bone metabolism, repair, and regeneration (Irie et al., 2018). Acquisition and analysis of bone volumes using microCT consists of the following steps: a) scout view and preprocessing on 2D section visualization; b) sample scanning; c) segmentation and 3D reconstruction; and d) microstructure quantification and analysis. In each stage of this process, some variables, such as resolution and the use of filters may affect the morphological outcomes (Christiansen, 2016). A guideline based on the need for standardized terminology and consistent reporting of parameters analyzed was published (Bouxsein et al., 2010), and described that besides following the manufacturer-specific instructions for regular quality control, images should be inspected visually to identify possible scanning artifacts. In this way, the influence of scanning and image processing during analysis and its influence on the results still needs to be accessed.

Image resolution is determined by voxel size. Morphological assessment of thinner structures, such as rat bone trabeculae (20-70 μm), can be affected by resolution (Kim et al., 2004; Müller et al., 1998). Scanning small structures with low resolution can underestimate bone mineral density and overestimate its thickness (Longo et al., 2017). Most microCT systems provide a resolution on the order of 6-73 μm (Chopra et al., 2009). Ideally, the smallest voxel size (highest resolution) should be used in animal experiments; however, using a small voxel size increases the scanning duration and data generation, being sometimes too much time-consuming. Moreover, the amount of radiation must be considered when *in vivo* microCT scanning is applied (Christiansen, 2016).

Other acquisition parameter that influences on the quality of the results is the use of filters. They may minimize artifacts present in the images. Beam

hardening is an artifact produced by a polychromatic X-ray beam with different energy spectra. When the X-ray beam propagates through the sample, the low-energy portion stops in the surface area, while the high-energy portion goes inside the sample. This phenomenon manifests as a higher-density image of the surface area of the sample. It is possible to minimize this artifact at the reconstruction stage. However, by placing a metal filter between the X-ray and the sample during image acquisition, the lower energy portion of the beam is filtered. The ideal filter and filter thickness to use will also depend on the sample size and density (Bouxsein et al., 2010).

The region-of-interest (ROI, e.g., the specific site where bone healing will be assessed in this study) should be delimited and separated from the other structures across the acquired field of view (Behrooz et al., 2017; Irie et al., 2018). This process could be done manually or in an automatic fashion. After ROI delimitation, determining a grayscale threshold (0-255) distinguishes bone from nonbone, a process called image segmentation (or binarization). This process can be performed by means of local or global values. Most commonly, global thresholding is performed, in which a chosen value (Hounsfield units or g/cm^3) distinguishes bone (above the threshold) from nonbone (below the threshold). The threshold is selected either visually, by analyzing the density of the histogram, or by setting a threshold value that will result in a volume dataset equal to the volume of the original bone sample (Ding et al., 1999). Local thresholds are based on the neighboring values of each voxel (Dufresne, 1998) or based on the local minima and local maxima values of the selected ROI. Diverse methods applying local threshold definition have been reported (Kuhn et al., 1990; Elmoutaouakkil et al., 2002) to overcome the limitations related to low resolution and nonhomogeneous samples that affects global thresholding. However, both processes (ROI delimitation and threshold setting) can be influenced by the examiner's experience.

The aim of this study was to *investigate whether* the acquisition voxel size, filter thickness, and operator experience affect the morphometric outcome of bone repair evaluation assessed by means of microCT. The null hypothesis

was that the acquisition voxel size, filter thickness, and examiner experience have no effect on the outcome.

Material and Methods

This study was approved by the Research Ethics Committee (approval number 093/17) of the institution and was carried out in strict compliance with the ethical principles for the care and use of laboratory animals, also according to the ARRIVE guidelines. Cortical bone defects of 1.6 mm in diameter were created using a cylindrical burr (Neodent®, Curitiba, Brazil) at a standardized location on the tibiae of 5 Wistar rats. The animals were euthanized 7 days after surgery, and the right tibiae were covered with moist gauze containing phosphate-buffered solution and stored in plastic tubes at -20 °C until scanning. The tibiae were positioned in the sample holder and left at room temperature before the scans. MicroCT scan of the 5 tibiae (Fig. 1) were acquired with a desktop SkyScan 1272 high-resolution 3D X-ray microscope based on micro computed tomography (microCT) technology (Bruker, Kontich, Belgium).

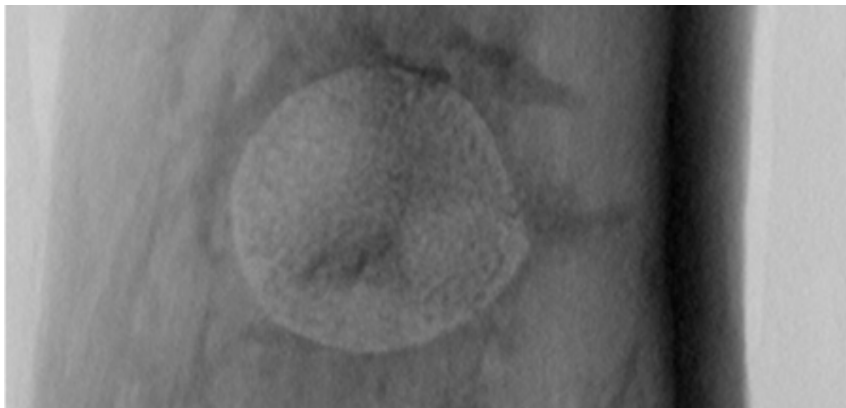


Fig. 1 MicroCT scout view of the tibia with the cortical defect (6 μm voxel size at 70 kV, 142 μA , a 0.2 rotation step, and a 1 mm aluminum filter).

Each sample was repeatedly scanned using the following acquisition parameters: voxel sizes of 6 μm and 12 μm , and aluminum filter thicknesses of 0.5 mm and 1.0 mm ($n = 5$). Image reconstruction was performed with NRecon software (version 1.6.6.0, Bruker, Kontich, Belgium). A single set of parameters

was chosen visually based on minimum artifacts, irrespective of the tested group. Ring artifact correction was set at 9, smoothing at 1, and beam hardening correction at 0%. The reconstructions included the entire lesion, as follows: new bone formation inside the tibia canal and at the lesion site was manually delimited in 2D slices (Fig. 2), from the bottom to the top of the lesion borders, delineated by a single examiner (LHST).

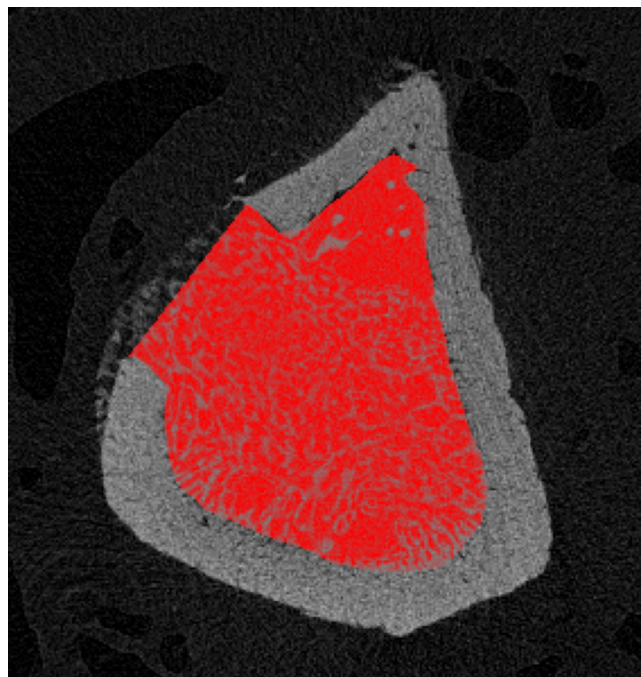


Fig. 2 Demonstration of the region of interest (ROI) delimitation of the defect area.

Morphometric data (bone volume ratio, BV/TV, and trabecular thickness in μm , Tb.Th) was evaluated by 5 experienced and 5 non-experienced examiners and assessed for each acquisition parameter. The non-experienced examiner's group included operators with experience in microCT analysis, but none has ever performed bone analysis before the study. The experienced examiner's group included researchers who had performed microCT analysis on rat bone tissue in previous experiments and other bone analysis. BV/TV and Tb.Th analyses were performed using the CTAn software (version 1.18.4.0, Bruker). Segmentation of the trabecular bone within the lesion area was manually

performed by each examiner. The entire lesion was defined by interpolation of the ROIs delineated by each examiner. Thresholds for segmentation of bone and nonbone (maximum and minimum gray levels) were visually and individually defined for each set of acquisition parameters. Then, BV/TV and Tb.Th measurements were calculated.

Statistical analysis was performed using SigmaPlot® (SigmaPlot v13.1; Systat Software Inc.) considering a significance level of $\alpha=0.05$. The influence of operator experience (experienced and non-experienced examiners), filter thickness (aluminum 0.5 and 1 mm) and scanning voxel size (6 and 12 μm) on BV/TV and Tb.Th were assessed using three-way analysis of variance (ANOVA) with Tukey's post hoc test. Intraclass correlation coefficients (ICCs) for absolute agreement among total tissue volume (TV) measurements were calculated (Salarian, 2019) (MATLAB MathWorks, Natick, MA) to evaluate interexaminer reliability (Koo & Li, 2016) for cortical and trabecular bone segmentation in both the experienced and non-experienced groups.

Results

The ICC between the experienced examiners was 0.84, indicating good reliability. Thus, ICC between the non-experienced examiners indicated poor reliability (0.06). The mean and standard deviation values for BV/TV and Tb.Th are shown in Tables 1 and 3, respectively. The factor interactions (operator experience, voxel size and filter) for BV/TV (Table 2) and Tb.Th are described in Table 4.

BV/TV

The operator experience ($p < .001$), the voxel size ($p < .001$) and the interaction between these factors ($p = .009$) had significant effects on the BV/TV values (Table 3). The analysis performed by experienced examiners resulted in significantly lower BV/TV values (17.8 ± 4.3) than that performed by non-experienced examiners (31.2 ± 2.1 , $p < .001$). The effect of voxel size depended on the examiner experience. No significant difference was observed for the experienced examiners after scanning at voxel sizes of 6 (15.8 ± 4.5) and 12 μm

(15.6 ± 5.2) (p = 0.900). However, for the non-experienced examiners, the analysis performed on the 12 µm volumes (32.7 ± 15.5) resulted in higher BV/TV than did that performed on the 6 µm group (25.1 ± 14.2, p < .001). The effects of the filter and its interactions with tested factors were not significant. No significant interaction was found among the 3 factors (p = 0.500).

Table 1. Mean BV/TV values (SDs) and results of Tukey HSD test

Examiner	6 µm voxel size		12 µm voxel size	
	0.5mm filter	1.0mm filter	0.5mm filter	1.0mm filter
Experienced	15.5 (4.0) ^{Aa}	16.0 (5.0) ^{Aa}	16.1 (5.6) ^{Aa}	15.1 (4.9) ^{Aa}
Non-experienced	25.4 (14.1) ^{Ba}	24.8 (14.5) ^{Ba}	32.4 (15.1) ^{Bb}	32.9 (16.1) ^{Bb}

Different uppercase letters in vertical columns indicate significant differences; different lowercase letters in horizontal rows indicate significant differences; Tukey HSD test (P<.05).

Table 2. Three-way ANOVA interactions for BV/TV measurements

Source of variation	P values
Operators x Filter	0.800
Operators x Voxel size	0.009*
Filter x Voxel size	0.800
Operators x Filter x Voxel size	0.500

**The mean difference is significant at the 0.05 level.*

Tb.Th

The examiner (p < .001), the voxel size (p < .001) and the interaction between factors (p = .040) had significant effects on the Tb.Th values (Table 4). The analysis performed by the experienced examiners resulted in lower Tb.Th

values (0.04 ± 0.01) than that performed by the non-experienced examiners (0.05 ± 0.02 , $p < .001$). The effect of the examiner depended on the voxel size of the volumes analyzed. There was no difference between experienced and non-experienced operators in the 6 μm group ($p = .900$); however, the analysis performed on 12 μm volumes resulted in higher ($p < .001$) Tb.Th values for the experienced examiners (0.06 ± 0.02) than for the non-experienced examiners (0.05 ± 0.01). The filter and interactions between 2 or 3 factors had no significant influence on Tb.Th values ($p = .900$).

Table 3. Mean Tb.Th values (SDs) and results of Tukey HSD test

Examiner	6 μm voxel size		12 μm voxel size	
	0.5mm filter	1.0mm filter	0.5mm filter	1.0mm filter
Experienced	0.04 (0.01) ^{Aa}	0.03 (0.01) ^{Aa}	0.06 (0.02) ^{Ab}	0.06 (0.02) ^{Ab}
Non-experienced	0.03 (0.00) ^{Aa}	0.03 (0.00) ^{Aa}	0.05 (0.01) ^{Bb}	0.05 (0.00) ^{Bb}

Different uppercase letters in vertical columns indicate significant differences; different lowercase letters in horizontal rows indicate significant differences; Tukey HSD test ($P < .05$).

Table 4. Three-way ANOVA interactions for Tb.Th measurements.

Source of variation	<i>P</i> values
Operators x Filter	0.400
Operators x Voxel size	0.040*
Filter x Voxel size	0.400
Operators x Filter x Voxel size	0.900

**The mean difference is significant at the 0.05 level.*

Discussion

The present study investigated whether the acquisition voxel size, filter thickness, and operator's experience influence on the results of the morphometric evaluation of bone volume and trabecular thickness, using an experimental model of bone repair in the rat tibiae. Both morphometric parameters of BV/TV and Tb.Th demonstrated some dependency upon examiner experience and acquisition voxel size. Regarding the filter thickness, this parameter had no effect on BV/TV and Tb.Th measurements. Thus, the null hypothesis that the acquisition voxel size, filter thickness, and experience of examiner parameters have no effect on the outcome of the morphometric evaluation was partially rejected. In this way, the present study pointed out two critical factors that should be considered for microCT analysis of a site with new bone formation: the acquisition voxel size and the experience of the examiners.

Several segmentation methods have been described to separate trabecular from cortical bone in microCT volumes (Korfiatis et al., 2017; Lublinsky et al., 2007; Behrooz et al., 2017). Automated segmentation to distinguish cortical from trabecular bone is not possible for bone repair sites in some specific models (mostly on the diaphysis of long bones), once the cortical contour is not intact and a detailed delimitation of the lesion edges cannot be achieved. If a ROI (e.g., standardized circle) is defined in the cancellous region, the analysis can be underestimated when only a fraction of the ROI (i.e., the trabecular bone undergoing healing) is included (Behrooz et al., 2017). An automated method to identify and separate the callus and/or newly formed bone, original cortical bone, and the marrow portion without requiring the delimitation of specific ROIs was proposed previously (Bissinger et al., 2017). The authors applied global thresholding for each structure visually determined by two independent examiners and by the associated histogram. This method was not time consuming; however, it did not provide volume-dependent microCT assessments of parameters such as BV/TV. In this case, the most accurate method for nonintact cortical analysis is manual drawing of contour lines on the outer edge of the lesion. Therefore, creating a VOI by interpolating several ROIs is feasible

considering the rupture in the cortical bone, the dimensions of which diverge in each section.

The ICC for total volume (TV) indicated good reliability between the VOIs of the experienced examiners. However, such good reliability was not observed between non-experienced examiners. This finding supports the difference in BV/TV outcomes between those groups. Bone volume fraction is one of the main morphological parameters for bone repair evaluation, and it depends on the total volume (Bouxsein et al., 2010). The results from the present study demonstrated that detailed volume of interest (VOI) delimitation by an experienced and calibrated examiner is critical for bone volume fraction analysis of a healing area. The relevance of examiner experience is also emphasized over the effect of resolution. BV/TV was influenced by the acquisition voxel size only for the non-experienced examiners. The analysis performed by an experienced examiner showed no difference between voxel sizes of 6 μm or 12 μm .

The influence of operator's experience was also observed for Tb.Th measurements. However, this difference was solely observed in the 12 μm group, indicating that Tb.Th analysis of bone repair in rats with the 6 μm voxel size volumes imply less bias than the examiner. When acquiring volumes at a larger voxel size, the bone surface is blurred, especially for trabecular structures within a healing area (which have higher resorption rates and even a thinner trabecula) (Glatt et al., 2007). This approach makes the binarization process more prone to bias, which was evident when the examiners had no previous experience in bone morphometric analysis. Longo *et al.* (2017) compared 9 μm and 18 μm voxel sizes in both *in vivo* and *ex vivo* microCT (Longo et al., 2017). The authors demonstrated that analysis with smaller voxel size volumes led to lower Tb.Th measurements in rat trabeculae. Similar results were found in the present study, in which a significant difference was observed between the 6- and 12- μm groups for Tb.Th. The findings of the present study supported the hypothesis that thinner trabecular structures are blurry when scanning at a larger voxel size, culminating in an increase in the mean measured thickness.

The effect of the acquisition voxel size on trabecular structures has also been demonstrated in human cadavers' investigations (Tjong et al., 2012).

While the effect of acquisition voxel size has been observed at larger dimensions, such as 41 μm in micro-CT compared to high-resolution peripheral quantitative computed tomography (HQ-pQCT) with acquisition voxel sizes of 41, 82 and 123 μm , the results of the present study revealed the same effect even for a narrow difference in the voxel size during image acquisition. A smaller voxel size may allow more accurate segmentation of the trabecular structure, which results in more accurate quantification of the trabecular microstructure parameters. The acquisition resolution should always be chosen based on the size of the structure being analyzed as well as the size of the expected microarchitecture changes that the experimenter aims to quantify (Palacio-Mancheno et al., 2014). However, the resolution might be critical if it involves remodeling areas. In this way, the findings from the present study have demonstrated that scanning at a 6 μm or 12 μm voxel size was not a limiting factor for BV/TV with calibrated examiners; rather, scanning at a 6 μm voxel size is a determinant for the Tb.Th measurements of a healing bone area.

In the present study, a global threshold for each acquisition parameter was used. The cortical bone was kept out of the analyzed area, and only trabecular bone within the lesion was analyzed, providing a homogenous structure analysis. A local threshold method was proposed (Waarsing et al., 2004), which was validated by histological analysis. The authors concluded that the performance of global threshold methods is equal to that of local thresholds when analyzing high-resolution scans of homogenous structures. However, when nonhomogeneous samples are analyzed (e.g., both thick cortices and thin trabeculae) or when the scan resolution is relatively low, the efficiency of the local threshold method overcomes that of the global methods. When analyzing high-resolution volumes of a homogeneous bone sample, as done in the present study, subjective thresholding performs similarly to objective thresholding. Nonetheless, definition of a reliable threshold should be performed considering 2D slicewise comparisons to the original, regardless of the segmentation method. Visual inspection of the segmentations to ensure that trabecular connectivity is maintained while excluding noise is crucial for micro-CT analysis (Tjong et al., 2012). It was also reported that segmentation limitations could be mitigated by

high-resolution scanning (Palacio-Mancheno et al., 2014), corrections for beam hardening, and the implementation of a density-based thresholding method.

The effect of beam hardening can be reduced by placing a metal filter during scanning and applying corrective algorithms during reconstruction (Gaêta-Araujo et al., 2019). In the present study, the beam hardening correction was set at 0% to verify the effect of the filter without algorithm correction. However, no difference was observed in either parameter (BV/TV or Tb.Th) between 0.5- and 1 mm-thick aluminum filters. It has been demonstrated that beam hardening leads to fewer artifacts for morphology than densitometric measurements (Meganck et al., 2009). However, one of the limitations of the present study is that bone mineral density was not assessed, to serve as a reference standard (i.e., the truth); thus, we can only assume that aluminum filter thickness did not influence the morphometric outcomes. Despite this limitation, the importance of a single experienced examiner for all the samples to avoid bias in the morphometric outcomes was clear.

Conclusions

Considering the limitations of the study design, it was possible to conclude:

- Acquisition voxel size (6 and 12 μm) and operators' experience influenced the outcome of the results obtained for trabecular thickness and bone volume ratio in a site of bone repair in an experimental model.
- Individual experience of the operator in micro-CT analysis is more critical for BV/TV, whereas for Tb.Th, voxel size has a major effect.
- It is recommended that high-resolution acquisitions should be used whenever possible, aiming to provide the most accurate measurements of bone microstructure parameters in an area on an active repair process.

References

ANAVI, Y., AVISHAI, G., CALDERON, S. & ALLON, D. M. (2011). Bone remodeling in

- onlay beta-tricalcium phosphate and coral grafts to rat calvaria: Microcomputerized tomography analysis. *J Oral Implantol* **37**, 379–386.
- BEHROOZ, A., KASK, P., MEGANCK, J. & KEMPNER, J. (2017). Automated quantitative bone analysis in in vivo x-ray micro-computed tomography. *IEEE Trans Med Imaging* **36**, 1955–1965.
- BISSINGER, O., GÖTZ, C., WOLFF, K. D., HAPFELMEIER, A., PRODINGER, P. M. & TISCHER, T. (2017). Fully automated segmentation of callus by micro-CT compared to biomechanics. *J Orthop Surg Res* **12**, 108.
- BOUXSEIN, M. L., BOYD, S. K., CHRISTIANSEN, B. A., GULDBERG, R. E., JEPSEN, K. J. & MÜLLER, R. (2010). Guidelines for assessment of bone microstructure in rodents using micro-computed tomography. *J Bone Miner Res* **25**, 1468–1486.
- CHOPRA, P. M., JOHNSON, M., NAGY, T. R. & LEMONS, J. E. (2009). Clinical device-related article micro-computed tomographic analysis of bone healing subsequent to graft placement. *J Biomed Mater Res - Part B Appl Biomater* **88**, 611–618.
- CHRISTIANSEN, B. A. (2016). Effect of micro-computed tomography voxel size and segmentation method on trabecular bone microstructure measures in mice. *Bone Reports* **5**, 136–140.
- DING, M., ODGAARD, A. & HVID, I. (1999). Accuracy of cancellous bone volume fraction measured by micro-CT scanning. *J Biomech* **32**, 323–326.
- DUFRESNE, T. (1998). Segmentation techniques for analysis of bone by three-dimensional computed tomographic imaging. *Technol Heal Care* **6**, 351–359.
- ELMOUTAOUAKKIL, A., PEYRIN, F., ELKAFI, J. & LAVAL-JEANTET, A. M. (2002). Segmentation of cancellous bone from high-resolution computed tomography images: Influence on trabecular bone measurements. *IEEE Trans Med Imaging* **21**, 354–362.
- GÂÊTA-ARAUJO, H., OLIVEIRA-SANTOS, N., BRASIL, D. M., DO NASCIMENTO, E. H. L., MADLUM, D. V., HAITER-NETO, F. & OLIVEIRA-SANTOS, C. DE (2019). Effect of micro-computed tomography reconstruction protocols on bone fractal dimension analysis. *Dentomaxillofacial Radiol* **48**, 20190235.

- GLATT, V., CANALIS, E., STADMEYER, L. & BOUXSEIN, M. L. (2007). Age-related changes in trabecular architecture differ in female and male C57BL/6J mice. *J Bone Miner Res* **22**, 1197–1207.
- IRIE, M. S., RABELO, G. D., SPIN-NETO, R., DECHICHI, P., BORGES, J. S. & SOARES, P. B. F. (2018). Use of micro-computed tomography for bone evaluation in dentistry. *Braz Dent J* **29**, 227–238.
- KIM, D. G., CHRISTOPHERSON, G. T., DONG, X. N., FYHRIE, D. P. & YENI, Y. N. (2004). The effect of microcomputed tomography scanning and reconstruction voxel size on the accuracy of stereological measurements in human cancellous bone. *Bone* **35**, 1375–1382.
- KOO, T. K. & LI, M. Y. (2016). A Guideline of Selecting and Reporting Intraclass Correlation Coefficients for Reliability Research. *J Chiropr Med* **15**, 155–163.
- KORFIATIS, V. C., TASSANI, S. & MATSOPOULOS, G. K. (2017). An Independent Active Contours Segmentation framework for bone micro-CT images. *Comput Biol Med* **87**, 358–370.
- KÜHL, S., BROCHHAUSEN, C., GÖTZ, H., FILIPPI, A., PAYER, M., D'HOEDT, B. & KREISLER, M. (2013). The influence of bone substitute materials on the bone volume after maxillary sinus augmentation: a microcomputerized tomography study. *Clin Oral Investig* **17**, 543–551.
- KUHN, J. L., GOLDSTEIN, S. A., FELDKAMP, L. A., GOULET, R. W. & JESION, G. (1990). Evaluation of a microcomputed tomography system to study trabecular bone structure. *J Orthop Res* **8**, 833–842.
- LONGO, A. B., SALMON, P. L. & WARD, W. E. (2017). Comparison of ex vivo and in vivo micro-computed tomography of rat tibia at different scanning settings. *J Orthop Res* **35**, 1690–1698.
- LUBLINSKY, S., OZCIVICI, E. & JUDEX, S. (2007). An automated algorithm to detect the trabecular-cortical bone interface in micro-computed tomographic images. *Calcif Tissue Int* **81**, 285–293.
- MEGANCK, J. A., KOZLOFF, K. M., THORNTON, M. M., BROSKI, S. M. & GOLDSTEIN, S. A. (2009). Beam hardening artifacts in micro-computed tomography scanning can be reduced by X-ray beam filtration and the resulting images can be used to accurately measure BMD. *Bone* **45**, 1104–1116.

- MÜLLER, R., VAN CAMPENHOUT, H., VAN DAMME, B., VAN DER PERRE, G., DEQUEKER, J., HILDEBRAND, T. & RÜEGSEGG, P. (1998). Morphometric analysis of human bone biopsies: A quantitative structural comparison of histological sections and micro-computed tomography. *Bone* **23**, 59–66.
- PALACIO-MANCHENO, P. E., LARRIERA, A. I., DOTY, S. B., CARDOSO, L. & FRITTON, S. P. (2014). 3D assessment of cortical bone porosity and tissue mineral density using high-resolution μ CT: Effects of resolution and threshold method. *J Bone Miner Res* **29**, 142–150.
- SALARIAN, A. (2019). *Intraclass Correlation Coefficient (ICC)*. MATLAB Central File Exchange.
- TJONG, W., KAZAKIA, G. J., BURGHARDT, A. J. & MAJUMDAR, S. (2012). The effect of voxel size on high-resolution peripheral computed tomography measurements of trabecular and cortical bone microstructure. *Med Phys* **39**, 1893–1903.
- WAARSING, J. H., DAY, J. S. & WEINANS, H. (2004). An improved segmentation method for in vivo μ CT imaging. *J Bone Miner Res* **19**, 1640–1650.

Acknowledgments

The authors are grateful to Rede de Biotérios de Roedores da Universidade Federal de Uberlândia, and to the Centro de Pesquisa Odontológico Biomecânico, Biomateriais e Biologia Celular (CPBIO – UFU). This study was supported by grants from the Fundação de Amparo à Pesquisa de Minas Gerais (FAPEMIG), the Coordenação de Aperfeiçoamento de Pessoal de Nível Superior – Brasil (CAPES) – Finance Code 001 and Conselho Nacional de Desenvolvimento Científico e Tecnológico (CNPq).

3.3 Capítulo 3

Artigo será submetido ao periódico Scientific Reports

Is there any effect of data binning and averaging for microCT image acquisition on morphometrics outcome of the bone repair?

Milena Suemi Irie¹, Juliana Borges Simeão¹, Rubens Spin-Neto², Priscilla Barbosa Ferreira Soares^{1*}

¹ Department of Periodontology and Implantology, School of Dentistry, Federal University of Uberlândia, Uberlândia, Brazil.

² Department of Dentistry and Oral Health, Section for Oral Radiology, Aarhus University, Aarhus C, Denmark

***Corresponding author:**

Dra. Priscilla Barbosa Ferreira Soares

Department of Periodontology and Implantology, School of Dentistry, Federal University of Uberlândia, Avenida Pará s/n°, Campus Umuarama, Bloco 4L, Bairro Umuarama, Uberlândia, Minas Gerais 38400-902, Brazil. E-mail: pbfsoares@yahoo.com.br. Phone: +55 (34) 99977-0088.

Abstract

Despite current advances in microCT analysis, the influence of some image acquisition parameters on the morphometric analysis have not been fully elucidated. Thus, the aim of this study was to determine if data binning and averaging affects morphometrics outcome of the bone repair tissue. Four Wistar rats' tibiae with the bone defect surgically created were individually scanned six times using a microCT unit. Each image acquisition was performed changing the frames averaging set for 1 and 2, while the software binning was configured for the values 1, 2 and 4. ANOVA two-way was performed to assess the effect of frame averaging and data binning, with Bonferroni post hoc test ($p < 0.01$). The effect of data averaging was not significant for all parameters and no interactions between the factors were observed. The more the data binning was increased, the larger was trabecular thickness values. In contrast, lowest values of bone volume fraction and bone volume were found as data binning increased. Trabecular number and trabecular separation were not influenced. In conclusion, morphometrics outcome of bone repair analysis in microCT demonstrated dependency upon software binning. Therefore, image acquisition of small structures such as rat trabeculae should be performed without data binning.

Keywords: X-Ray Microtomography; image Processing, Computer-Assisted; image pixel size; bone repair

Introduction

Bone is a dynamic tissue and its repair process involves innumerable events to achieve bone formation and to restore the damaged tissue¹⁻³. Systemic and local conditions such as osteoporosis⁴, uncontrolled diabetes⁵ and radiotherapy⁶ have been associated with an arrest of the physiological bone formation and microarchitecture deterioration⁷. Comprehension of the mechanical and biological behavior of the bone tissue as well as the therapeutic strategies in compromised situations is necessary to overcome the impairment caused by these conditions⁸.

Microtomographic analysis in animal rodents provides a novel perspective of therapies that aim bone healing enhancement. Animal models of several diseases, treatments and the pre-clinical understanding of disease manifestations are assessed through microCT. It is currently considered the gold standard to evaluate bone tissue microarchitecture three-dimensionally (3D) which complements the traditional histomorphometry⁹⁻¹². The non-destructive technique, convenience, time-saving, and volumetric analyses provided by the method are appealing to analyze bone cortical and trabecular architecture¹³⁻¹⁵.

Due to the polychromatic characteristics of X rays beams in microCT, several parameters settings can be selected for image acquisition in microCT in order to achieve signal to noise ratio (SNR) improvement. SNR compares the level of the desired signal to the level of the undesirable background noise within an image¹⁶. The number of projections taken (frame averaging) in each rotation step of the sample (*ex vivo* scanning) or the tube-detector system (*in vivo* scanning) during image acquisition is previously determined. A set of projections is obtained and only the mean image is recorded⁹. Thus, the noise can be reduced by increasing frame averaging, but longer scan time is needed in detriment of more scan cycles^{9,14,17}.

During image acquisition each pixel of the detector can be counted individually, although the resulting signals are low. In 2x camera binning, a pixel size becomes 2x2 pixels and in 4x, camera binning is 4x4 pixels. The detector hardware allows the pixel combination during image acquisition that generates more contrast and less noise at the cost of image resolution, which is reduced. However, to boost the contrast might be desirable in certain situations, especially when scanning strongly attenuating structures. Implementing image binning reduces file sizes, thus leading to faster image processing¹⁶⁻¹⁸.

Despite current advances, the influence of some image acquisition parameters on the morphometric analysis have not been fully elucidated. Parameter settings for image acquisition such as the software binning and data averaging, are rarely reported¹⁷ and little is known regarding its effects on the results of structural quantification. To our knowledge, no study has already evaluated the effect of these parameters on microCT analysis of bone repair.

Thus, the aim of this study was to answer the following question: “Is there any effect of the software binning and averaging data for μ CT image acquisition on the morphometrics outcome of the bone repair?” The null hypothesis was that the parameters would not influence the outcome from μ CT analysis.

Methods

This study was carried out following the ethical principles for the care and use of laboratory animals and according to the ARRIVE guidelines. The samples were obtained from a previous approved study in The Committee on the Ethics of Animal Experiments of Universidade Federal de Uberlândia (Protocol Number: 076/17, CEUA-UFU), thus it was exempted from reviewing. The surgical procedure was performed as previously described²⁸. Briefly, four animals were submitted to general anesthesia intraperitoneally and surgical access to the left tibial metaphysis was obtained. A bone defect was performed with a drill measuring 1.6mm diameter (Neodent, Curitiba, Brazil) at 12.000 rpm, under copious irrigation with sterile saline solution of 0.9% sodium chloride. The suture was performed with 4-0 nylon surgical monofilament. All procedures were performed by a single operator (MSI). After 7 days, the animals were submitted to euthanasia by intraperitoneal overdose of thiopental (150 mg/kg). The tibiae were removed and covered with moist gauze containing sterile saline solution of 0.9% sodium chloride and frozen at -20°C until the time of analysis.

Four Wistar rats' tibiae with the bone defect were individually scanned six times using a microCT unit (μ CT 40, Scanco Medical, Bruttisellen, Switzerland). Each sample was wrapped in wet paper and positioned with the long axis perpendicular to the horizontal plane. The following scanning settings were used: 70 kV, 114 μ A, 10 μ m voxel size, 1 mm-thick Al filter, rotation step of 0.5° and 180° rotation. Each image acquisition was performed changing the frames averaging set for 1 and 2, while the software binning was configured for the values 1, 2 and 4.

The raw data were exported to NRecon software (Bruker, Kontich, Belgium). The images were reconstructed using the following settings: 30% for beam hardening correction, 0 for smoothing and 5 to reduce ring artifacts. Bone

volume (BV) (mm^3), tissue volume (TV) (mm^3), Bone volume fraction (BV/TV), trabecular thickness (Tb.Th), trabecular number (Tb.N) and trabecular separations (Tb.Sp) of the reconstructed volumes were assessed using the software CtAn (Bruker microCT, Kontich, Belgium). For this, the region of interest (ROI) was manually draw in each slice to delineate the lesion area. The same threshold (50-255) was set in all samples for bone segmentation. A single experient operator (PBFS) performed all analyses. The system of the device used for image acquisition (Scanco Medical, Bruttisellen, Switzerland) was distinct from the software employed for data reconstruction and analysis (Bruker, Kontich, Belgium). Thus, data binning of pixel matrices during image acquisition were computed in the results obtained from CtAn (Bruker, Kontich, Belgium) by multiplying linear measurements for 2 (binning 2x2) and 4 (binning 4x4), while volumetric measurements were multiplied for 7.99 (binning 2x2) and 64.94 (binning 4x4). These calculations allowed compatible linear and volumetric data between image acquisition and processing.

Statistical Analysis

Statistical analysis was performed using Sigma Plot software (version 13.1; Systat Software Inc., San Jose, CA, USA). Data were tested for normal distribution (Shapiro–Wilk's test) and equality of variances (Levene's test). ANOVA two-way was performed to assess the effect of frame averaging and data binning on the morphometric parameters, with Bonferroni post hoc test to compare the mean and standard deviation of the groups. Due to the multiple tests ($n=5$) for each parameter, the Bonferroni correction was applied, which adjusted the significance level from 0.05 to 0.01.

Results

TV mean values and standard deviations of the groups are shown in Table 1. Two-way ANOVA showed no significant effect of the data binning ($P = 0.78$) and frame averaging ($P = 0.63$). Interaction between them ($P = 0.80$) was not observed.

BV mean values and standard deviations for each group are demonstrated in Table 2. Two-way ANOVA showed a significant effect of the binning parameter ($P = 0.01$), however no significant effect was observed for data averaging ($P = 0.91$), and for interaction between both parameter ($P = 0.95$). There was no difference between Bin1 and Bin2 groups ($P = 0.76$), or between Bin2 and Bin4 ($P = 0.11$). However, Bin1 was statistically different ($P = 0.009$) from Bin4, irrespective of the levels of data averaging used.

BV/TV mean values and standard deviations of each group are shown in Table 3. The influence of data averaging and binning on BV/TV was in agreement with the results from BV analysis. Two-way ANOVA showed a significant effect of the binning parameter ($P < 0.001$), however no significant effect was observed for data averaging ($P = 0.72$), and for interaction between both parameters ($P = 0.99$). There was no difference between Bin1 and Bin2 groups ($P = 0.66$), or between Bin2 and Bin4 ($P = 0.02$). However, Bin1 was statistically different ($P < 0.001$) from Bin4, irrespective of the levels of data averaging used.

Tb.Th mean values and standard deviations of each group are shown in Table 4. The effect of data averaging was not significant ($P = 0.68$). However, data binning effect on Tb.Th was observed in all levels ($P < 0.001$), without interaction with frame averaging parameters ($P = 0.86$). The more the data binning was increased, the larger was Tb.Th. Statistical differences with a P value < 0.001 were found in all comparisons.

Tb.N and Tb.Sp mean values and standard deviations are presented in Table 5 and 6, respectively. Data averaging did not affect neither Tb.N ($P = 0.88$), nor Tb.Sp ($P = 0.81$). In the same way, there was no influence of image binning in Tb.N ($P = 0.16$) and Tb.Sp ($P = 0.17$). Thus, no interaction was found between the parameters for both Tb.N ($P = 0.96$) and Tb.Sp ($P = 0.74$).

Figure 1 shows a representative slice of the reconstructed data of each acquisition parameter of the correspondent region in the same sample.

Discussion

MicroCT is one of the most commonly used methods to improve the knowledge of the microstructures of bone tissue under several pathological conditions. The aim of this study was to determine if data binning and averaging affects the morphometric outcome of the bone tissue repair. This study showed that data binning affected specific bone microstructure measurements. In contrast, no significant difference was observed in the evaluated parameters after comparison of one or two projections averaging during image acquisition.

The samples of the experiment were sequentially scanned and reconstruction parameters were the same for all groups. Every effort was made to reduce the influence of confounding factors in the analysis. However, a degree of error was unavoidable. Each sample had its region of interest manually delineated because of the different pixel binning, thus tissue volume (TV) variations could be slightly detected. Despite that, no significant difference in volume extracted was shown.

Scanning at 10 μm voxel size for rat trabeculae assessment is considered suitable for the analysis¹², however image quality relies on further factors determined by the spatial resolution. Spatial resolution is the minimum difference between two objects that is needed to be able to distinguish them as separate sources in the reconstructed image¹⁹. In other words, it indicates the ability to differentiate small structures. Image processing can be impacted by other factors rather than voxel size, such as image resolution, noise, artifacts, and post-acquisition processing (e.g., filtering)²⁰.

Data binning decreases image resolution. Our findings revealed that this operation affected trabecular thickness measurements significantly. The more the data binning was increased, the larger was Tb.Th. The same behavior has been demonstrated by previous studies in which Tb.Th was consistently found to increase as voxel size increased^{21,22}. This pattern of dependence was expected mainly because larger voxel size scans led to the loss of detection of small trabeculae (partial volume effect). However, software binning shows a distinct mechanism that increases pixel/voxel size only after signal acquisition without affecting scan time¹⁶. Higher contrast was observed, as expected, but this

effect was noted only in the largest and most mineralized structures such as cortical bone. In the bone defect area, the trabeculae are thinner and closely arranged. Distinct levels of mineralization of the woven bone led to the occurrence of pixels displaying wider gray level intervals in this area, most of them indicating lower attenuation degree. When software binning is used, only the thickest portion of the trabeculae were segmented. Thinner structures less mineralized had its attenuation dissolved by pixel binning since a global threshold was further applied. Bone volume fraction (BV/TV) and BV reduction also reflects this effect. Although an increase in Tb.N and Tb.Sp values is expected as a result of this trabeculae “disruption” after segmentation, they did not demonstrate dependency of the binning process. Probably, not only the smallest portion of the trabeculae were undetected, but also the finest trabeculae dispersed in the healing area that counterbalancing the measurements.

Signal to noise ratio is simultaneously dependent from the number of incident photons in the detector and the sensitivity of the charge-coupled detector¹⁹. Frame averaging can reduce the noise from intensity fluctuations above and below the actual image intensity. This noise has a random pattern even for continuous exposure parameters²³. In the present study the increase in data averaging (1 to 2) had no effect in the evaluated parameters. This result should be cautiously interpreted. First, only the repair tissue of rats' tibia was analyzed in this study. The effect of data averaging on root resorption volume in rats has been previously demonstrated¹⁷. Therefore, further studies should investigate if such findings remain on different bony tissues and structures. Besides, Bonferroni correction was applied to reduce inflated type I error since multiple comparisons were performed. It warrants higher reliability and reproducibility of the differences observed in our findings. An impractical sample size would be required to ensure the data averaging influence on the analysis of our samples. Considering the ethical aspects of studies in animals, it seemed inappropriate an enormous increase in the sample size in order to verify the occurrence of small differences in stereological measurements due to different data averaging values. Moreover, in bone repair investigations, the size effects of assessed independent variables are usually great enough to be clinically

relevant²⁴. This fact would probably make the data averaging influence on bone repair analysis become irrelevant, if it exists. Despite that, using the same parameter throughout image acquisition of all groups is strongly recommended.

In microCT experimentations two features must be considered: time consumption and data storage. Time consumption is pertinent to both human resources and equipment depreciation. Besides, taking into account *in vivo* scanning, it is even more critical. It has been demonstrated that a standard microCT scan resulted in consistently high radiation doses (0.295–0.507 Gy per scan)²⁵. The radiation levels in microCT observed in the mentioned experiment are usually not lethal; but have the potential to influence the experimental outcomes by disturbing the immune response and other physiological processes. Moreover, *in vivo* scanning requires the subject to be anesthetized making longer scanning unfeasible. In this context, increased data averaging requires longer scanning periods¹⁷ and image binning impact the file size¹⁶. The required disc space for data storage involves some practical questions regarding the maintenance and sharing of such a large amount of data²⁶. Thus, to evaluate image parameters are necessary to provide information to assist the researchers in the determination of the scan protocols weighing factors such as scan time, field of view, and image resolution.

Selection of parameters during the analysis in microCT may have significant effects on the results and affect reproducibility^{22,27}. There is limited information in the current literature regarding standardization of important parameters during scanning, reconstruction, analysis and reporting of data from bone repair tissue, which makes it difficult to compare with other models and studies. Based on the results found in the present study, it is also opportune to study the influence of others image acquisition parameters, and different microCT devices should be assessed.

In conclusion, the morphometric outcome of bone repair analysis in microCT demonstrated dependency upon software binning. Trabecular thickness was the most influenced parameter. Image acquisition of small structures such as rat trabeculae should be performed without data binning. In contrast, no difference was observed by increasing the frame averaging value to 2 and further

studies are desired to elucidate the influence of different values of averaged projections during image acquisition.

References

1. Schmidt-Bleek, K., Petersen, A., Dienelt, A., Schwarz, C. & Duda, G. N. Initiation and early control of tissue regeneration-bone healing as a model system for tissue regeneration. *Expert Opinion on Biological Therapy* vol. 14 (2014).
2. Lin, C. Y. *et al.* 2,3,5,4'-Tetrahydroxystilbene-2-O-beta-D-glucoside promotes the effects of dental pulp stem cells on rebuilding periodontal tissues in experimental periodontal defects. *J. Periodontol.* doi:10.1002/jper.19-0563.
3. Vieira, A. E. *et al.* Intramembranous bone healing process subsequent to tooth extraction in mice: Micro-computed tomography, histomorphometric and molecular characterization. *PLoS One* **10**, (2015).
4. de Oliveira, D. *et al.* Short term sodium alendronate administration improves the periimplant bone quality in osteoporotic animals. *J. Appl. Oral Sci.* **25**, (2017).
5. Pitol-Palin, L. *et al.* Different stages of alveolar bone repair process are compromised in the type 2 diabetes condition: An experimental study in rats. *Biology (Basel)*. **9**, (2020).
6. Mendes, E. M. *et al.* Effects of ionizing radiation on woven bone: influence on the osteocyte lacunar network, collagen maturation, and microarchitecture. *Clin. Oral Investig.* **24**, (2020).
7. Chen, H., Liu, N., Xu, X., Qu, X. & Lu, E. Smoking, Radiotherapy, Diabetes and Osteoporosis as Risk Factors for Dental Implant Failure: A Meta-Analysis. *PLoS One* **8**, (2013).
8. Ribeiro, F. V. *et al.* Resveratrol reverses the negative effect of smoking on peri-implant repair in the tibia of rats. *Clin. Oral Implants Res.* **30**, (2019).
9. Bouxsein, M. L. *et al.* Guidelines for assessment of bone microstructure in rodents using micro-computed tomography. *J. Bone Miner. Res.* **25**, 1468–

- 1486 (2010).
10. Faot, F., Chatterjee, M., de Camargos, G. V., Duyck, J. & Vandamme, K. Micro-CT analysis of the rodent jaw bone micro-architecture: A systematic review. *Bone Reports* vol. 2 (2015).
 11. Mashiatulla, M., Ross, R. D. & Sumner, D. R. Validation of cortical bone mineral density distribution using micro-computed tomography. *Bone* **99**, (2017).
 12. van 't Hof, R. J. & Dall'Ara, E. Analysis of bone architecture in rodents using micro-computed tomography. in *Methods in Molecular Biology* vol. 1914 (2019).
 13. Irie, M. S. *et al.* Use of micro-computed tomography for bone evaluation in dentistry. *Braz. Dent. J.* **29**, 227–238 (2018).
 14. Chavez, M. B. *et al.* Guidelines for Micro-Computed Tomography Analysis of Rodent Dentoalveolar Tissues. *JBMR Plus* vol. 5 (2021).
 15. Lyu, H. Z. & Lee, J. H. Correlation between two-dimensional micro-CT and histomorphometry for assessment of the implant osseointegration in rabbit tibia model. *Biomater. Res.* **25**, (2021).
 16. Nair, M., Shepherd, J. H., Best, S. M. & Cameron, R. E. MicroCT analysis of connectivity in porous structures: Optimizing data acquisition and analytical methods in the context of tissue engineering. *J. R. Soc. Interface* **17**, (2020).
 17. Friedrichsdorf, S. P., Arana-Chavez, V. E., Cattaneo, P. M., Spin-Neto, R. & Dominguez, G. C. Effect of the software binning and averaging data during microcomputed tomography image acquisition. *Sci. Rep.* **9**, (2019).
 18. Oliviero, S., Lu, Y., Viceconti, M. & Dall'Ara, E. Effect of integration time on the morphometric, densitometric and mechanical properties of the mouse tibia. *J. Biomech.* **65**, (2017).
 19. Rueckel, J., Stockmar, M., Pfeiffer, F. & Herzen, J. Spatial resolution characterization of a X-ray microCT system. *Appl. Radiat. Isot.* **94**, (2014).
 20. Campbell, G. M. & Sophocleous, A. Quantitative analysis of bone and soft tissue by micro-computed tomography: applications to ex vivo and in vivo studies. *Bonekey Rep.* **3**, (2014).

21. Cooper, D., Turinsky, A., Sensen, C. & Hallgrímsson, B. Effect of voxel size on 3D micro-CT analysis of cortical bone porosity. *Calcif. Tissue Int.* **80**, (2007).
22. Longo, A. B., Salmon, P. L. & Ward, W. E. Comparison of ex vivo and in vivo micro-computed tomography of rat tibia at different scanning settings. *J. Orthop. Res.* **35**, 1690–1698 (2017).
23. Takeda, K. *et al.* Periodontal regenerative effect of enamel matrix derivative in diabetes. *PLoS One* **13**, e0207201 (2018).
24. Serdar, C. C., Cihan, M., Yücel, D. & Serdar, M. A. Sample size, power and effect size revisited: Simplified and practical approach in pre-clinical, clinical and laboratory studies. *Biochem. Medica* **31**, (2021).
25. Willekens, I. *et al.* Evaluation of the radiation dose in micro-CT with optimization of the scan protocol. *Contrast Media Mol. Imaging* **5**, (2010).
26. Cengiz, I. F., Oliveira, J. M. & Reis, R. L. Micro-computed tomography characterization of tissue engineering scaffolds: effects of pixel size and rotation step. *J. Mater. Sci. Mater. Med.* **28**, (2017).
27. Pyka, G., Kerckhofs, G., Schrooten, J. & Wevers, M. The effect of spatial micro-CT image resolution and surface complexity on the morphological 3D analysis of open porous structures. *Mater. Charact.* **87**, (2014).
28. OSUNA, L. G. G. *et al.* Influence of bone defect position and span in 3-point bending tests: experimental and finite element analysis. *Braz. Oral Res.* **35**, (2021).

Acknowledgments

The authors are grateful to Rede de Biotérios de Roedores da Universidade Federal de Uberlândia, to the Department of Radiology da Universidade do Triângulo Mineiro (UFTM) for the animals's radiotherapy and the Research Laboratory of the Department of Dentistry and Oral Health (Aarhus University).

This study was supported by grants from the Fundação de Amparo à Pesquisa de Minas Gerais (FAPEMIG), the Coordenação de Aperfeiçoamento de Pessoal

de Nível Superior – Brasil (CAPES) – Finance Code 001 and Conselho Nacional de Desenvolvimento Científico e Tecnológico (CNPq)

Competing interests

The author(s) declare no competing interests.

Figure 1

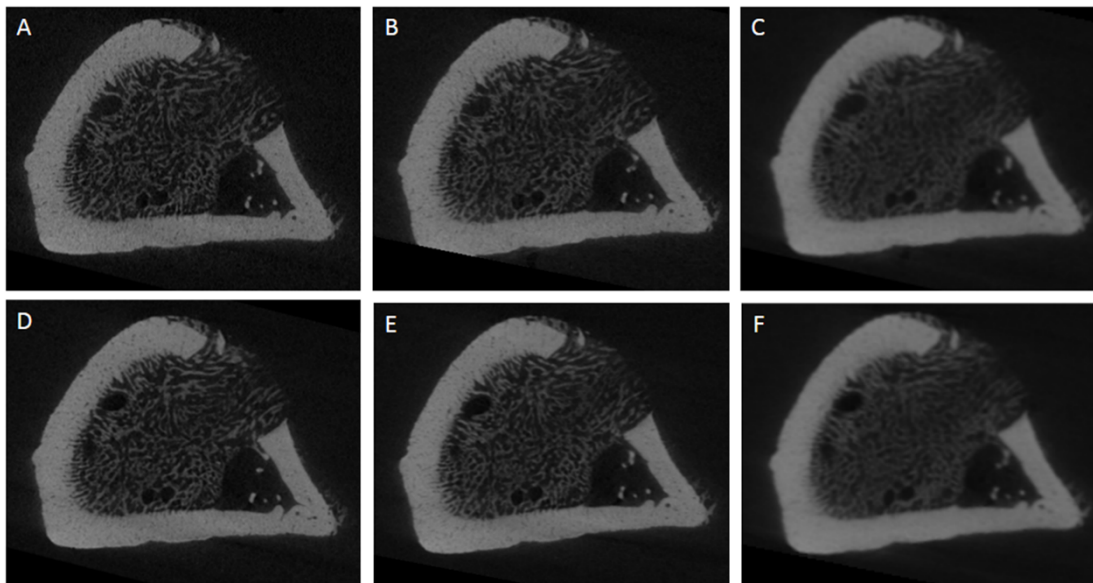


Figure caption

Figure 1. Representative slice of the reconstructed data of each acquisition parameter (A) Frame averaging = 1, data binning = 1; (B) Frame averaging = 1, data binning = 2; (C) Frame averaging = 1, data binning = 4; (D) Frame averaging = 2, data binning = 2; (E) Frame averaging = 2, data binning = 2; (F) Frame averaging = 2, data binning = 4.

Tables

Table 1. Mean and standard deviation of TV values

	TV (mm ³)	
	Avg 1	Avg 2
Bin 1	309.4 ± 39.1 ^{Aa}	291.9 ± 39 ^{Aa}
Bin 2	289.1 ± 33.4 ^{Aa}	290.8 ± 23 ^{Aa}
Bin 4	297.1 ± 12.1 ^{Aa}	294.8 ± 28 ^{Aa}

Different uppercase letters in vertical columns indicate significant differences; different lowercase letters in horizontal rows indicate significant differences; Bonferroni posthoc test (P<.05).

Table 2. Mean and standard deviation of BV values

	BV (mm ³)	
	Avg 1	Avg 2
Bin 1	50.2 ± 18.6 ^{Aa}	48.2 ± 17.3 ^{Aa}
Bin 2	39.9 ± 14.3 ^{Aa}	42.0 ± 13.4 ^{Aa}
Bin 4	24.1 ± 7.4 ^{Ba}	26.0 ± 10.6 ^{Ba}

Different uppercase letters in vertical columns indicate significant differences; different lowercase letters in horizontal rows indicate significant differences; Bonferroni posthoc test (P<.05).

Table 3. Mean and standard deviation of BV/TV values

	BV/TV (%)	
	Avg 1	Avg 2
Bin 1	15.9 ± 4.1 ^{Aa}	16.2 ± 3.7 ^{Aa}
Bin 2	13.5 ± 3.5 ^{Aa}	14.2 ± 3.4 ^{Aa}
Bin 4	8.1 ± 2.2 ^{Ba}	8.6 ± 2.8 ^{Ba}

Different uppercase letters in vertical columns indicate significant differences; different lowercase letters in horizontal rows indicate significant differences; Bonferroni posthoc test (P<.05).

Table 4. Mean and standard deviation of Tb.Th values

	Tb.Th	
	Avg 1	Avg 2
Bin 1	0.13 ± 0.00 ^{Aa}	0.14 ± 0.01 ^{Aa}
Bin 2	0.17 ± 0.01 ^{Ba}	0.18 ± 0.01 ^{Ba}
Bin 4	0.27 ± 0.02 ^{Ca}	0.26 ± 0.03 ^{Ca}

Different uppercase letters in vertical columns indicate significant differences; different lowercase letters in horizontal rows indicate significant differences; Bonferroni posthoc test (P<.05).

Table 5. Mean and standard deviation of Tb.N values

	Tb.N	
	Avg 1	Avg 2
Bin 1	1.20 ± 0.3 ^{Aa}	1.16 ± 0.6 ^{Aa}
Bin 2	1.63 ± 0.7 ^{Aa}	1.65 ± 0.6 ^{Aa}
Bin 4	1.22 ± 0.4 ^{Aa}	1.33 ± 0.4 ^{Aa}

Different uppercase letters in vertical columns indicate significant differences; different lowercase letters in horizontal rows indicate significant differences; Bonferroni posthoc test (P<.05).

Table 6. Mean and standard deviation of Tb.Sp values

	Tb.Sp	
	Avg 1	Avg 2
Bin 1	1.18 ± 0.6 ^{Aa}	1.30 ± 0.6 ^{Aa}
Bin 2	1.69 ± 0.3 ^{Aa}	1.66 ± 0.3 ^{Aa}
Bin 4	2.01 ± 0.1 ^{Aa}	1.90 ± 0.1 ^{Aa}

Different uppercase letters in vertical columns indicate significant differences; different lowercase letters in horizontal rows indicate significant differences; Bonferroni posthoc test (P<.05).

3.4 Capítulo 4

Artigo será submetido ao periódico Oral Surgery, Oral Medicine, Oral Pathology, and Oral Radiology

Effect of ionizing radiation and LLLT (low-level laser therapy) on grafted and non-grafted lesions – an experimental study

Milena Suemi Irie¹, Rubens Spin-Neto², Paula Dechichi¹, Ann Wenzel², Priscilla Barbosa Ferreira Soares¹

¹ Department of Periodontology and Implantology, School of Dentistry, Federal University of Uberlândia, Avenida Pará s/nº, Campus Umuarama, Bloco 4L, Bairro Umuarama, 38400-902, Uberlândia, Minas Gerais, Brazil.

² Department of Dentistry and Oral Health, Section for Oral Radiology, Health, Aarhus University, Arhuus C, 8000, Aarhus, Denmark

Corresponding author:

Priscilla Barbosa Ferreira Soares

Address: Avenida Pará s/nº, Campus Umuarama, Bloco 4L, Bairro Umuarama. Uberlândia - Minas Gerais – Brazil, 38.400-902. Phone/ Fax: +55 (34) 3225-8106. e-mail: pbfsoares@yahoo.com.br

Acknowledgements

The authors are grateful to Rede de Biotérios de Roedores da Universidade Federal de Uberlândia, to the Department of Radiology da Universidade do Triângulo Mineiro (UFTM) for the animals's radiotherapy and the Research Laboratory of the Department of Dentistry and Oral Health (Aarhus University).

This study was supported by grants from the Fundação de Amparo à Pesquisa de Minas Gerais (FAPEMIG), the Coordenação de Aperfeiçoamento de Pessoal de Nível Superior – Brasil (CAPES) – Finance Code 001 and Conselho Nacional de Desenvolvimento Científico e Tecnológico (CNPq)

Effect of ionizing radiation and LLLT (low-level laser therapy) on grafted and non-grafted lesions – an experimental study

Abstract

Objectives: Evaluate the effects of a single dose of ionizing radiation (15 Gy) and infrared LLLT (low-level laser therapy) application in grafted and non-grafted defects on bone microarchitecture and collagen maturity.

Materials and Methods: Bone defects were surgically created on rats femurs. The right side was filled by clot and the left side deproteinized bovine bone mineral (DBBM) graft were inserted (Xenograft groups). Animals were aleatory divided into four groups (n = 8): nRTX: without ionizing radiation; RTX: with ionizing radiation; nRTX/LLLT: without ionizing radiation with LLLT application; RTX/LLLT: with ionizing radiation and without LLLT application. Microtomographic, histological and histomorphometric analyses were performed 14 days after the surgery. Three-way ANOVA with Tukey post-hoc test was used to compare the groups ($\alpha = 5\%$).

Results: MicroCT analysis revealed that radiotherapy led to lower values of BV/TV, relative BV/TV and Tb.N in both Clot and Xenograft groups. Regardless the radiotherapy treatment, defects filled with xenograft showed higher values of Relative BV/TV and Tb.N , in contrast, Clot groups demonstrated increased values of BV/TV ($p < 0.001$) and Tb.Th. Application of infrared LLLT did not affect the results. Histomorphometric results was in agreement with microCT analysis. Intermediately and densely packed collagen were predominant among the groups. Histological analysis revealed a disorganized bone formation bridging the cortical borders of the lesion in RTX groups. Primary bone involving the particles was commonly observed in all Xenograft groups and radiotherapy and LLLT treatments did not affect the percentage of bone-graft contact ($p > .05$)

Conclusions: Ionizing radiation affected the bone repair demonstrated by a smaller amount of newly formed bone in both grafted and non-grafted defects. However, the incorporation of the graft particles was maintained after irradiation. LLLT did not improve the bone healing. The promising results related to the osteoconductive property of the bone graft particles applied before irradiation

should encourage more efforts to investigate its application in clinical conditions before the radiotherapy onset.

Keywords Ionizing radiation; bone repair; bone substitutes; x-ray microtomography; collagen; low-level laser therapy.

Introduction

Worldwide new cases of cancer are estimated to 19.3 million in 2020.¹ Most of the patients undergo radiation therapy. While tumor radiation improves patient survival, it also has an effect on healthy tissue. Ionizing radiation (IR) in the bone might affect its volume, composition and microarchitecture.² Both organic and mineral components of the matrix are damaged³. Osteoradionecrosis (ORN) is one of the most severe complications due to radiation of head and neck tumors. Blood vessel narrowing leads to hypocellular tissue, hypoxia and necrosis of the bone.⁴ Tooth extraction after radiotherapy is a risk factor for ORN. Thus, it has been suggested to perform pretreatment extraction and surgical intervention when it is indicated.⁵

Squamous cell carcinoma treatment usually requires surgical resection and radiotherapy which lead to functional maxillofacial sequelae.⁶ Prosthetic rehabilitation with implants might be an option for these patients who have suffered considerable tissue loss. In this context, timing of implant installation is still under discussion. Despite the risk of ORN, some studies have shown the viability of dental implant placement in a delayed timing (after radiotherapy).⁷⁻⁹ However, to avoid a second intervention, implant placement has more recently been placed simultaneously at the time of ablative surgery and free flap reconstruction with elevated success rates.¹⁰⁻¹² The viability of immediate implant placement after tooth extractions performed at the time of the ablative surgery or in routine dental evaluations before radiotherapy has also been demonstrated.¹³

In a healthy condition, socket preservation has been recommended to maintain bone volume after dental extraction. In cases of insufficient bone tissue for further implant placement, socket preservation is of greater importance. Techniques using socket grafting biomaterials seem to be more effective in the

reduction of the bone height remodeling than non-grafted sockets.¹⁴ As mentioned above, dental implant in patients who undergo postoperative radiotherapy has become widely accepted recently as a method to restore function and esthetic due to ablative surgeries.¹⁵ The association of a particulate bone graft might be advantageous for volume maintenance of the reconstruction site in these cases. There is no evidence about using xenogeneic bone substitute in areas that will be further included in the radiation field for head and neck cancer treatment. A proper clinical management and reconstruction techniques with dental implants can greatly improve the rehabilitative potential for these patients.¹¹

Low level laser therapy has been considered an important approach for various medical issues including tissue healing¹⁶. Its biological effects, known as photobiomodulation, is resulted from light application that stimulate cell responses. In the bone tissue, an increase in osteocyte number was observed after LLLT.¹⁷ Ionizing radiation compromises bone metabolism by reducing angiogenesis and osteogenesis.¹⁸ On the opposite side, LLLT (830nm) resulted in positive effects on healing represented by a greater amount of bone formation and blood vessels in the fracture area.¹⁶ LLLT also has provided favorable results in bone defects filled with biomaterials (bovine inorganic bone and hydroxyapatite).¹⁹ However, there is no evidence regarding LLLT effect on bone repair in defects filled with inorganic biomaterial before radiation. Thus, the aim of this study was to assess the effect of a single dose of ionizing radiation (15 Gy) and LLLT application in grafted and non-grafted defects.

Materials and Methods

Study design

This study followed the normative guidelines of the National Council for Animal Control and Experimentation (CONCEA), a constituent of the Ministry of Science, Technology and Innovation (MCTI; Law 11.794, 08/19/2008), Brazil. The Bioethics Committee for Animal Experimentation of the Universidade Federal de Uberlândia has approved the experimental protocol (CEUA #093/17). Thirty-

Two *Rattus norvegicus* rats (average of 300g), were kept in cages with a 12-hour light-dark cycle, and controlled temperature conditions (average 22 ± 2 oC). Diet consisted of standard laboratory pellets (Labina, Purina®, Paulínia, SP, Brazil) and water ad libitum.

Initially, the animal legs were trimmed and cleaned with a 0.2% chlorhexidine solution (Rioquímica, São José do Rio Preto, SP, Brazil) to prevent possible infections. Then, the animals were submitted to intraperitoneal anesthesia combining 100mg/kg of 10% ketamine hydrochloride (Ketamina Agener®; Agener União Ltda, São Paulo, SP, Brazil) with 10mg/kg of 2% xylazine hydrochloride (Rompum ® Bayer SA, São Paulo, SP, Brazil). Incisions of 3 cm length were performed and bone defects were created using a spherical carbide burr (no 8) (Angelus Prima Dental, Londrina, PR, Brazil) measuring 2.1 mm of diameter. The depth of perforation was limited to the rupture of the cortical bone. The right side was left ungrafted filled only by clot (Clot groups). The left side was filled with inorganic particulate xenogeneic bone graft (Xenograft groups) (Bio-oss® Small, Geistlich Pharma AG, Wolhusen, Switzerland). Aliquots of the bone graft particles were previously separated in eppendorf tubes in a sterile environment (laminar flow cabinet). After the surgery, the animals were randomly divided into four groups (n = 8): (a) nRTX: without ionizing radiation; (b) RTX: with ionizing radiation (single dose 15Gy); (c) nRTX/LLLT: without ionizing radiation with LLLT application; (d) RTX/LLLT: with ionizing radiation (single dose 15Gy) and without LLLT application. The randomization was obtained on the website *random.org*. All the procedures were performed by a single research (MSI).

Application of LLLT

The groups nRTX/LLLT and RTX/LLLT were submitted to laser therapy using a gallium-aluminum-arsenide (GaAlAs) infrared laser diode (Flash lase III, DMC Equipamentos/São Carlos, SP, Brazil) with a continuous wavelength of 830 nm, 50 mW of potency, and 0.028-cm² beam diameter. The protocol consisted of transcutaneous applications in four points equidistant (6mm) from each other around the defect, with a fluence of 16 J/cm² with the laser tip positioned over and perpendicular to the long axis of the bone.

Applications were made immediately after the surgery and every 48h, extending for 15 days.²⁰

Ionizing radiation

Seven days after surgical procedure, RTX and RTX/LLLT groups received a single dose of 15 Gy of ionizing radiation on both legs through a medical linear accelerator 6MeV (Varian 600-C © Varian Medical System Inc Palo Alto, California, USA). Animals were submitted to general anesthesia by an intraperitoneal injection of 100 mg/kg ketamine and 70 mg/kg xylazine hydrochloride to be immobilized and fixed with tape. A bolus measuring 1,5cm of width was placed over the legs of all animals. Animals of nonirradiated (nRTX and nRTX/LLLT) group were also anesthetized (sham method). All animals were euthanized 14 days after the surgical procedure with intravenous injection of 150mg/kg of 2.5% thiopental. Femurs were removed and immediately fixed in 4% phosphate-buffered paraformaldehyde solution during 48h (Figure 1). The samples were first scanned using X-ray microcomputed tomography (micro-CT). Subsequently, the samples were decalcified in 4% EDTA for 5 weeks, dehydrated with graded ethanol and embedded in paraffin. Longitudinal histological sections of 5 µm were obtained and stained with hematoxylin and eosin (H&E) for qualitative analysis, Mallory's trichrome stain for histomorphometric analysis and Picrosirius Red for quantitative collagen analysis.

Histomorphometric analysis Micro-CT analysis

The samples were scanned using microcomputed tomography Skyscan 1176 microcomputed tomography (Bruker, Kontich, Belgium) with a nominal isotropic voxel size of 9 µm (X-ray source 70 kV, 276 µA) using an aluminum filter (1 mm of thickness) and 180° rotation with an angular increment of 0.4° and averaging of 2 frames. The reconstructions were performed using the software nRecon (version 1.6.10.1, SkyScan, Bruker, Belgium), following the parameters of smoothing (0), ring artifacts reduction (12) and beam-hardening (30%) for all samples. Each dataset was opened in the software DataViewer (version 1.5 1.2. SkyScan, Bruker, Belgium) and the samples were rotated until

the longitudinal axis of the tibiae were parallel to the horizontal plane. The coronal views were saved for further analysis. The images were analyzed in CTAn software (version 1.14.4.1, SkyScan, Bruker, Belgium) using a standard threshold 82-255 for the Clot groups. The threshold was defined as the mean of the automatic threshold values (Otsu method) calculated from 10 samples. For Xenograft groups analysis, the volume of the graft particles was calculated applying the threshold value of 129-255. This value was obtained by calculating the predominant gray values in the histogram of the particles selected alone. The mean value obtained from 10 samples was used. The bone volume fraction (BV/TV) results were obtained using the threshold of 82-128. The region of interest included only the area of the newly formed bone using a circular predefined shape measuring 2.3 mm (size of the lesion), respecting the limits of the top to the bottom of the lesion. In order to obtain a standard protocol of analysis, the number of slices comprising the perforated cortical was assessed and the 50 slices (approximately 0.45mm) in the middle were selected. This volume of interest (VOI) corresponded to the cortical portion of the lesion. A single operator carried out all the analysis. The percent bone volume (BV/TV), trabecular thickness (Tb. Th), trabecular number (Tb. N), trabecular separation (Tb. Sp), were analyzed. In Xenograft groups, the bone volume fraction was also calculated subtracting the bone graft volume from the total volume, denominated "Relative BV/TV".

Bone matrix quantification and qualitative analysis

Masson's trichrome-stained and hematoxylin eosin (HE) sections were used to obtain histologic images of the lesion captured using a light microscope (Olympus BX61, Olympus Corporation, Tokyo, Japan) connected to a digital camera (Olympus DP80, Olympus Corporation, Tokyo, Japan) with an objective lens of 20x.

For the histomorphometric analysis, the Masson's trichrome-stained sections were evaluated. The HE sections were used for a general histologic analysis. A dedicated software (ImageJ 1.51k, Wayne Rasband, National Institute of Health, USA) was used for the quantitative analysis. A rectangular

area of interest (AOI) drawn between the cortices and the borders of the lesion was defined for each section. The software aleatorily generated a “grid”, providing an area of 3,675 pixels on top of each image. The grid was represented by intersecting lines with a distance between neighboring counting points of 40 µm. This grid configuration was determined in order to avoid over and under-sampling of the histologic sections, as reported by Hartlev et al., 2020.²¹ Each point was classified as: (a) bone; (b) soft tissue; or, in the grafted groups, (c) biomaterial. The graft particles were recognizable by their color and pattern. In the same AOI, the percentage of direct contact between biomaterial particles and bone was assessed in Xenograft groups. The values were expressed as a percentage of bone-graft contact over the total surface of the particles. Intraclass correlation coefficient was calculated for intra-examiner calibration in 10 samples for the quantitative histological measurements. A high correlation coefficient (ICC =09) was obtained before the analysis.

Collagen analysis

The collagen packing density was evaluated on Picrosirius Red-stained sections of five chosen equal areas within the AOI of lesion. Images were captured by polarized light microscopy (Nikon Eclipse Ti - S) with a 20x objective lens against a black background. Collagen analysis of each area was performed using ImageJ (ImageJ 1.51k, Wayne Rasband, National Institute of Health, USA). The birefringence color changes from green to red (shorter to longer wavelength) as the density of the collagen packing increases.²² Color thresholds were determined by individual pixel selection using the tool *Color Threshold*, and each pixel was categorized as: red, representing densely packed collagen; yellow representing intermediately packed collagen; and green, representing loosely packed collagen. The results were obtained calculating the number of pixels stained between an intensity threshold in bins determined by 8-bit hue values (0–25 for red, 26-52 for yellow, and 53–110 for green; modified from Smith & Barton, 2014.²³ The proportion of colors within birefringent tissue was normalized and compared between groups.

Statistical analysis

The data were analyzed using Shapiro-Wilk normality. The influence of LLLT, RTX and defect filling treatments on bone morphometric parameters were assessed using three-way analysis of variance (ANOVA). The percentage of bone volume graft among the Xenograft groups was compared using one-way ANOVA. In addition, two-way ANOVA was used to calculate the effect of LLLT and RTX treatments on bone-graft contact in histological pictures. Tukey's *post hoc* test was applied for multiple comparisons when significant differences were detected. The differences were considered statistically significant at $\alpha=0.05$. Statistical analyses were performed using Sigma Plot (v. 12., Systat Software, Inc., San Jose, California, USA).

Results

The animals showed no signs of infection at the surgical site. A reduction of the body weight (approximately 5%) after 5 days of the surgery was noted in all animals. The radiation was well tolerated and did not induce alopecia or weight loss monitored until the day of euthanasia.

Micro-CT analysis - morphological parameters

The mean and standard deviation values of the micro-CT parameters are listed in Table 1. Radiotherapy resulted in lower values of BV/TV ($P=0.005$), Relative BV/TV ($P=0.026$), Tb.N ($P<0.001$) in both Clot and Xenograft groups, whereas a decrease in Tb.Sp ($P<<0.001$) was observed only in Clot groups. Defects filled with xenograft showed higher values of Relative BV/TV ($P=0.022$) and Tb.N ($P<0.001$) in both nRTX and RTX groups. In contrast, Clot groups demonstrated increased values of BV/TV ($P<0.001$) and Tb.Th ($P<0.001$) regardless the radiotherapy treatment, while Tb.Sp was greater ($P<0.001$) only in RTX group. Application of LLLT did not affect the results. There was not a statistically significant difference ($P=0.114$) in the percentage of graft particles volume among the groups.

Histomorphometric analysis and histological findings

The results of the histomorphometric analysis are presented in Figure 1. In both groups (Clot and Xenograft) the LLLT did not affect the amount of newly formed bone (BV/TV) and soft tissue (%) within the repair area ($P > .05$). In agreement with microCT results, the amount of woven bone formed was significantly diminished in the RTX groups ($P < .001$) and in Xenograft groups ($P < .001$). The presence of soft tissue was also higher ($P \leq .05$) in these groups. No interaction between the three factors (LLLT, radiotherapy and defect filling) was noted ($P = 0.7$). Radiotherapy and LLLT application did not affect the percentage of bone graft contact ($P > .05$) (Table 2).

The degree of collagen packing was determined by Picrosirius Red-stained sections evaluation under polarized light. The extent of collagen packing was analyzed as a proportion of collagen area (Figure 2). Intermediately (yellow) and densely packed collagen (red) were predominant among the groups. A very small fraction of collagen area ($< 1\%$) was occupied by loosely packed collagen (green) in all groups. The proportions of densely and intermediately packed collagen were similar ($P > .05$) in all groups filled by clot regardless the LLLT and RTX treatment. However, radiotherapy resulted in a decreased amount ($P \leq .05$) of densely packed collagen in Xenograft group. LLLT treatment did not affect ($P > .05$) collagen packing of the woven bone.

Histological section analysis showed similar bone healing in nLLLT and LLLT both in Xenograft and Clot groups. In the Clot group (Figure 3), nRTX showed predominantly trabecular bone and the defect closure was almost reached. The periosteum was well organized above the newly formed bone. The cortical portion of the lesion in the irradiated groups (RTX) were filled by woven bone with more elongated trabecular bone. The presence of granulation and medullary tissue between the trabecula was common. The healing pattern showed a disorganized bone formation bridging the cortical borders of the lesion. The presence of blood vessels were more frequently observed in nRTX groups. Figure 4 represents the grafted samples sections. Histological sections revealed a larger periosteum invagination in the AOI in grafted groups. In the nRTX groups, the cortical portion of the lesion showed mostly a primary bone (woven bone) around the particles and a more mature healing pattern aiming the wound

closure. In contrast, the presence of soft tissue was more evident in the RTX groups observed mainly in the external portion of the AOI. However, primary bone involving the particles was evident in the AOI near the medullary area of the lesion and within the cavity. The presence of multinucleated cells was more frequent in the grafted groups.

Discussion

This experimental study assessed the effect of a single dose of irradiation (15Gy) and infrared LLLT application on bone repair. Ionizing radiation impaired the bone healing characterized by alterations in the woven bone microstructure, which was observed in both graft and non-grafted defects. In contrast, LLLT had no effect on the bone formation and its microarchitecture. Bone repair process in irradiated areas has been extensively evaluated in the literature. Despite that, few studies have focused on the effect of radiotherapy in ongoing healing surgical sites.²⁶⁻²⁸ However, it assumes greater relevance considering the possibility of defects reconstructions and dental implant osseointegration before the onset of radiotherapy sessions.

It has been observed a strong tendency towards implant placement in the same intervention of the ablative surgery in order to prevent surgical procedure in irradiated tissue and to shorten the time for prosthetic rehabilitation.¹¹ This approach usually involves free flaps reconstruction of the jaws and has shown to be a feasible option for prosthetic rehabilitation of oral cancer.^{29,30} Data from a retrospective study¹⁰ involving 210 patients revealed a greater overall success rate of implant osseointegration in irradiated patients when installed immediately at the time of flap transfer than those that a delayed setting was adopted (86 percent versus 64 percent). Evidences of increased damage when radiotherapy had been delivered preoperatively and minimal effects on bone healing when it had been applied after the surgery, can sustain this clinical finding.^{28,31} It seems that planning the rehabilitation treatment before radiotherapy sessions provides more time for integration of the graft and the implant.³² Therefore, the rationale to investigate the effect of ionizing radiation on

bone repair of defects filled with particulate bone graft has been based on these findings.

In our previous study,²⁶ 30Gy delivered 2 weeks postsurgically did not affect the bone volume fraction of defects in rabbits. Interestingly, a decreased amount of bone volume fraction was evident in this experiment after 7 days of the irradiation procedure. To explain these findings, the mechanisms involved in the repair process and radiation delivery timing have to be considered. Bone healing of burr hole defect in long bones comprises, in summary, 2 healing stages. First, a phase of predominant woven bone formation along the lateral periosteal bridging the cortical, and then a second phase characterized by woven bone replacement by lamellar bone. In rats, the first phase has been observed until day 7. Then, the woven bone is remodeled to lamellar bone to reach the defect closure and the resorption of the woven bone inside the medullary cavity is observed.³³ Associating the healing phase with the irradiation timing is determinant for a proper interpretation of the results. It has been demonstrated that the effect of the radiotherapy on bone healing diverges as the degree of maturation of the tissue changes. The interval of 4 days or more between the surgery and the postoperative irradiation dramatically decreased the deleterious effect of ionizing radiation on bone healing in rats. At the same time, when radiotherapy had been delivered before the surgical intervention or in an early postoperative period (within 3 days) a decrease in bone formation was observed.²⁸ Thus, it seems that the divergent results among the studies might be due to the distinct intervals between the surgery and the postoperative irradiation and because of the different animal models used.

This effect on bone microstructure could probably be observed in a short period after irradiation because radiotherapy affects mainly the proliferative capacity of osteogenic precursor cells.³⁴ The induced lesion is characterized as a challenge for the physiologic environment that requires the recruitment and differentiation of the mesenchymal cells,³⁵ which were affected by high dose of ionizing radiation during this process. This mechanism, involving metabolism acceleration in both hard and soft tissues in order to potentiate tissue healing and local tissue defensive reactions.³³ Without this trigger, otherwise, radiation effect on the

mineralized portion of the bone probably would take longer to become apparent as reported previously.³⁶ The ionizing radiation was delivered in a single dose of 15 Gy. It promotes a rapid death of the most sensitive cells to ionizing radiation, whereas the fractionated applications induce a dose- and delay dependent response.^{37,38} The most commonly used protocol for head and neck cancer, when radiotherapy is given alone, is 2 Gy in a single fraction per day, five days a week, for six to seven weeks.³⁹ However, fractionated dose delivery in animal experiment was not suitable due the tight schedule of the linear accelerator device used for the patients treatment and anesthetics difficulties related to animal experimentation. For this reason, the application of 15 Gy in a single dose was performed in order to simulate the effect of 60 Gy delivered in 2 Gy fractions. The more fractionated is the dose, the more the total final dose must be increased to achieve the same biologic effect.

Regarding the grafted defects, the radiation did not interrupt the bone integration with the grafted particles, despite the indication of decreased amount of bone observed in the morphometric results when the percentage of newly formed bone was calculated as a fraction of the total volume. In the histomorphometric analysis only the area of actual bone was measured precluding the area of graft particles. Deproteinized bovine bone mineral particles (DBBM) degrade very slowly. These bone graft particles have been found after 4 to 10 years after implantation.⁴⁰ This characteristic allows the volume maintenance of the grafted areas to persist over the time, being advantageous especially in areas where bone dehiscence's affect function and esthetic.¹⁴ Thus, it was expected to find a lower percentage of newly formed bone in grafted groups in this initial healing period. Biomaterials that take long periods for complete resorption result in a reduction of newly formed bone amount because of the continued space occupied by the particle.⁴¹ An ideal experimental model to assess the bone formation in grafted areas for longer periods is critical defects in which spontaneous bone healing does not occur during the lifetime of the animal. Larger defects in rats tibiae might lead to fractures, thus calvarial critical defect are the most frequent used. However, radiation delivery of 15 Gy in single dose is not possible in this area making this model unfeasible in the present study.

In order to allow a direct comparison between grafted and non-grafted groups without the intervention of the volume occupied by the particles, microCT analysis of the bone volume fraction was also assessed subtracting the graft volume from the total volume. The results revealed an increase percentage of bone volume observed in both RTX and nRTX groups. Despite the difficult to set a reliable threshold for bone and bone graft, the morphometric results from microCT agreed to the histomorphometric findings. Bio-oss® particles (Geistlich Pharma AG, Wolhusen, Switzerland) were visually distinguished from newly formed bone due its different gray levels. The threshold for the particles segmentation was obtained by selecting the graft alone and further histogram analysis of 10 samples to minimize any possible bias that arises from microCT methodological analysis. Even though, misleading measurements in the bone-graft interface might occur in microCT analysis, thus histological analysis was also performed to ensure the reliability of the results. Histological analysis showed that the osteoconductive property of the xenogeneic granules was maintained with no sign of necrosis after irradiation. Besides, irradiation delivery did not affect the bone graft incorporation as demonstrated by the percentage of particles surface in contact to bone after radiotherapy.

Few studies have evaluated the influence of postoperative irradiation on bone properties around particulate bone substitutes.^{37,43–45} Malard *et al.* (2005),³⁷ investigated the possibility of bone reconstruction using macroporous biphasic calcium phosphate (CaP) inserted 3 weeks before radiotherapy associated to autologous bone marrow (BM) graft injected after irradiation. The results showed that CaP were osseointegrated even without marrow graft association. Histological analysis revealed the absence of fibrous tissue between bone and implanted CaP similar to the findings of the present study. The authors suggest that this integration had initiated before irradiation and was preserved contributing to bone bonding and stability. The same behavior has been noted in the osseointegration of implants coated with hydroxyapatite: the more organized the peri-implant bone was at irradiation onset, the less was the radiation damage on bone formation.³² However, as the bone remodeling of irradiated bone has shown to be altered in a long-term period,⁴² future studies should evaluate the

behavior of the grafted tissues over the time as well as the implant osseointegration in these areas. Nonetheless, the findings of the present study are promising, mainly because osteoconductive biomaterials can enhance bone deposition in unfavorable regions,⁴⁶ which has been demonstrated preserved after irradiation.

Mineralized bone graft has shown to be effective for volume maintenance when bone augmentation is required. The literature is extensive regarding the osteoconductive property of xenogeneic bone grafts.⁴⁷ From a clinical perspective, its association with vascularized free flaps might be considered as an option for larger reconstructions considering that the particles serve as a scaffold for osteogenic cells⁴⁸ supporting the consolidation of the free flap and the host before radiotherapy. The employment of nonautologous particulate grafts for socket preservation after tooth extraction is another condition that should be further explored in this context. The increased volumetric loss in postsurgical irradiated extraction sockets when compared to non-irradiated patients has been demonstrated.⁴⁹ The oral rehabilitation supported by implants could be improved in specific cases through biomaterials association in order to minimize bone resorption and volumetric loss over the time as demonstrated in non-irradiated bone.⁵⁰ Lower survival rate of implant installed in irradiated grafted bone when compared to native bone has been reported.⁹ These results were expected because of the increased complexity of the anatomical sites in cases that grafting procedures are required. However, a recent systematic review has demonstrated that the survival rate is still high (90.4%) for dental implants placed in both native and grafted bone during ablative surgery.⁵¹

Another fundamental aspect that requires more investigation to ensure the previsibility of the oncologic treatment is the backscattering effect in the presence of biomaterials. The particulate graft used in this experiment is a deproteinized bovine bone material, which has crystalline hydroxyapatite as constituent. Stenson *et al.*,⁵⁸ reported that stainless steel and titanium alloy caused increased radiation dose proximal to the interface and attenuated dose distal to the interface. Hydroxyapatite showed a relatively minor effect whereas poly-L-lactide PLA (bioabsorbable polymer) led to minimal radiation-dose

inhomogeneities for photons and electrons.⁵² Considering the difficult to obtain a biomaterial with ideal physical and mechanical properties, the biological implications of the backscatter and attenuation effects caused by the presence of reconstruction devices should also be evaluated.

Collagen cross-linking is highly associated with bone mechanical properties. Therefore, it has been considered as a key predictor of bone fracture risks.⁵³ The early post-radiotherapy increase in osteoclastic activity is followed by long-term depletion of local osteoclast. The decrease in bone resorption results in a low rate of remodeling that allows bone tissue to remain longer than normal. Consequently, collagen hyper-mineralization and hyper-orientation takes place.⁴² This effect has been reported in mature bone. In newly formed bone, a decrease in collagen density has been demonstrated after a single dose of 30Gy.²⁶ In the present study, fifteen grays delivered postsurgically did not affect collagen-packing density in defects filled with clot. However, a smallest percentage of densely packed collagen in irradiated grafted defects was observed. This finding can be attributed to the fact that the proportion between soft and hard tissue in grafted defects is higher than the clot group. Quantification analysis of fibrillar collagen levels after Picrosirius Red staining involves both mineralized and non-mineralized tissue. Thus, since components of the irradiated wound have different degrees of sensitivity,⁵⁴ it is not possible to assume that the collagen packing density specifically of the newly formed bone was affected. Histological sections revealed a greater periosteum collapse inside the AOI in grafted groups. It is possible that ionizing radiation has an initial major effect in the periosteal collagen organization during this healing phase, although validation of this hypothesis requires further investigation.

The protocol of the LLLT applied in this study was based on a previous study that has been demonstrate to be able to reach bone tissue due to its high penetrability potential.²⁰ Unfortunately, photobiomodulation therapy using low-level laser is still controversial in the literature due to the large variety of existing protocol.⁵⁵ Our findings failed to demonstrate the effect of LLLT on newly formed bone in all groups. Batista et al., reported that LLLT was not efficient to overcome the deleterious effect of 30 Gy preoperatively delivered on bone healing. Some

authors also reported that LLLT did not improve bone formation in grafted sites.^{56–58} However, this is contrast to most of the studies that have evaluated the LLLT alone^{55,59} or in combination with bone grafts.^{60–62} It can be attributed to many factors, such as the divergence among the studies in the type of animal, the bone defect characteristics (size and area), evaluation period and method of analysis. Besides, it has been demonstrated an increased bone metabolism (resorption and formation) in LLLT treated defects that did not culminate in more bone volume fraction.⁶³ Thus, it seems that the LLLT effects is relative to several aspect not only the application protocol but also the type of tissue and the experimental model.⁶²

In conclusion, preoperative delivery of 15 Gy lead to a delay in the bone repair demonstrated by a smaller amount of newly formed bone in both grafted and non-grafted defects. In addition, LLLT did not improve the bone healing. However, graft particles integration with the newly formed bone was preserved after 7 days of the irradiation delivery. The oral environment was not reproduced in this study, but the promising results related to the osteoconductive property of the bone graft particles applied before irradiation should encouraging more efforts to investigate its application in clinical conditions before the radiotherapy begin.

Compliance with Ethical Standards

Conflict of Interest: The authors declare that they have no conflict of interest.

Funding: This study was supported by grants from the Fundação de Amparo à Pesquisa de Minas Gerais (FAPEMIG), the Coordenação de Aperfeiçoamento de Pessoal de Nível Superior – Brasil (CAPES) – Finance Code 001 and Conselho Nacional de Desenvolvimento Científico e Tecnológico (CNPq).

Ethical approval: All applicable international, national, and/or institutional guidelines for the care and use of animals were followed.

Informed consent: For this type of study, formal consent is not required.

Tables

Table 1. Mean and standard deviation values of the microCT analysis

	nRTX		RTX	
	nLLLLT	LLLLT	nLLLLT	LLLLT
Percentage of graft volume (GV)				
Clot	-	-	-	-
Xenograft	25.0 (5.5) ^a	30.8 (8.3) ^a	31.8 (6.0) ^a	28.0 (5.9) ^a
Bone volume fraction (BV/TV)				
Clot	59.5 (5.4) ^{Aa}	60.6 (7.9) ^{Aa}	51.1 (10.1) ^{Ab}	56.9 (6.3) ^{Ab}
Xenograft	45.0 (7.9) ^{Ba}	45.8 (4.5) ^{Ba}	41.1 (4.5) ^{Bb}	41.6 (5.5) ^{Bb}
Relative Bone volume fraction (BV/(TV-GV))				
Clot	59.5 (5.4) ^{Aa}	60.6 (7.9) ^{Aa}	51.1 (10.1) ^{Ab}	56.9 (6.3) ^{Ab}
Xenograft	60.0 (9.5) ^{Ba}	68.2 (9.6) ^{Ba}	61.7 (9.5) ^{Bb}	58.5 (9.4) ^{Bb}
Trabecular thickness (Tb.Th)				
Clot	0.09 (0.01) ^{Aa}	0.1 (0.03) ^{Aa}	0.11 (0.02) ^{Aa}	0.11 (0.01) ^{Aa}
Xenograft	0.06 (0.01) ^{Ba}	0.05 (0.00) ^{Ba}	0.05 (0.00) ^{Ba}	0.05 (0.00) ^{Ba}
Trabecular number (Tb.N)				
Clot	6.2 (0.5) ^{Aa}	5.8 (1.2) ^{Aa}	4.6 (1.1) ^{Ab}	5.2 (0.9) ^{Ab}
Xenograft	7.9 (0.4) ^{Ba}	8.6 (0.7) ^{Ba}	7.4 (0.6) ^{Bb}	7.4 (0.8) ^{Ba}
Trabecular separation (Tb.Sp)				
Clot	0.09 (0.01) ^{Aa}	0.1 (0.03) ^{Aa}	0.19 (0.07) ^{Ab}	0.14 (0.06) ^{Ab}
Xenograft	0.10 (0.01) ^{Aa}	0.1 (0.01) ^{Aa}	0.11 (0.01) ^{Ba}	0.12 (0.01) ^{Ba}

Different uppercase letters indicate significant difference between the rows; different lowercase letters indicate significant difference the columns.

Table 2. Mean and standard deviation values of the percentage of bone/graft contact

	nLLLT	LLLT
xRTX	52 (18) ^{Aa}	63 (12) ^{Aa}
RTX	63 (12) ^{Aa}	47 (15) ^{Aa}

Different uppercase letters indicate significant difference between the rows; different lowercase letters indicate significant difference the columns.

Figure captions

Figure 1. Histograms showing the histomorphometric results (mean±SD). Percentage of new bone area (A) and soft tissue (B) among the groups: bone formation was significantly increased in nRTX and the percentage of soft tissue was higher in RTX groups. These differences were observed in both Clot and Xenograft groups. LLLT did not affect the amount of bone formation and soft tissue in both clot and xenograft groups. Xenograft groups showed a smaller amount of BV/TV and higher levels of soft tissue in comparison to the Clot group regardless RTX and LLLT treatment. Photomicrographs (Masson's Trichrome stained) of the cortical portion of the defect in Clot (C) and Xenograft (D) groups. (Different uppercase letters indicate significant difference between Clot and Xenograft groups; different lowercase letters indicate significant difference between nRTX and RTX groups).

Figure 2. Quantification analysis of fibrillar collagen levels (mean±SD). (A) Polarized photomicrograph (PicroSirius Red stained) of the woven bone. (B) Red pixels selected (white area) by color threshold. (C) Yellow pixels selected (white area). (D) Green pixels selected (white area). (E) The normalized proportion of green, yellow and red birefringent collagen bundles in Clot groups. (F) The normalized proportion of green, yellow and red birefringent collagen bundles in

Xenograft groups. (Different uppercase letters indicate significant difference between Clot and Xenograft groups; different lowercase letters indicate significant difference between nRTX and RTX groups)

Figure 3. Photomicrograph (H&E stained) of the non grafted groups 14 days after the surgery. The healing stages of the lesions were evaluated from the longitudinal femur sections. Approximated view shows the woven bone formed in the cortical portion of the lesion. Thinner trabecula with granulation tissue between them were observed in RTX groups. An impairment of the defect closure was also noted. (Asterisk: bone; square: medullary tissue; circle: granulation tissue; black arrow: osteoclast; blue arrow: osteocyte being embedded).

Figure 4. Photomicrograph (H&E stained) of the grafted groups 14 days after the surgery. Overview of the longitudinal femur sections. Approximated view shows the remodeling process around the particles. Note the bone formation in the nRTX groups and the presence of granulation tissue in the RTX groups (Asterisk: bone; square: grafted material; circle: granulation tissue). Multinucleated cells (black arrow) were observed on the biomaterial surface.

References

1. Sung H, Ferlay J, Siegel RL, et al. Global Cancer Statistics 2020: GLOBOCAN Estimates of Incidence and Mortality Worldwide for 36 Cancers in 185 Countries. *CA Cancer J Clin.* 2021;71(3). doi:10.3322/caac.21660
2. Soares PBF, Soares CJ, Limirio PHJO, et al. Effect of ionizing radiation after-therapy interval on bone: histomorphometric and biomechanical characteristics. *Clin Oral Investig.* 2019;23(6). doi:10.1007/s00784-018-2724-3
3. Bartlow CM, Mann KA, Damron TA, Oest ME. Limited field radiation therapy results in decreased bone fracture toughness in a murine model. *PLoS One.* 2018;13(10). doi:10.1371/journal.pone.0204928
4. Lyons A, Ghazali N. Osteoradionecrosis of the jaws: current understanding of its pathophysiology and treatment. *Br J Oral Maxillofac Surg.* 2008;46(8). doi:10.1016/j.bjoms.2008.04.006

5. Wang TH, Liu CJ, Chao TF, Chen TJ, Hu YW. Risk factors for and the role of dental extractions in osteoradionecrosis of the jaws: A national-based cohort study. *Head Neck*. 2017;39(7). doi:10.1002/hed.24761
6. Schiødt M, Hermund NU. Management of oral disease prior to radiation therapy. *Support Care Cancer*. 2002;10(1). doi:10.1007/s005200100284
7. Di Carlo S, De Angelis F, Ciolfi A, et al. Timing for implant placement in patients treated with radiotherapy of head and neck. *Clin Ter*. 2019;170(5). doi:10.7417/CT.2019.2153
8. Zen Filho EV, Tolentino EDS, Santos PSS. Viability of dental implants in head and neck irradiated patients: A systematic review. *Head Neck*. 2016;38. doi:10.1002/hed.24098
9. Schiegnitz E, Al-Nawas B, Kämmerer PW, Grötz KA. Oral rehabilitation with dental implants in irradiated patients: A meta-analysis on implant survival. *Clin Oral Investig*. 2014;18(3). doi:10.1007/s00784-013-1134-9
10. Urken ML, Buchbinder D, Costantino PD, et al. Oromandibular reconstruction using microvascular composite flaps: Report of 210 cases. *Arch Otolaryngol - Head Neck Surg*. 1998;124(1). doi:10.1001/archotol.124.1.46
11. Korfage A, Schoen PJ, Raghoobar GM, Roodenburg JLN, Vissink A, Reintsema H. Benefits of dental implants installed during ablative tumour surgery in oral cancer patients: A prospective 5-year clinical trial. *Clin Oral Implants Res*. 2010;21(9). doi:10.1111/j.1600-0501.2010.01930.x
12. Ch'Ng S, Skoracki RJ, Selber JC, et al. Osseointegrated implant-based dental rehabilitation in head and neck reconstruction patients. In: *Head and Neck*. Vol 38. ; 2016. doi:10.1002/hed.23993
13. Albergia JM, Korfage A, Bonnema I, Witjes MJH, Vissink A, Raghoobar GM. Mandibular dental implant placement immediately after teeth removal in head and neck cancer patients. *Support Care Cancer*. 2020;28(12). doi:10.1007/s00520-020-05431-y
14. Iocca O, Farcomeni A, Pardiñas Lopez S, Talib HS. Alveolar ridge preservation after tooth extraction: a Bayesian Network meta-analysis of grafting materials efficacy on prevention of bone height and width

- reduction. *J Clin Periodontol*. 2017;44(1). doi:10.1111/jcpe.12633
15. Alberga JM, Vosselman N, Korfage A, et al. What is the optimal timing for implant placement in oral cancer patients? A scoping literature review. *Oral Dis*. 2021;27(1). doi:10.1111/odi.13312
 16. Fávaro-Pípi E, Feitosa SM, Ribeiro DA, et al. Comparative study of the effects of low-intensity pulsed ultrasound and low-level laser therapy on bone defects in tibias of rats. *Lasers Med Sci*. 2010;25(5). doi:10.1007/s10103-010-0772-2
 17. Dörtbudak O, Haas R, Mailath-Pokorny G. Effect of low-power laser irradiation on bony implant sites. *Clin Oral Implants Res*. 2002;13(3). doi:10.1034/j.1600-0501.2002.130308.x
 18. Rottensteiner-Brandl U, Distel L, Stumpf M, et al. Influence of Different Irradiation Protocols on Vascularization and Bone Formation Parameters in Rat Femora. *Tissue Eng - Part C Methods*. 2017;23(10). doi:10.1089/ten.tec.2017.0170
 19. Obradović RR, Kesić LG, Peševska S. Influence of low-level laser therapy on biomaterial osseointegration: A mini-review. *Lasers Med Sci*. 2009;24(3). doi:10.1007/s10103-008-0573-z
 20. Marques L, Holgado LA, Francischone LA, Ximenez JPB, Okamoto R, Kinoshita A. New LLLT protocol to speed up the bone healing process—histometric and immunohistochemical analysis in rat calvarial bone defect. *Lasers Med Sci*. 2015;30(4). doi:10.1007/s10103-014-1580-x
 21. Hartlev J, Erik Nørholt S, Spin-Neto R, Kraft D, Schou S, Isidor F. Histology of augmented autogenous bone covered by a platelet-rich fibrin membrane or deproteinized bovine bone mineral and a collagen membrane: A pilot randomized controlled trial. *Clin Oral Implants Res*. 2020;31(8). doi:10.1111/clr.13605
 22. Junqueira LCU, Bignolas G, Brentani RR. Picrosirius staining plus polarization microscopy, a specific method for collagen detection in tissue sections. *Histochem J*. 1979;11(4). doi:10.1007/BF01002772
 23. Smith LR, Barton ER. Collagen content does not alter the passive mechanical properties of fibrotic skeletal muscle in mdx mice. *Am J Physiol*

- *Cell Physiol.* 2014;306(10). doi:10.1152/ajpcell.00383.2013
24. Marx RE. Osteoradionecrosis: A new concept of its pathophysiology. *J Oral Maxillofac Surg.* 1983;41(5). doi:10.1016/0278-2391(83)90294-X
 25. Granström G. Radiotherapy, osseointegration and hyperbaric oxygen therapy. *Periodontol* 2000. 2003;33. doi:10.1046/j.0906-6713.2002.03312.x
 26. Mendes EM, Irie MS, Rabelo GD, et al. Effects of ionizing radiation on woven bone: influence on the osteocyte lacunar network, collagen maturation, and microarchitecture. *Clin Oral Investig.* 2020;24(8). doi:10.1007/s00784-019-03138-x
 27. Pelker RR, Friedlaender GE. The Nicolas Andry Award-1995. Fracture healing: Radiation induced alterations. *Clin Orthop Relat Res.* 1997;(341). doi:10.1097/00003086-199708000-00038
 28. Arnold M, Stas P, Kummermehr J, Schultz-Hector S, Trott KR. Radiation-induced impairment of bone healing in the rat femur: Effects of radiation dose, sequence and interval between surgery and irradiation. *Radiother Oncol.* 1998;48(3). doi:10.1016/S0167-8140(98)00039-5
 29. Allen RJ, Nelson JA, Polanco TO, et al. Short-Term Outcomes following Virtual Surgery-Assisted Immediate Dental Implant Placement in Free Fibula Flaps for Oncologic Mandibular Reconstruction. *Plast Reconstr Surg.* Published online 2020. doi:10.1097/PRS.00000000000007352
 30. Schoen PJ, Reintsema H, Raghoobar GM, Vissink A, Roodenburg JLN. The use of implant retained mandibular prostheses in the oral rehabilitation of head and neck cancer patients. A review and rationale for treatment planning. *Oral Oncol.* 2004;40(9). doi:10.1016/j.oraloncology.2003.08.024
 31. Brogniez V, Nyssen-Behets C, Grégoire V, Reychler H, Lengelé B. Implant osseointegration in the irradiated mandible: A comparative study in dogs with a microradiographic and histologic assessment. *Clin Oral Implants Res.* 2002;13(3). doi:10.1034/j.1600-0501.2002.130302.x
 32. Weinländer M, Beumer J. III, Kenney EB, et al. Histomorphometric and fluorescence microscopic evaluation of interfacial bone healing around three different dental implants before and after radiation therapy

- [Histomorphometrische und fluoreszenzmikroskopische analyse der knochenheilung im kontaktbereich. *Implantologie*. 2007;15(2).
33. Schilling T, Müller M, Minne HW, Ziegler R. Influence of inflammation-mediated osteopenia on the regional acceleratory phenomenon and the systemic acceleratory phenomenon during healing of a bone defect in the rat. *Calcif Tissue Int*. 1998;63(2). doi:10.1007/s002239900508
 34. Matsumura S, Jikko A, Hiranuma H, Deguchi A, Fuchihata H. Effect of X-ray irradiation on proliferation and differentiation of osteoblast. *Calcif Tissue Int*. 1996;59(4). doi:10.1007/s002239900129
 35. Green DE, Rubin CT. Consequences of irradiation on bone and marrow phenotypes, and its relation to disruption of hematopoietic precursors. *Bone*. 2014;63. doi:10.1016/j.bone.2014.02.018
 36. Mitchell MJ, Logan PM. Radiation-induced Changes in Bone. *Radiographics*. 1998;18(5). doi:10.1148/radiographics.18.5.9747611
 37. Malard O, Guicheux J, Bouler JM, et al. Calcium phosphate scaffold and bone marrow for bone reconstruction in irradiated area: A dog study. *Bone*. 2005;36(2). doi:10.1016/j.bone.2004.07.018
 38. Rubin P. Regeneration of bone marrow in rabbits following local, fractionated irradiation. *Cancer*. 1973;32(4). doi:10.1002/1097-0142(197310)32:4<847::AID-CNCR2820320416>3.0.CO;2-V
 39. Baujat B, Bourhis J, Blanchard P, et al. Hyperfractionated or accelerated radiotherapy for head and neck cancer. *Cochrane Database Syst Rev*. 2010;2010(12). doi:10.1002/14651858.CD002026.pub2
 40. Piattelli M, Favero GA, Scarano A, Orsini G, Piattelli A. Bone reactions to anorganic bovine bone (Bio-Oss) used in sinus augmentation procedures: a histologic long-term report of 20 cases in humans. *Int J Oral Maxillofac Implants*. 14(6):835-840. <http://www.ncbi.nlm.nih.gov/pubmed/10612920>
 41. MacNeill SR, Cobb CM, Rapley JW, Glaros AG, Spencer P. In vivo comparison of synthetic osseous graft materials. A preliminary study. *J Clin Periodontol*. 1999;26(4). doi:10.1034/j.1600-051X.1999.260407.x
 42. Oest ME, Gong B, Esmonde-White K, et al. Parathyroid hormone attenuates radiation-induced increases in collagen crosslink ratio at

- periosteal surfaces of mouse tibia. *Bone*. 2016;86:91-97. doi:10.1016/j.bone.2016.03.003
43. Pinholt EM, Kwon PHJ. The effect of therapeutic radiation on canine alveolar ridges augmented with hydroxylapatite. *J Oral Maxillofac Surg*. 1992;50(3). doi:10.1016/0278-2391(92)90321-P
 44. Khateery S, Waite PD, Lemons JE. The influence of radiation therapy on subperiosteal hydroxyapatite implants in rabbits. *J Oral Maxillofac Surg*. 1991;49(7). doi:10.1016/S0278-2391(10)80237-X
 45. Kudo M, Matsui Y, Ohno K, Michi K. A histomorphometric study of the tissue reaction around hydroxyapatite implants irradiated after placement. *J Oral Maxillofac Surg*. 2001;59(3). doi:10.1053/joms.2001.20998
 46. Mendoza-Azpur G, de la Fuente A, Chavez E, Valdivia E, Khouly I. Horizontal ridge augmentation with guided bone regeneration using particulate xenogenic bone substitutes with or without autogenous block grafts: A randomized controlled trial. *Clin Implant Dent Relat Res*. 2019;21(4). doi:10.1111/cid.12740
 47. Fernandez de Grado G, Keller L, Idoux-Gillet Y, et al. Bone substitutes: a review of their characteristics, clinical use, and perspectives for large bone defects management. *J Tissue Eng*. 2018;9. doi:10.1177/2041731418776819
 48. Tapety FI, Amizuka N, Uoshima K, Nomura S, Maeda T. A histological evaluation of the involvement of Bio-Oss® in osteoblastic differentiation and matrix synthesis. *Clin Oral Implants Res*. 2004;15(3). doi:10.1111/j.1600-0501.2004.01012.x
 49. Agbaje JO, Jacobs R, Michiels K, Abu-Ta'a M, Van Steenberghe D. Bone healing after dental extractions in irradiated patients: A pilot study on a novel technique for volume assessment of healing tooth sockets. *Clin Oral Investig*. 2009;13(3). doi:10.1007/s00784-008-0231-7
 50. Araújo MG, Lindhe J. Ridge preservation with the use of Bio-Oss® collagen: A 6-month study in the dog. *Clin Oral Implants Res*. 2009;20(5). doi:10.1111/j.1600-0501.2009.01705.x
 51. In 't Veld M, Schulten EAJM, Leusink FKJ. Immediate dental implant

- placement and restoration in the edentulous mandible in head and neck cancer patients: a systematic review and meta-analysis. *Curr Opin Otolaryngol Head Neck Surg.* 2021;29(2). doi:10.1097/MOO.0000000000000685
52. Stenson KM, Balter JM, Campbell JH, Carroll WR. Effects of implantable biomaterials on radiation dosimetry. *Head Neck.* 1997;19(5). doi:10.1002/(sici)1097-0347(199708)19:5<384::aid-hed4>3.0.co;2-w
 53. Saito M, Marumo K. Collagen cross-links as a determinant of bone quality: A possible explanation for bone fragility in aging, osteoporosis, and diabetes mellitus. *Osteoporos Int.* 2010;21(2). doi:10.1007/s00198-009-1066-z
 54. Jegoux F, Malard O, Goyenvalle E, Aguado E, Daculsi G. Radiation effects on bone healing and reconstruction: interpretation of the literature. *Oral Surgery, Oral Med Oral Pathol Oral Radiol Endodontology.* 2010;109(2). doi:10.1016/j.tripleo.2009.10.001
 55. Escudero JSB, Perez MGB, de Oliveira Rosso MP, et al. Photobiomodulation therapy (PBMT) in bone repair: A systematic review. *Injury.* 2019;50(11). doi:10.1016/j.injury.2019.09.031
 56. Oliveira P, Ribeiro DA, Pippi EF, Driusso P, Parizotto NA, Renno ACM. Low level laser therapy does not modulate the outcomes of a highly bioactive glass-ceramic (Biosilicate®) on bone consolidation in rats. *J Mater Sci Mater Med.* 2010;21(4). doi:10.1007/s10856-009-3945-4
 57. Pinto KNZ, Tim CR, Crovace MC, et al. Effects of biosilicate® scaffolds and low-level laser therapy on the process of bone healing. *Photomed Laser Surg.* 2013;31(6). doi:10.1089/pho.2012.3435
 58. Kim J-R, Kim S-H, Kim I-R, Park B-S, Kim Y-D. Low-level laser therapy affects osseointegration in titanium implants: resonance frequency, removal torque, and histomorphometric analysis in rabbits. *J Korean Assoc Oral Maxillofac Surg.* 2016;42(1). doi:10.5125/jkaoms.2016.42.1.2
 59. Abramoff MMF, Pereira MD, De Seixas Alves MT, Segreto RA, Guilherme A, Ferreira LM. Low-level laser therapy on bone repair of rat tibiae exposed to ionizing radiation. *Photomed Laser Surg.* 2014;32(11).

- doi:10.1089/pho.2013.3692
60. de Oliveira GJPL, Aroni MAT, Pinotti FE, Marcantonio E, Marcantonio RAC. Low-level laser therapy (LLLTL) in sites grafted with osteoconductive bone substitutes improves osseointegration. *Lasers Med Sci.* 2020;35(7). doi:10.1007/s10103-019-02943-w
 61. Márquez Gerbi ME, Barbosa Pinheiro AL, Marzola C, et al. Assessment of bone repair associated with the use of organic bovine bone and membrane irradiated at 830 nm. *Photomed Laser Surg.* 2005;23(4). doi:10.1089/pho.2005.23.382
 62. de Oliveira Rosso MP, Oyadomari AT, Pomini KT, et al. Photobiomodulation therapy associated with heterologous fibrin biopolymer and bovine bone matrix helps to reconstruct long bones. *Biomolecules.* 2020;10(3). doi:10.3390/biom10030383
 63. Nicolau RA, Jorgetti V, Rigau J, Pacheco MTT, Dos Reis LM, Zângaro RA. Effect of low-power GaAlAs laser (660 nm) on bone structure and cell activity: An experimental animal study. *Lasers Med Sci.* 2003;18(2). doi:10.1007/s10103-003-0260-z

Figure 1

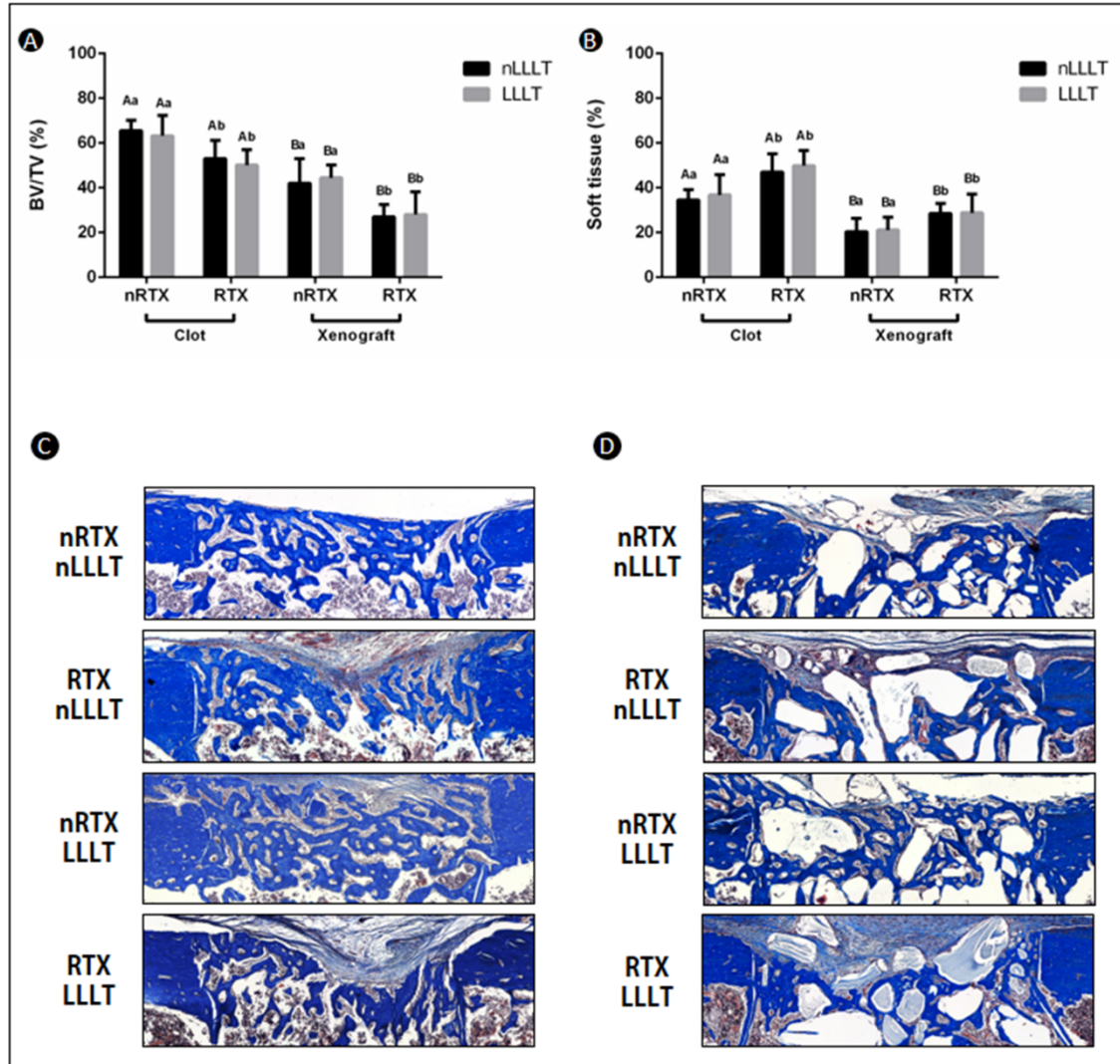


Figure 2

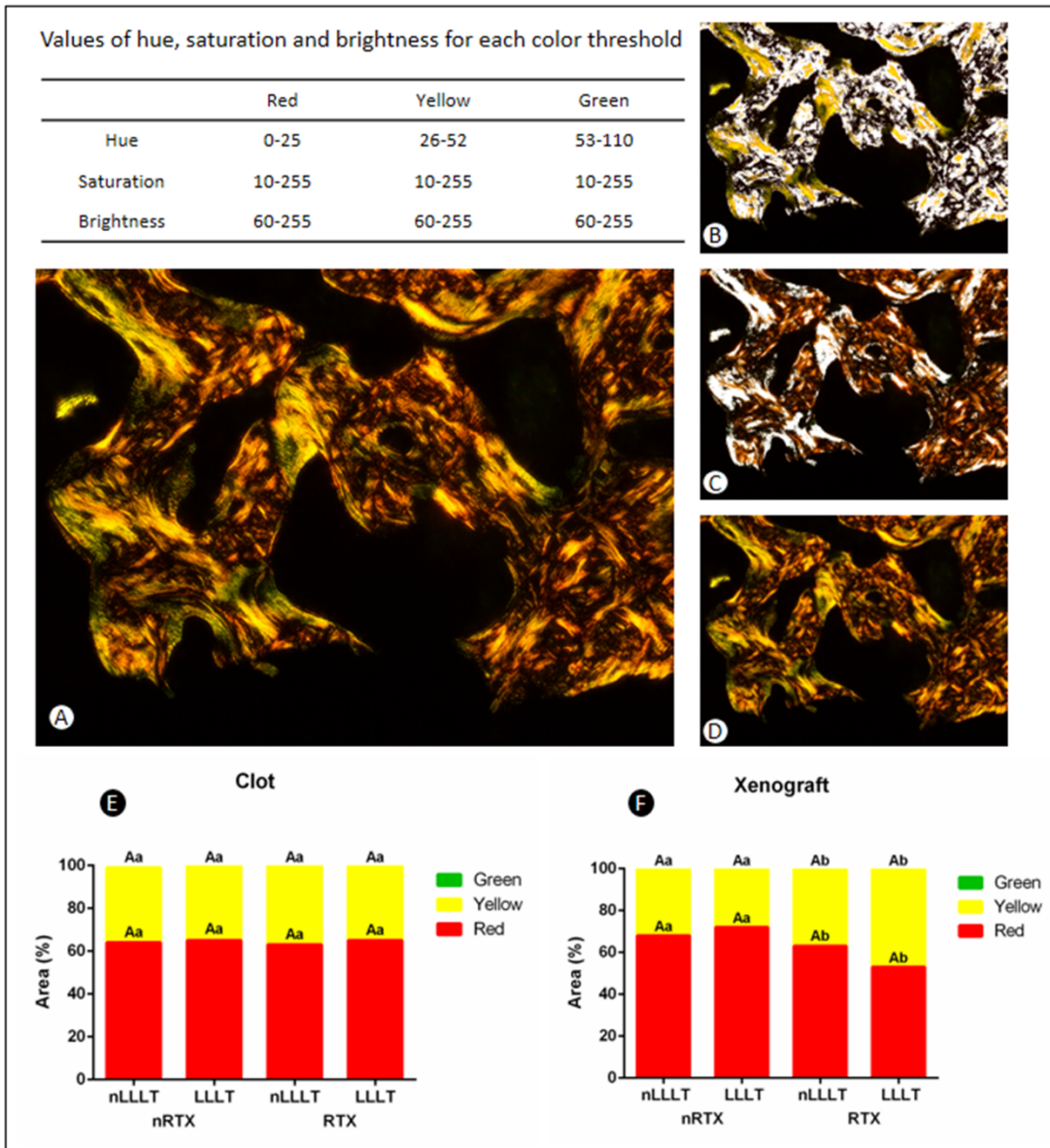


Figure 3

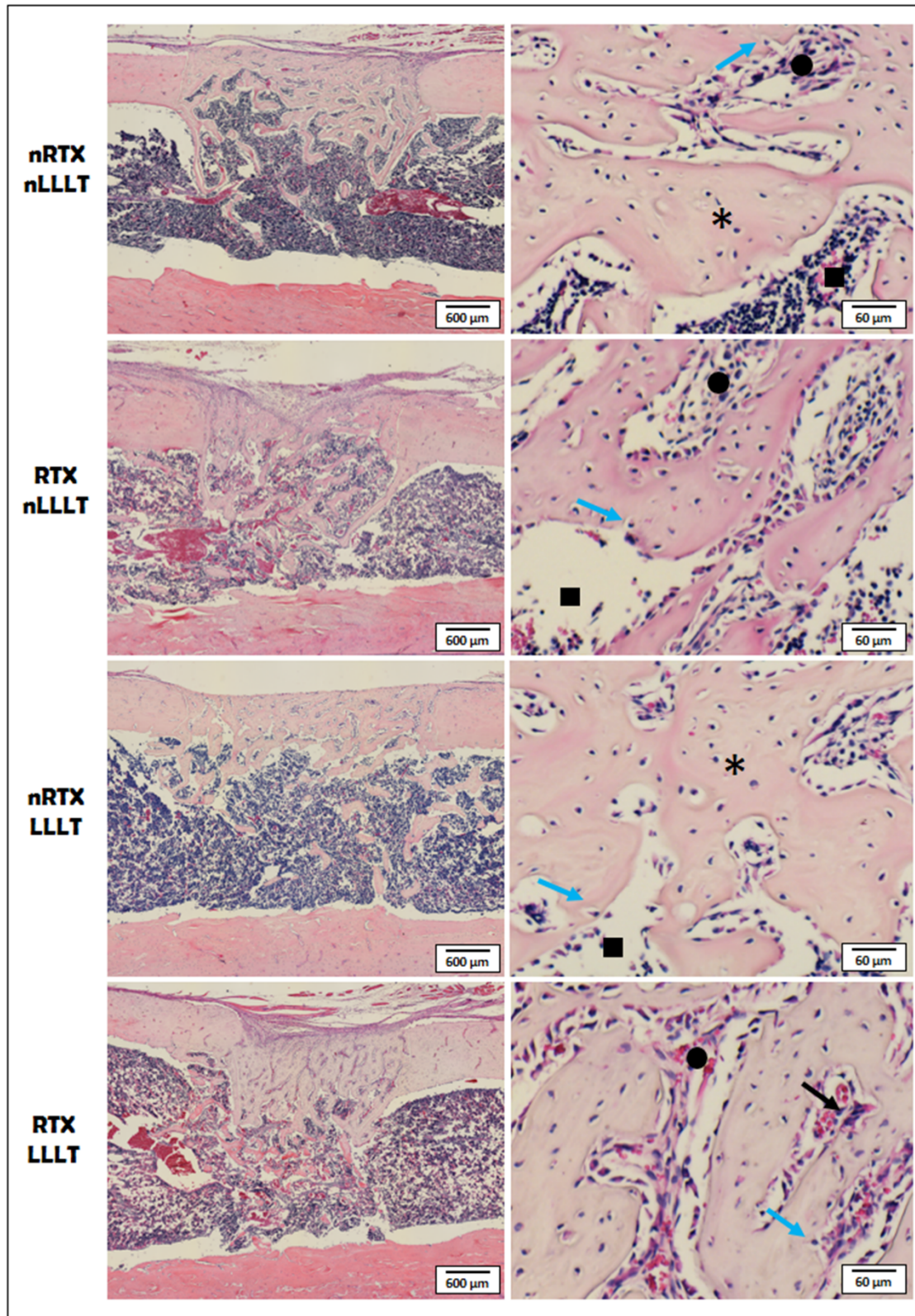
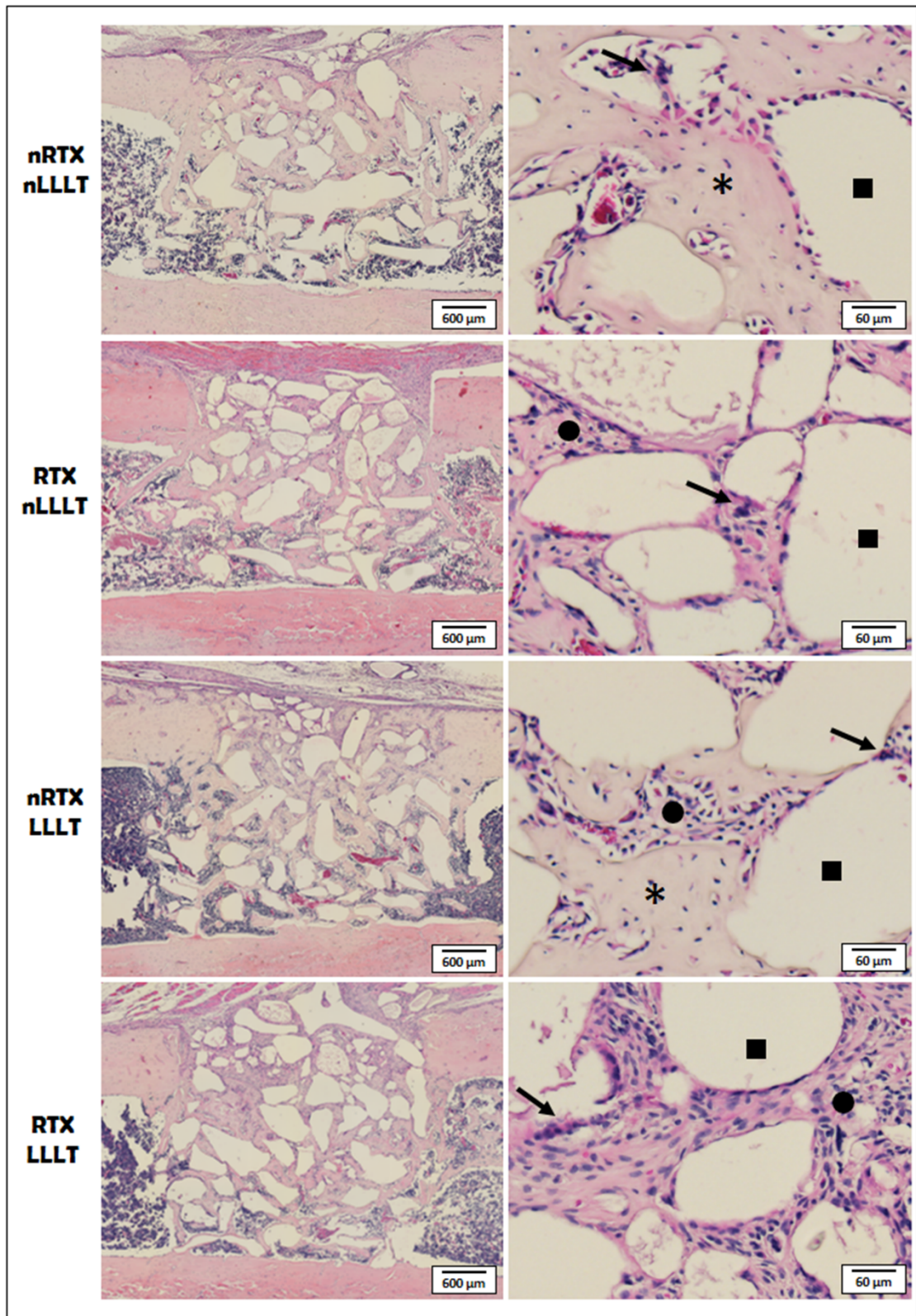


Figure 4



4. CONCLUSÕES

Com base nas metodologias utilizada e nos resultados obtidos destes estudos, pode-se concluir que:

- Diversas aplicações da análise microtomográfica dos tecidos ósseos dentro da Odontologia são utilizadas, tais como: avaliação de doenças e condições que afetam o metabolismo e a estrutura óssea; análise de procedimentos de reparo e regeneração; avaliação de novas terapias e intervenções cirúrgicas; avaliação da eficácia e uso de biomateriais e implantes. Portanto, para cada tipo de análise devem ser consideradas: características da amostra; o preparo da amostra; metodologias associadas (processamento histológico, testes mecânicos); a resolução e os parâmetros de aquisição ideais e, por fim, os parâmetros a serem avaliados.

- Determinados parâmetros de aquisição podem afetar a análise microtomográfica do reparo ósseo em um modelo experimental. O tamanho do voxel (6 e 12 μm) e a experiência dos examinadores influenciaram os resultados obtidos para a Tb.Th e BV/TV. A análise dos dados morfométricos da BV/TV foi influenciada pelo tamanho do voxel apenas para os examinadores não experientes. De forma que não houve diferença nos dados provenientes das análises em 6 e 12 μm quando realizada por examinadores experientes. A influência da experiência do operador também foi observada nos dados de Tb.Th. No entanto, essa diferença foi observada apenas no grupo de 12 μm , indicando que a análise de Tb.Th do reparo ósseo em ratos em volumes com voxel de 6 μm implica em menor viés inerente à experiência do examinador.

- O *binning* de pixels realizado durante a aquisição de imagens microtomográficas também influenciou a análise do reparo ósseo. Quanto maior o *binning* de dados, maiores valores de Tb.Th e menores valores de BV/TV e BV foram observados. Não foi observada diferença nos dados de Tb.N e Tb. Sp. Os mesmos parâmetros morfométricos avaliados não apresentam diferença estatística ao aumentar o número de projeções em que a imagem é calculada (*frame averaging*) de 1 para 2.

- A análise histomorfométrica e microtomográfica do reparo do tecido ósseo irradiado (15Gy) 7 dias após cirurgia resultou em menor neoformação

óssea tanto em defeitos enxertados por DBBM, quanto em defeitos não enxertados preenchidos por coágulo. A aplicação da laserterapia de baixa intensidade não apresentou efetividade em acelerar o processo de reparo demonstrado pela quantidade de tecido ósseo neoformado. A incorporação das partículas do enxerto com o osso recém-formado foi preservada mesmo após 7 dias da radioterapia, demonstrando que a osteocondutividade do biomaterial foi preservada.

5. REFERÊNCIAS¹

Alberga JM, Vosselman N, Korfage A, Delli K, Witjes MJH, Raghoobar GM et al. What is the optimal timing for implant placement in oral cancer patients? A scoping literature review. **Oral Dis**. 2021;27(1):94-110.

<https://doi.org/10.1111/odi.13312>.

Anas EM, Kim JG, Lee SY, Hasan K. Comparison of ring artifact removal methods using flat panel detector based CT images. **Biomed Eng Online**. 2011;10:72.

<https://doi.org/10.1186/1475-925X-10-72>.

Anavi Y, Avishai G, Calderon S, Allon DM. Bone remodeling in onlay beta-tricalcium phosphate and coral grafts to rat calvaria: microcomputerized tomography analysis. **J Oral Implantol**. 2011;37(4):379-86.

<https://doi.org/10.1563/AAID-JOI-D-09-00128.1>.

Arnold M, Stas P, Kummermehr J, Schultz-Hector S, Trott KR. Radiation-induced impairment of bone healing in the rat femur: effects of radiation dose, sequence and interval between surgery and irradiation. **Radiother Oncol**. 1998;48(3):259-65.

[https://doi.org/10.1016/s0167-8140\(98\)00039-5](https://doi.org/10.1016/s0167-8140(98)00039-5).

Barth HD, Zimmermann EA, Schaible E, Tang SY, Alliston T, Ritchie RO. Characterization of the effects of x-ray irradiation on the hierarchical structure and mechanical properties of human cortical bone. **Biomaterials**. 2011;32(34):8892-904.

<https://doi.org/10.1016/j.biomaterials.2011.08.013>.

¹ De acordo com a Norma da FOUFU, baseado nas Normas de Vancouver. Abreviaturas dos periódicos com conformidade com Medline (Pubmed).

Bartlow CM, Mann KA, Damron TA, Oest ME. Limited field radiation therapy results in decreased bone fracture toughness in a murine model. **PLoS One**. 2018;13(10):e0204928.

<https://doi.org/10.1371/journal.pone.0204928>.

Baselet B, Sonveaux P, Baatout S, Aerts A. Pathological effects of ionizing radiation: endothelial activation and dysfunction. **Cell Mol Life Sci**. 2019;76(4):699-728.

<https://doi.org/10.1007/s00018-018-2956-z>.

Boerckel JD, Mason DE, McDermott AM, Alsberg E. Microcomputed tomography: approaches and applications in bioengineering. **Stem Cell Res Ther**. 2014;5(6):144.

<https://doi.org/10.1186/scrt534>.

Borges JS, Rabelo GD, Irie MS, Paz JLC, Spin-Neto R, Soares PBF. Cortical Bone Modifications after Radiotherapy: Cortex Porosity and Osteonal Changes Evaluated Over Time. **Braz Dent J**. 2021;32(1):9-15.

<https://doi.org/10.1590/0103-6440202103384>.

Borrelli J Jr, Pape C, Hak D, Hsu J, Lin S, Giannoudis P et al. Physiological challenges of bone repair. **J Orthop Trauma**. 2011;26(12):708-11.

<https://doi.org/10.1097/BOT.0b013e318274da8b>.

Bouxsein ML, Boyd SK, Christiansen BA, Guldberg RE, Jepsen KJ, Müller R. Guidelines for assessment of bone microstructure in rodents using micro-computed tomography. **J Bone Miner Res**. 2010;25(7):1468-86.

<https://doi.org/10.1002/jbmr.141>.

Brown AP, Wendler DS, Camphausen KA, Miller FG, Citrin D. Performing nondiagnostic research biopsies in irradiated tissue: a review of scientific, clinical, and ethical considerations. **J Clin Oncol**. 2008;26(24):3987-94.

<https://doi:10.1200/JCO.2008.16.9896>

Buie HR, Campbell GM, Klinck RJ, MacNeil JA, Boyd SK. Automatic segmentation of cortical and trabecular compartments based on a dual threshold technique for in vivo micro-CT bone analysis. **Bone**. 2007;41(4):505-15.

<https://doi.org/10.1016/j.bone.2007.07.007>.

Cengiz IF, Oliveira JM, Reis RL. Micro-computed tomography characterization of tissue engineering scaffolds: effects of pixel size and rotation step. **J Mater Sci Mater Med**. 2017;28(8):129.

<https://doi.org/10.1007/s10856-017-5942-3>.

Chavez MB, Chu EY, Kram V, de Castro LF, Somerman MJ, Foster BL. Guidelines for Micro-Computed Tomography Analysis of Rodent Dentoalveolar Tissues. **JBMR Plus**. 2021;5(3):e10474.

<https://doi.org/10.1002/jbm4.104>.

Cho S, Bian J, Pelizzari CA, Chen CT, He TC, Pan X. Region-of-interest image reconstruction in circular cone-beam microCT. **Med Phys**. 2007;34(12):4923-33.

<https://doi.org/10.1118/1.2804924>.

Christiansen BA. Effect of micro-computed tomography voxel size and segmentation method on trabecular bone microstructure measures in mice. **Bone Rep**. 2016;5:136-40.

<https://doi.org/10.1016/j.bonr.2016.05.006>.

Clark DP, Badea CT. Micro-CT of rodents: state-of-the-art and future perspectives. **Phys Med**. 2014;30(6):619-34.

<https://doi.org/10.1016/j.ejmp.2014.05.011>.

Dalle Carbonare L, Valenti MT, Bertoldo F, Zanatta M, Zenari S, Realdi G et al. Bone microarchitecture evaluated by histomorphometry. **Micron**. 2005;36(7-8):609-16.

<https://doi.org/10.1016/j.micron.2005.07.007>.

de Lange GL, Overman JR, Farré-Guasch E, Korstjens CM, Hartman B, Langenbach GE et al. A histomorphometric and micro-computed tomography study of bone regeneration in the maxillary sinus comparing biphasic calcium phosphate and deproteinized cancellous bovine bone in a human split-mouth model. **Oral Surg Oral Med Oral Pathol Oral Radiol**. 2014;117(1):8-22.

<https://doi.org/10.1016/j.oooo.2013.08.008>.

de Oliveira GJPL, Aroni MAT, Medeiros MC, Marcantonio E Jr, Marcantonio RAC. Effect of low-level laser therapy on the healing of sites grafted with coagulum, deproteinized bovine bone, and biphasic ceramic made of

hydroxyapatite and β -tricalcium phosphate. In vivo study in rats. **Lasers Surg Med**. 2018. Epub ahead of print.

<https://doi.org/10.1002/lsm.22787>.

Donnelly E. Methods for assessing bone quality: a review. **Clin Orthop Relat Res**. 2011;469(8):2128-38.

<https://doi.org/10.1007/s11999-010-1702-0>.

Dörtbudak O, Haas R, Mailath-Pokorny G. Effect of low-power laser irradiation on bony implant sites. **Clin Oral Implants Res**. 2002;13(3):288-92.

<https://doi.org/10.1034/j.1600-0501.2002.130308.x>.

Farlay D, Boivin G. Bone mineral quality. **Osteoporosis**. Yannis Dionyssiotis, IntechOpen. 2012;953-78.

<https://doi.org/10.5772/29091>. Disponível em:

<https://www.intechopen.com/books/osteoporosis/bone-mineral-quality>.

Fávaro-Pípi E, Feitosa SM, Ribeiro DA, Bossini P, Oliveira P, Parizotto NA et al. Comparative study of the effects of low-intensity pulsed ultrasound and low-level laser therapy on bone defects in tibias of rats. **Lasers Med Sci**. 2010;25(5):727-32.

<https://doi.org/10.1007/s10103-010-0772-2>.

Fenner M, Park J, Schulz N, Amann K, Grabenbauer GG, Fahrig A et al. Validation of histologic changes induced by external irradiation in mandibular bone. An experimental animal model. **J Craniomaxillofac Surg**. 2010;38(1):47-53.

<https://doi.org/10.1016/j.jcms.2009.07.011>.

Friedrichsdorf SP, Arana-Chavez VE, Cattaneo PM, Spin-Neto R, Dominguez GC. Effect of the software binning and averaging data during microcomputed tomography image acquisition. **Sci Rep**. 2019;9(1):10562.

<https://doi.org/10.1038/s41598-019-46530-z>.

Garcia VG, de Lima MA, Okamoto T, Milanezi LA, Júnior EC, Fernandes LA et al. Effect of photodynamic therapy on the healing of cutaneous third-degree-burn: histological study in rats. **Lasers Med Sci**. 2010;25(2):221-8.

<https://doi.org/10.1007/s10103-009-0694-z>.

Green DE, Rubin CT. Consequences of irradiation on bone and marrow phenotypes, and its relation to disruption of hematopoietic precursors. **Bone**. 2014;63:87-94.

<https://doi.org/10.1016/j.bone.2014.02.018>.

Guda T, Labella C, Chan R, Hale R. Quality of bone healing: perspectives and assessment techniques. **Wound Repair Regen**. 2014;22 Suppl 1:39-49.

<https://doi.org/10.1111/wrr.12167>.

Gupta A, Dai T, Hamblin MR. Effect of red and near-infrared wavelengths on low-level laser (light) therapy-induced healing of partial-thickness dermal abrasion in mice. **Lasers Med Sci**. 2014;29(1):257-65.

<https://doi.org/10.1007/s10103-013-1319-0>.

Higham CES, Faithfull S. Bone Health and Pelvic Radiotherapy. **Clinical Oncology**. 2015;27(11):668 – 78.

<https://doi.org/10.1016/j.clon.2015.07.006>.

Hutchinson JC, Shelmerdine SC, Simcock IC, Sebire NJ, Arthurs OJ. Early clinical applications for imaging at microscopic detail: microfocus computed tomography (micro-CT). **Br J Radiol**. 2017;90(1075):20170113.

<https://doi.org/10.1259/bjr.20170113>

Iocca O, Farcomeni A, Pardiñas Lopez S, Talib HS. Alveolar ridge preservation after tooth extraction: a Bayesian Network meta-analysis of grafting materials efficacy on prevention of bone height and width reduction. **J Clin Periodontol**. 2017;44(1):104-14.

<https://doi.org/10.1111/jcpe.12633>.

Jovanović Z, Khan F, Enzmann F, Kersten M. Simultaneous segmentation and beam-hardening correction in computed microtomography of rock cores. **Comput Geosci**. 2013;56:142-50.

<https://doi.org/10.1016/j.cageo.2013.03.015>.

Kalpakcioglu BB, Morshed S, Engelke K, Genant HK. Advanced imaging of bone macrostructure and microstructure in bone fragility and fracture repair. **J Bone Joint Surg Am**. 2008;90 Suppl 1:68-78.

<https://doi.org/10.2106/JBJS.G.01506>.

Kamburoglu K, Kolsuz E, Murat S, Eren H, Yüksel S, Paksoy CS. Assessment of buccal marginal alveolar peri-implant and periodontal defects using a cone beam CT system with and without the application of metal artefact reduction mode. **Dentomaxillofac Radiol.** 2013;42(8):20130176.

<https://doi.org/10.1259/dmfr.20130176>.

Koontz BF, Verhaegen F, De Ruyscher D. Tumour and normal tissue radiobiology in mouse models: how close are mice to mini-humans? **Br J Radiol.** 2017;90(1069):20160441.

<https://doi.org/10.1259/bjr.20160441>.

Kühl S, Götz H, Hansen T, Kreisler M, Behneke A, Heil U et al. Three-dimensional analysis of bone formation after maxillary sinus augmentation by means of microcomputed tomography: a pilot study. **Int J Oral Maxillofac Implants.** 2010.25(5):930-8.

Limirio PHJO, Soares PBF, Emi ETP, Lopes CCA, Rocha FS, Batista JD, Rabelo GD et al. Ionizing radiation and bone quality: time-dependent effects. **Radiat Oncol.** 2019;14(1):15.

<https://doi.org/10.1186/s13014-019-1219-y>.

Lucatto SC, Guilherme A, Dib LL, Segreto HR, Alves MT, Gumieiro EH et al. Effects of ionizing radiation on bone neoformation: histometric study in Wistar rats tibiae. **Acta Cir Bras.** 2011;26(6):475-80.

<https://doi.org/10.1590/s0102-86502011000600012>.

Mackiewicz Z, Niklińska WE, Kowalewska J, Chyczewski L. Bone as a source of organism vitality and regeneration. **Folia Histochem Cytobiol.** 2011;49(4):558-69.

<https://doi.org/10.5603/fhc.2011.0079>.

McDougald WA, Collins R, Green M, Tavares AAS. High Dose MicroCT Does Not Contribute Toward Improved MicroPET/CT Image Quantitative Accuracy and Can Limit Longitudinal Scanning of Small Animals. **Front. Phys.** 2017;5:50.

<https://doi.org/10.3389/fphy.2017.00050>.

Mendes EM, Irie MS, Rabelo GD, Borges JS, Dechichi P, Diniz RS et al. Effects of ionizing radiation on woven bone: influence on the osteocyte lacunar network,

collagen maturation, and microarchitecture. **Clin Oral Investig.** 2020;24(8):2763-771.

<https://doi.org/10.1007/s00784-019-03138-x>.

Mendoza-Azpur G, de la Fuente A, Chavez E, Valdivia E, Khouly I. Horizontal ridge augmentation with guided bone regeneration using particulate xenogenic bone substitutes with or without autogenous block grafts: A randomized controlled trial. **Clin Implant Dent Relat Res.** 2019;21(4):521-30.

<https://doi.org/10.1111/cid.12740>.

Mueller M, Schilling T, Minne HW, Ziegler R. A systemic acceleratory phenomenon (SAP) accompanies the regional acceleratory phenomenon (RAP) during healing of a bone defect in the rat. **J Bone Miner Res.** 1991;6(4):401-10.

<https://doi.org/10.1002/jbmr.5650060412>.

Müller R, Van Campenhout H, Van Damme B, Van Der Perre G, Dequeker J, Hildebrand T et al. Morphometric analysis of human bone biopsies: a quantitative structural comparison of histological sections and micro-computed tomography. **Bone.** 1998;23(1):59-66.

[https://doi.org/10.1016/s8756-3282\(98\)00068-4](https://doi.org/10.1016/s8756-3282(98)00068-4).

Obradović RR, Kesić LG, Pesevska S. Influence of low-level laser therapy on biomaterial osseointegration: a mini-review. **Lasers Med Sci.** 2009; 24(3):447-51.

<https://doi.org/10.1007/s10103-008-0573-z>.

Pauwels R, Beinsberger J, Collaert B, Theodorakou C, Rogers J, Walker A et al. Effective dose range for dental cone beam computed tomography scanners. **Eur J Radiol.** 2012;81(2):267-71.

<https://doi.org/10.1016/j.ejrad.2010.11.028>.

Queiroz PM, Rovaris K, Santaella GM, Haiter-Neto F, Freitas DQ. Comparison of automatic and visual methods used for image segmentation in Endodontics: a microCT study. **J Appl Oral Sci.** 2017;25(6):674-79.

<https://doi.org/10.1590/1678-7757-2017-0023>.

Rabelo GD, Beletti ME, Dechichi P. Histological analysis of the alterations on cortical bone channels network after radiotherapy: A rabbit study. **Microsc Res Tech.** 2010;73(11):1015-8.

<https://doi.org/10.1002/jemt.20826>.

Schilling T, Müller M, Minne HW, Ziegler R. Influence of inflammation-mediated osteopenia on the regional acceleratory phenomenon and the systemic acceleratory phenomenon during healing of a bone defect in the rat. **Calcif Tissue Int.** 1998;63(2):160-6.

<https://doi.org/10.1007/s002239900508>.

Schindeler A, Mills RJ, Bobyn JD, Little DG. Preclinical models for orthopedic research and bone tissue engineering. **J Orthop Res.** 2018;36(3):832-40.

<https://doi.org/10.1002/jor.23824>.

Schneider CA, Rasband WS, Eliceiri KW. NIH Image to ImageJ: 25 years of image analysis. **Nat Methods.** 2012;9(7):671-5.

<https://doi.org/10.1038/nmeth.2089>.

Schoen PJ, Reintsema H, Raghoobar GM, Vissink A, Roodenburg JL. The use of implant retained mandibular prostheses in the oral rehabilitation of head and neck cancer patients. A review and rationale for treatment planning. **Oral Oncol.** 2004;40(9):862-71.

<https://doi.org/10.1016/j.oraloncology.2003.08.024>.

Schulze R, Heil U, Gross D, Bruellmann DD, Dranischnikow E, Schwanecke U et al. Artefacts in CBCT: a review. **Dentomaxillofac Radiol.** 2011;40(5):265-73.

<https://doi.org/10.1259/dmfr/30642039>.

Schulze RK, Berndt D, d'Hoedt B. On cone-beam computed tomography artifacts induced by titanium implants. **Clin Oral Implants Res.** 2010;21(1):100-7.

<https://doi.org/10.1111/j.1600-0501.2009.01817.x>.

Szymczyk KH, Shapiro IM, Adams CS. Ionizing radiation sensitizes bone cells to apoptosis. **Bone.** 2004;34(1):148-56.

<https://doi.org/10.1016/j.bone.2003.09.003>.

Soares PBF, Soares CJ, Limirio PHJO, de Jesus RNR, Dechichi P, Spin-Neto R, Zanetta-Barbosa D. Effect of ionizing radiation after-therapy interval on bone: histomorphometric and biomechanical characteristics. **Clin Oral Investig.** 2019 Jun;23(6):2785-2793.

<https://doi.org/10.1007/s00784-018-2724-3>.

Soares PBF, Soares CJ, Limirio PHJO, Lara VC, Moura CCG, Zanetta-Barbosa D. Biomechanical and morphological changes produced by ionizing radiation on bone tissue surrounding dental implant. **J Appl Oral Sci.** 2020;28:e20200191.

<https://doi.org/10.1590/1678-7757-2020-0191>.

Versiani MA, Silva-Sousa YTC, Leoni GB, Lopes RT, Sousa-Neto OMD. Microtomografia aplicada à pesquisa odontológica. In: Estrella C. **Metodologia Científica – Ciência, Ensino, Pesquisa.** 3 ed. Artes Médicas; 2018. p.637-66.

Waarsing JH, Day JS, Weinans H. An improved segmentation method for in vivo microCT imaging. **J Bone Miner Res.** 2004;19(10):1640-50.

<https://doi.org/10.1359/JBMR.040705>.

Wong AK, Schönmeyr BH, Soares MA, Li S, Mehrara BJ. Hyperbaric oxygen inhibits growth but not differentiation of normal and irradiated osteoblasts. **J Craniofac Surg.** 2008;19(3):757-65.

<https://doi.org/10.1097/SCS.0b013e31816aac19>.

ANEXOS



Universidade Federal de Uberlândia

– Comissão de Ética na Utilização de Animais –



CERTIFICADO

Certificamos que o projeto intitulado “Efeito da radioterapia e laser de baixa intensidade no reparo ósseo em defeito preenchido com enxerto ósseo particulado”, protocolo nº 093/17, sob a responsabilidade de **Priscilla Barbosa Ferreira Soares** – que envolve a produção, manutenção e/ou utilização de animais pertencentes ao filo Chordata, subfilo Vertebrata, para fins de pesquisa científica – encontra-se de acordo com os preceitos da Lei nº 11.794, de 8 de outubro de 2008, do Decreto nº 6.899, de 15 de julho de 2009, e com as normas editadas pelo Conselho Nacional de Controle da Experimentação Animal (CONCEA), e foi APROVADA pela COMISSÃO DE ÉTICA NA UTILIZAÇÃO DE ANIMAIS (CEUA) da UNIVERSIDADE FEDERAL DE UBERLÂNDIA, em reunião **18 de Outubro de 2019**.


(We certify that the project entitled “Efeito da radioterapia e laser de baixa intensidade no reparo ósseo em defeito preenchido com enxerto ósseo particulado”, protocol 093/17, under the responsibility of **Priscilla Barbosa Ferreira Soares** - involving the production, maintenance and/or use of animals belonging to the phylum Chordata, subphylum Vertebrata, for purposes of scientific research - is in accordance with the provisions of Law nº 11.794, of October 8th, 2008, of Decree nº 6.899 of July 15th, 2009, and the rules issued by the National Council for Control of Animal Experimentation (CONCEA) and it was approved for ETHICS COMMISSION ON ANIMAL USE (CEUA) from FEDERAL UNIVERSITY OF UBERLÂNDIA, in meeting of October 18th, 2019).

Vigência do Projeto	Início: 20/06/2018 Término: 02/11/2020
Espécie / Linhagem / Grupos Taxonômicos	<i>Rattus norvegicus</i>
Número de animais	64
Peso / Idade	300g / 18 semanas
Sexo	Machos
Origem / Local	Rede de Biotérios de Roedores da UFU
Local onde serão mantidos os animais:	Rede de Biotérios de Roedores da UFU

Alterações realizadas:

Aumento de 16 ratos machos, serão utilizados 64 ratos machos *Rattus norvegicus*, da linhagem Wistar, clinicamente sadios com 18 semanas de idade e peso aproximado de 300g.

Uberlândia, 04 de Novembro de 2019.


Prof. Dr. Lúcio Vilela Carneiro Girão
UNIVERSIDADE FEDERAL DE UBERLÂNDIA
Comissão de Ética na Utilização de Animais /UFU
Coordenador da CEUA
Portaria Nº 1234 DE 01 DE OUTUBRO DE 2019